THE UNIVERSITY *of* EDINBURGH

Stochastic effects in systems of aligning self-propelled particles

Eoin Ó Laighléis

Doctor of Philosophy
The University of Edinburgh
July 2022

Lay summary

In this thesis, we study systems of entities that move under their own power (self-propelled particles) such as birds, fish or bacteria, known as active matter systems. Much like how fluids such as water are made up of many microscopic individual water molecules, active matter systems can be approximated as an active fluid to explore their behaviour at large scales. Fluids are usually described by a set of equations for the change in the fluid's density and velocity over time, whose solutions give the behaviour of the fluid in time and space.

An example of a large-scale behaviour seen in an active matter system is the flocking of birds. Here, birds that are close together move in the same direction, creating a highly organised cluster. Occasionally, a flock of birds will rapidly change direction *en masse* with no obstacles or predators in sight. In this thesis, we study particle models where flocking is observed in simulations and derive fluid equations to explore the conditions needed for this random change in direction to be able to occur.

We introduce and use a method of deriving fluid equations for active matter systems and compare the solutions of these equations to the behaviour of the particle system. Our key finding is that the mathematical form of the randomness in these fluid equations plays a large role in determining whether the fluid behaves the same way as the particle system. We then show that using the method we introduced gives the correct mathematical form, and the fluid equations derived this way can be used to better understand the system as a whole. These results show why getting the random element of fluid equations right is important and outline a method to better understand the random behaviour of other active matter systems.

Abstract

Systems of self-propelled particles are often capable of exhibiting complex behaviours on a macroscopic scale with only simple interactions between the active microscopic agents. In systems where the particles interact by attempting to align their directions of motion, the ordered steady state tends towards a dense coherent grouping of particles (a "flock") travelling in the same direction. Continuum theories where the particles are treated as an active fluid allow for a greater understanding of the macroscopic behaviour of these flocks, although these theories have typically focussed on understanding the behaviour of the flock in a steady state. In this thesis, we are interested in deriving continuum theories of aligning self-propelled particle systems and in understanding the role that stochasticity has in ensuring the dynamical behaviour of the underlying agent-based model is maintained.

The focus of this thesis is a family of models of aligning self-propelled particles on a lattice that interact by aligning with a subset of nearby particles. We use the Kramers-Moyal approximation to derive stochastic Langevin equations directly from the microscopic interactions. Our goal is to obtain equations for the evolution of the system's density and polarisation such that their trajectories match the dynamic behaviour of the underlying agent-based models and, in doing so, to demonstrate that the form of the stochastic prefactor in the polarisation equation can greatly affect the macroscopic behaviour of the system.

In Chapter 2, we study the ordered state of a system of aligning self-propelled particles on a one-dimensional lattice. The aligning interaction between particles allows for the formation of a flock capable of alternating the direction it travels through the lattice. We derive a set of stochastic differential equations for the density and polarisation of the system and introduce a numerical integration scheme to demonstrate that the order parameter of each of the agent-based and continuum systems scales identically with increasing noise strength. We then use

the continuum equations to obtain a minimal set of interactions for a flock to exist in one dimension and demonstrate how alignment interactions with three particles are necessary for a flock to form on a one dimensional lattice.

This motivates the work in the remainder of this thesis, wherein we examine a family of two-dimensional models to explore whether we can derive stochastic differential equations whose trajectories demonstrate the same behaviour as in the agent-based models. We introduce a family of four lattice-based agent-based models in Chapter 3 and map out the behaviour of the ordered state in each of these models. These models consist of all combinations of two interaction types (exponential or linear in local polarisation) and two interaction neighbourhoods (fixed or varying with local density). One of these models shows the "banding" present in traditional Vicsek models, while the other three show the occasional macroscopic change in direction observed in flocks of birds such as starlings.

In Chapter 4, we use the Kramers-Moyal approximation again to derive stochastic differential equations for the density and polarisation of the four models above. Using linear stability analysis, we explain why the ordered state in each model consists of a flock that will either be capable or incapable of turning. The linear stability analysis shows why the choice of interaction neighbourhood does not affect the ability of the flocks with a linear interaction to macroscopically alter direction and why that choice *does* affect the ability of a flock to turn for systems with an exponential interaction, although some calculation remains here to demonstrate linear stability exactly matching that of the agent-based systems. We also explore a numerical integration scheme for the two dimensional models, laying out a procedure that may result in integrated trajectories matching the behaviour of the agent-based model as in one dimension.

The work in this thesis explores the effects of different stochastic terms in continuum equations describing systems of aligning self-propelled particles and introduces a mechanism to derive these terms to ensure the behaviour matches that of the underlying agent-based models. We demonstrate the power of this mechanism by identifying a minimal model of flocking in one dimension and by exploring when flocks can turn in two dimensions. These examples provide a pathway for exploring the dynamic behaviour of other interacting particle models on a macroscopic scale.

Declaration

I declare that this thesis was composed by myself, that the work contained herein is my own except where explicitly stated otherwise in the text, and that this work has not been submitted for any other degree or professional qualification except as specified.

Parts of this work have been published in [81].

(*Eoin Ó Laighléis, July 2022*)

Acknowledgements

I would like to express my grateful thanks to my fantastic supervisors, Richard Blythe and Martin Evans, who guided my work and supported me over the last six years. Their guidance and direction shaped this work greatly, and I'm grateful for all they've done.

I would also like to thank my partner, Susanna, who provided the support and encouragement I needed to complete this work, and my cat, Mylo, who provided endless distractions and let me know every time a bird was nearby.

Many thanks to my parents and sister, who supported me throughout this academic journey.

Thanks also to my friends - to Emily, Iain and Katherine, who sense-checked my assumptions and approximations and let me know when I was overcomplicating things; to David, Michael, Chloe, Heather, Jon, Amy, Sophie and Laura, who ensured I made time for socialising and breaks from work; and to Eimear, Caoimhe and Orna, who have always been there for me.

A final thanks to Taylor Swift, whose album *folklore* helped me through the start of the pandemic when it seemed like everything was going wrong.

Contents

Lay summary i

Abstract ii

Declaration iv

Acknowledgements v

Contents vi

List of Figures x

1 Background 1

1.1 Non-equilibrium steady states 1

1.2 Agent-based models of self-propelled particles 3

1.2.1 The Vicsek model 3

1.2.2 Agent-based flocking models in one dimension 8

1.2.3 Reaction-diffusion models of aligning self-propelled particles 11

1.2.4 Alternative neighbourhoods for a self-propelled particle model 12

1.3 Active hydrodynamics 14

1.3.1 Phenomenological equations 15

1.3.2 Microscopic to Macroscopic 16

1.4 The structure of this thesis 25

2 Stochastic field equations for one-dimensional flocking 27

2.1 Agent-based model 30

2.1.1 Model definition 30

2.1.2 ABM behaviour 31

2.1.3 Differences from O'Loan model 33

2.2 Kramers-Moyal approximation 34

2.2.1 Arriving at a set of Langevin equations 34

2.2.2 The density equation 35

2.2.3 The magnetisation equation 37

2.2.4 Choice of stochastic variable 39

2.3 Numerical integration 40

2.3.1 Truncating the noise term 40

2.3.2 Comparison of continuum equations with agent-based model 44

2.4 Interpretation of the continuum equations 46

2.4.1 Density equation 46

2.4.2 Magnetisation equation 47

2.5 Minimal model 48

2.6 Modifications to the alignment rule 51

2.6.1 Particle self-interaction - persistence or uncertainty 52

2.6.2 Alternative neighbourhood definitions 53

2.7 Summary 56

3 Agent-based flocking in two dimensions on a lattice 57

3.1 Agent-based models 59

3.1.1 Exponentially aligning model (lattice-gas cellular automata) 59

3.1.2 Linearly aligning model 62

3.1.3 Ordered phase behaviour 63

3.2 Topological interaction 64

3.2.1 Definition of the neighbourhood 64

3.2.2 Changes to the ordered state 65

3.3 Robustness of the ordered phase behaviour to model changes 67

3.3.1 Constraining particles to a lattice 67

3.3.2 Implementation of stochastic uncertainty 68

3.3.3 Removing the "fixed-speed" assumption 70

3.4 Summary 72

4 Continuous space flocking in two dimensions 75

4.1 Continuous equation derivation 76

4.1.1 Jump moments of probability density 78

4.1.2 Field equation for particle density 79

4.1.3 Field equation for magnetisation 80

4.1.4 Review of key assumptions 82

4.2 Comparison between interaction types 84

4.2.1 EA model 85

4.2.2 LA model 86

4.3 Stability analysis 87
4.3.1 Fluctuations to the neighbourhood magnetisation **M** 87
4.3.2 Fluctuations to particle flux and directional density 89
4.3.3 Linearised equations and dispersion relations 90
4.3.4 Inconsistencies in the linear stability analysis 96
4.4 Numerical analysis 98
4.4.1 Numerical integration 98
4.4.2 Results of the numerical integration 100
4.5 Summary 102

5 Discussion & conclusion 104

A The Kramers-Moyal approximation 110

B Beta-type distribution 112

C Run-and-tumble velocity derivation 114

D Exponentially-aligning Fourier transform and matrix solution 117

Bibliography 120

List of Figures

(1.1) The phases of the two-dimensional Vicsek model as the noise strength is varied. Each of these snapshots contains 300 particles. The arrowhead indicates the current direction of motion, with the short lines indicating the particle's trajectory over the preceding 20 time-steps. (a) High density and high noise ($L = 7, \eta_0 = 2.0$), early time. No coherent orientational order is observed. Particles move as is performing a random walk in continuous space. (b) Low density and low noise ($L = 25, \eta_0 = 0.1$). Distinct groups form that move in random directions. Motion within each group is coherent (c) Later time of (a). Small correlation is observed, though particles still move largely at random. (d) High density and low noise ($L = 5, \eta_0 = 0.1$) results in highly ordered motion. Image reproduced from [116] with permission. 5

(1.2) Banding in a two-dimensional Vicsek model (top) and a two-dimensional active Ising model. The number of bands in the Vicsek model increases as the total density is increased and remains constant as they propagate through the system. Figure reproduced with permission from [104]. 7

(1.3) The dynamics of a trajectory of the one-dimensional Vicsek SPP model with $L = 300$, $N = 600$ and $\eta_0 = 2.0$. The darker area represent regions of higher particle density, and time increases in the negative y direction. Particles undergo phase separation and clustering into condensates, with the condensate alternating direction stochastically. Note that η_0 here is much larger than for the ordered state of the two-dimensional SPP model [116]. Figure reproduced with permission from [35]. 8

(1.4) The dynamics of a trajectory of a discrete space one-dimensional SPP model with $L = 1000$ and $N = 1000$. The darker area represent regions of higher particle density. (a) $\eta = 0.2$, time between snapshots $\Delta t = 1$. Particles change direction frequently and no ordered flock is observed. (b) $\eta = 0.02, \Delta t = 5$. Particles undergo phase separation and clustering into condensates, with the condensate alternating direction stochastically. Figure reproduced from [82]. © IOP Publishing. Reproduced with permission. All rights reserved. 10

(1.5) (A) The neighbourhood of the i-th particle (shaded blue) in a limited field-of-view Vicsek model. Here, $n_{ij} = 1$ if the j-th particle lies within a sector of angle 2ϕ of a fixed radius circle centred on particle i. (B) An example of a non-reciprocal interaction. While $n_{ij} = 1$, $n_{ji} = 0$ due to the directional vision. Reproduced with permission from [44]. 12

(1.6) An example of a non-metric neighbourhood where the $k = 5$ nearest particles are considered neighbours in a dense (a) and dilute (b) system. Reproduced from [55]. 13

(1.7) Representation of the propagation of turning information in a real flock and a Vicsek model. (a) The turning information is undamped in a real flock, propagating throughout the system and causing a macroscopic turn. (b) In a Vicsek model, turning information is damped. Reproduced with permission from [23]. . . 14

(1.8) (a) A typical rotational diffusive "kick", where a random angle η has been applied to a particle moving in a direction θ to give it a new velocity with angle θ'. (b) A typical collision between two particles with directions θ_1 and θ_2, where the average angle $\bar{\theta}$ (1.19) is given by the dashed line. After the collision, each particle assumes a new velocity that differs from $\bar{\theta}$ by a random noise η_1 and η_2 respectively. 17

(2.1) Sample trajectories of the agent-based model at different values of the noise strength η. Points with darker colours have more particles on that site, with black denoting the most dense regions. Left: $\eta = 0.02$. Here, a condensed group (red) is moving through the lattice before stochastically alternating direction. Other than the large flock, the lattice is sparsely populated with a small number of travelling particles (yellow). Right: $\eta = 0.2$. The stochastic effects dominate here and no condensate forms. Particle density is approximately uniform and no coherent motion is observed. For both trajectories, $N = L = 2000$ and $\beta = 2.0$. For these plots, $\Delta x = 1$ and $\Delta t = 5$. 28

(2.2) Graphical representation of the update rules for a single time-step. Once a particle has been selected (red above), a new direction is chosen with probabilities given by (2.1), represented by the diverging paths. Once the particle has a new velocity, it travels one space in that direction, then the process repeats. 30

(2.3) Plot of the mean site velocity v as a function of the site polarisation p for (left) varying strengths of non-linear interactions β and (right) varying strengths of stochasticity η. Note that the $\beta \to \infty$ limit approaches a step function of height $2 - 4\eta$. 31

(2.4) Plot of a measure of order in the system as a function of the stochasticity η. Below the phase transition $\eta = \eta_c \approx 0.05$, the system exhibits order, while above the critical noise strength, no global order is observed. 32

(2.5) Plots of $Beta_{\alpha,\beta}(y)$ for various α and β. We have kept $\alpha + \beta$ constant for comparison. This relates to a constant density (here, $\rho \approx \frac{2}{N}$). 43

(2.6) The order parameter of the system φ vs the noise strength η for three different implementations of the continuum equations and compared with the ABM (dots). In all of these implementations, we had $N = L = 100$, $\beta = 2.0$, $\delta t = \frac{1}{N} = 0.01$, $T = 50000$. 44

(2.7) Sample space-time trajectories for (2.22, 2.34) using beta noise (left) and truncated Gaussian noise (right). Both trajectories show the existence of a phase separated ordered flock. For the same system parameters ($N = L = 2000$, $\beta = 2$, $\eta = 0.02$), the flock in the truncated Gaussian model is more dense, suggesting this treatment of the noise gives rise to greater order. This can be seen more clearly in Fig. 2.6 46

(2.8) A purely deterministic version of the agent-based model with a small pulse sent in from the right. This pulse is enough to turn the flock around, demonstrating that the flock is unstable to a sufficiently persistent fluctuation in the nose. 49

(2.9) When $\beta = 0$, all values of η have low order parameter φ. Other parameters: $N = L = 1000$, $T = 90000$. 50

(2.10) Space-time trajectories of the field equations (2.22, 2.34) for a linear interaction (left) (2.47) and a third order interaction (right) (2.48). Parameters are $N = L = 2000$, $\beta = 2$, $\eta = 0.02$, $r = 1$. . . 51

(2.11) The multiplicative change in p due to uncertainty instead of directional persistence. No difference is made when $\Delta = 1$, thus the low density regime $N\rho < 5$ has a large change in the mean velocity v due to particle uncertainty. 54

(2.12) A measure of the order parameter φ (2.5) against noise strength η for various neighbourhood definitions. The dots denote models where particles count themselves as their own neighbour, even if they would not normally meet the criteria for inclusion, while the crosses are for models where particles exclude themselves from their own neighbourhood, even if they would normally meet the criteria for inclusion. 54

(3.1) Particles moving on a section of a lattice in an LGCA model. Note that the direction of motion is determined by the spin state particles occupy on the lattice site, with particles sitting in the centre spin states remaining stationary. Sites can contain multiple particles, while spin states within sites typically have a maximum occupancy of 1. 60

(3.2) Order parameter of selected trajectories of the ABM models. Order is present in each trajectory, as evidenced by the magnitude of the order parameter being close to 1. The LA model with metric interactions exhibits a change in orientation of the ordered flock, while the EA model does not. The average magnitude of the order parameter is lower for the LA model than the EA model. $N = L_x = L_y = 100$, $\beta = 0.75$, $\eta = 0.02$. 63

(3.3) Mean velocity of selected trajectories of topological neighbourhood ABMs. Order is present in each trajectory, evidenced by the magnitude of the order parameter (left plot) being close to 1. Unlike for metric neighbourhood ABMs, both the EA and LA models exhibit macroscopic turning here, as evidenced by the non-constant angle of the mean velocity (right plot). Parameters were $N = L_x = L_y = 100$, $\beta = 0.75$, $\eta = 0.02$. 66

(3.4) Top: The order parameter in the metric EA model above as a function of system density using either intrinsic or extrinsic noise as a function of ρ or β. Bottom: The order parameter in the metric LA model above as a function of system density using either intrinsic or extrinsic noise as a function of ρ or η. The behaviour of the order parameter in the ordered state is similar between the two noise types, although it is closer quantitatively in the EA model than the LA model. $L_x = L_y = 100$, $R = 16$, $\beta = 0.3$ (top left), $\eta_0 = 0.005$ (bottom left), $\rho_0 = 0.01$ (top right and bottom right). . 68

(3.5) Order parameter of selected trajectories of the ABM models. Order is present in each trajectory, as evidenced by the magnitude of the order parameter being close to 1. Changes in direction occur more frequently in the metric LA model with intrinsic noise than the metric LA model with extrinsic noise. $N = L_x = L_y = 100$, $\eta = 0.02$. 69

(3.6) Top: The order parameter in the metric EA model above using either a stochastic or simultaneous update rule as a function of ρ or β. Bottom: The order parameter in the metric LA model above using either a stochastic or simultaneous update rule as a function of ρ or η. While the position of the phase transition may differ between the two selections, the overall behaviour remains similar between the two update types. $N = L_x = L_y = 100$, $R = 16$, $\beta = 0.3$ (top left), $\eta_0 = 0.005$ (bottom left), $\rho = 0.01$ (top right and bottom right). 71

(4.1) The real values of the Fourier-transformed spatial correlation function of fluctuations in particle direction in our ABMs. The fluctuations are shown to be long-range, as indicated by the rapid decrease as k increases. Rising values for large k are due to the periodicity of the lattice. $N = L_x = L_y = 100$, $\beta = 0.75$, $\eta = 0.02$. 83

(4.2) Autocorrelation function of polarisation (4.26) within our ABMs. The correlation function drops sharply for $r \neq 0$, therefore correlations between neighbouring sites are significantly smaller than self-correlations.$N = L_x = L_y = 100$, $\beta = 0.75$, $\eta = 0.02$. . . 84

(4.3) Top: The order parameter in the ABM EA model vs the numerically integrated field equations as a function of system density with metric (left) or topological (right) interactions. Bottom: The order parameter in the ABM LA model vs the numerically integrated field equations as a function of system density with metric (left) or topological (right) interactions. For all four models, the order parameter for the numerically integrated SDE trajectories is close to 1 and does not change significantly as density increases. However, for trajectories of the ABMs that exhibit macroscopic turning in the ordered state (top right, bottom left and bottom right), the order parameter is lower than 1 and decreases further as density increases. This indicates that the macroscopic turning present in the topological EA and both LA ABMs is not observed in the trajectories of the numerically integrated field equations, as we see from Fig.s 3.2 and 3.3 that the order parameter drops as the flock changes direction. The ABM data was obtained using a stochastic update with scalar noise. $L_x = L_y = 100$, $\beta = 0.75$, $\eta = 0.02$. 101

Chapter 1

Background

1.1 Non-equilibrium steady states

The designation of a non-equilibrium system can typically be applied to two major groups: a system that is in the process of relaxation towards equilibrium, such as a "glassy" system wherein particles are moving towards equilibrium on a time-scale much longer than the typical time-scales of the constituent particles [13, 103]; or a driven system where external forces are applied to keep the system from reaching equilibrium, such as particles in a constant or oscillating field [69, 97]. States in driven systems where one or more macroscopic quantities of the system remain constant in time are typically referred to as non-equilibrium steady states.

Active matter systems are examples of driven systems for which the external forces are generated by the individual constituents [91]. These constituents, termed "active particles", consume energy to produce propulsion. As such, the external force acting on the system is a sum of individual internal forces. Most active matter systems can be characterised as being along three main axes: dense vs dilute, wet vs dry, and aligning vs repulsion [29, 30]. Dense systems typically have a higher ratio of three or more body interactions to two body interactions, compared to dilute systems where interactions are less frequent; wet systems tend to be momentum-conserving due to hydrodynamic interactions, while dry systems are non-momentum conserving; aligning systems [116] tend to have a much larger particle interaction radius compared to repulsive systems [18]. While not every active matter system can be neatly characterised as being on one or other end

of each of these axes [43, 49, 56, 93, 101], the three axes can be a good way to categorise and differentiate active matter systems.

Interest in active matter typically focuses on the complex motion that these systems can exhibit. Under certain systematic conditions, active matter systems can produce macroscopic motion, whether in the form of a particle current [112] or a non-zero vorticity [64]. While simulations of agent-based models can be used to observe and identify macroscopic behaviours [100], an understanding of why and how these behaviours manifest typically requires more direct study of how macroscopic observables behave. This is often done by examining differential equations appropriate to the system, whether obtained phenomenologically [112], directly from the particle interactions [88, 118] or through experimental observations [24, 62, 83].

In this thesis, we derive stochastic differential equations describing a sample of dry, aligning, dense active matter systems to investigate the role of the stochastic prefactor in the dynamics of the system. We seek to understand this role by studying the impact of the stochastic prefactor on the ability of a coherent ordered condensate (hereafter "flock") to form and spontaneously change direction. In this chapter, we explore the background to our goal, discussing various agent-based models of aligning self-propelled particles and the differential equations that describe the large-scale behaviour of these systems.

We begin by introducing the Vicsek model in two or more dimensions in Section 1.2.1, which consists of a fixed number of self-propelled particles aligning with other particles within a fixed radius and travelling with a fixed speed and is the basis for the Vicsek class of models. Models within this class exhibit a transition between a disordered state where no coherent motion is observed and an ordered state where particles travel through the system in the same direction. In Section 1.2.2, we examine Vicsek-class models in one spatial dimension, and discuss how the change to a discrete rotational symmetry affects the behaviour observed in these models. Sections 1.2.3 and 1.2.4 introduce modifications to the base Vicsek model, the former reproducing the behaviour of the ordered state, the latter introducing macroscopic turning based on observations of flocks of starlings. Section 1.3 describes various methods of obtaining differential equations describing Vicsek-class models, from phenomenological approaches in Section 1.3.1 to derivations from microscopic models in Section 1.3.2, finishing with the Kramers-Moyal expansion that will be the focus of much of the analytical work in the thesis. Finally, in Section 1.4, we outline the structure of the remainder of

this thesis.

1.2 Agent-based models of self-propelled particles

Throughout this thesis, we discuss non-equilibrium steady states in the context of systems of aligning self-propelled particles, which we hereafter abbreviate as SPPs. SPP models aim to capture behaviours of ordered systems in the physical world consisting of active particles [95], such as birds flocking [20, 33], fish schooling or milling [64], locust swarming [12, 15], pedestrian motion in crowds [77] or bacterial motion [109, 117]. Ordered motion arises in such systems from the spontaneous breaking of a rotational symmetry [90] that is continuous in systems with two or more dimensions. In this work, we focus on "polar particles", defined as particles with a clearly defined "head" and "tail" that move in the direction given by a vector from their tail to head. Thus, the "angle" of a particle in two dimensions is the angle that their orientation or velocity vector makes to the horizontal.

Early work in this field [93] focussed on the interplay between short-range repulsive interactions, mid-range aligning interactions, and long-range attractive interactions in polar particle systems to generate system trajectories that would qualitatively behave like real-life flocks of birds. While this combination of interactions produced system trajectories that behaved similarly to such flocks, the number of parameters required made it difficult to analyse conceptually. By reducing the set of possible interactions to alignment only, a clearer understanding of the physics underpinning this motion can be obtained.

1.2.1 The Vicsek model

In this thesis, we focus on a reduced set of models where only aligning interactions are included. The field of aligning SPPs is perhaps best exemplified by the Vicsek model [35, 116]. The Vicsek model presented below is a simplified version of how real-world agents such as birds or fish flock, acting as a prototype from which more complicated dynamics can be created.

In the two-dimensional Vicsek model, a fixed number N of polar particles move about in a space of size L^2 with periodic boundary conditions, each with a

constant speed v_0. Time is scaled such that the time Δt between updates of particles' position and velocity is 1. In a single time-step, the i-th particle's position $\mathbf{r}_i^t$ and velocity $\mathbf{v}_i^t$ are updated according to

$$\mathbf{r}_i^{t+1} = \mathbf{r}_i^t + \mathbf{v}_i^t, \tag{1.1}$$

$$\mathbf{v}_i^{t+1} = v_0 \cos\theta_i^{t+1}\hat{\mathbf{x}} + v_0 \sin\theta_i^{t+1}\hat{\mathbf{y}}, \tag{1.2}$$

$$\theta_i^{t+1} = \langle\theta\rangle_R^t + \eta_i^t, \tag{1.3}$$

where $\langle\theta\rangle_R^t$ is the average angle of all particles (including particle i) within a given radius R of particle i at time-step t, and η_i^t is a random number drawn from the uniform distribution $\left[\frac{-\eta_0}{2}, \frac{\eta_0}{2}\right]$. The average angle is typically computed as

$$\langle\theta\rangle_R^t = \arctan\left(\frac{\sum_{j=1}^N n_{ij}^t \sin\theta_j^t}{\sum_{j=1}^N n_{ij}^t \cos\theta_j^t}\right), \tag{1.4}$$

where n_{ij}^t is the neighbourhood matrix at time t whose entries are 1 if j is a neighbour of i and are zero otherwise. Note that, in general, this matrix is not constant in time, such that particles may no longer be neighbours if they move too far apart. Using the neighbourhood matrix is the most general way of writing Eq. (1.4), allowing for calculations and code to be generalised for other definitions of the neighbourhood.

For the Vicsek model, the neighbourhood matrix is defined as

$$n_{ij}^t = \Theta(R - |\mathbf{r}_i^t - \mathbf{r}_j^t|) \tag{1.5}$$

where the Heaviside function, $\Theta(x)$, restricts the interactions to the fixed radius R. As n_{ij} is symmetric for the Vicsek model, the interaction is reciprocal, i.e. if particle i is in j's neighbourhood at a given time t, then j must be in i's neighbourhood at time t.

The noise term η_i^t in Eq. (1.3) can be thought of as an error arising from the particle's inability to accurately determine the average of its neighbours [95]. For this reason, a noise term affecting the angle of the particle directly as in Eq. (1.3) is typically referred to as "intrinsic" noise. In contrast, "extrinsic" noise refers to an error arising from a particle's inability to accurately follow the direction it has determined to be the local average. Extrinsic noise can be implemented by

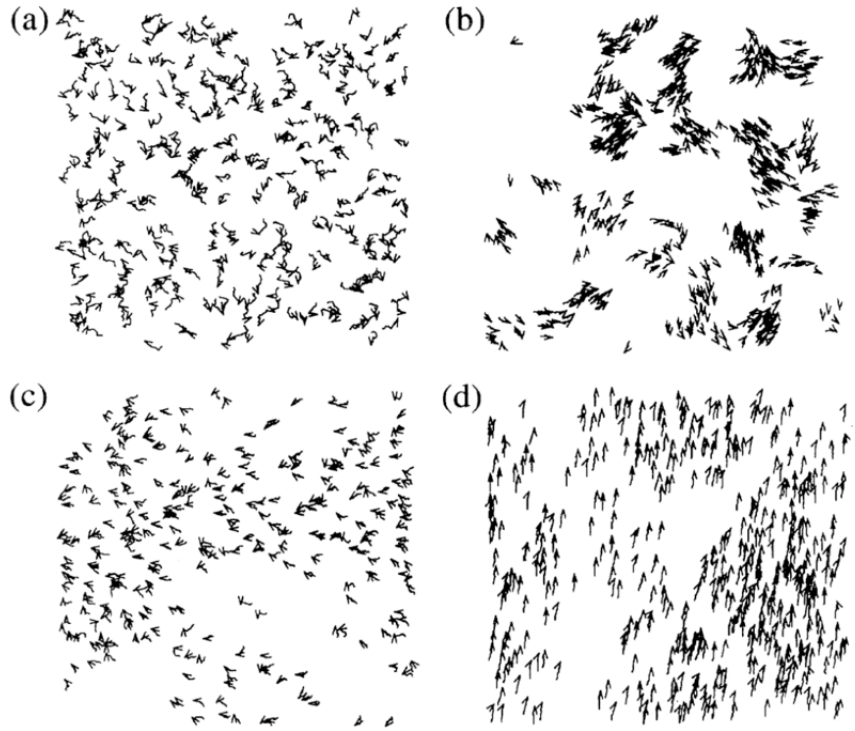

Figure 1.1 *The phases of the two-dimensional Vicsek model as the noise strength is varied. Each of these snapshots contains 300 particles. The arrowhead indicates the current direction of motion, with the short lines indicating the particle's trajectory over the preceding 20 time-steps. (a) High density and high noise ($L = 7, \eta_0 = 2.0$), early time. No coherent orientational order is observed. Particles move as is performing a random walk in continuous space. (b) Low density and low noise ($L = 25, \eta_0 = 0.1$). Distinct groups form that move in random directions. Motion within each group is coherent (c) Later time of (a). Small correlation is observed, though particles still move largely at random. (d) High density and low noise ($L = 5, \eta_0 = 0.1$) results in highly ordered motion. Image reproduced from [116] with permission.*

replacing (1.2, 1.3) with

$$\mathbf{v}_i^{t+1} = v_0 \frac{\sum_{j=1}^{N} n_{ij}^t (\mathbf{v}_j^t + \boldsymbol{\xi}_i^t)}{\left| \sum_{j=1}^{N} n_{ij}^t (\mathbf{v}_j^t + \boldsymbol{\xi}_i^t) \right|}, \tag{1.6}$$

where $\boldsymbol{\xi}_i^t$ is a random vector of fixed magnitude η_0 [87]. Intrinsic and extrinsic noise are often called "scalar" and "vectorial" noise respectively, due to their implementation. For sufficiently large system size, the choice of noise type causes no difference in the essential macroscopic properties of the system discussed below [53]. Alternative versions of the extrinsic noise equation (1.6) scale the stochastic vector $\boldsymbol{\xi}_i^t$ differently with the number of particles in the neighbourhood [87], but these alterations do not affect the macroscopic properties of the system either.

Behaviour of the Vicsek model

The behaviour of particles at a macroscopic level in a Vicsek model is determined by the magnitude of the intrinsic noise strength η_0. In the limit as $\eta_0 \to 2\pi$, no orientational order is observed in the system (Fig. 1.1a) and particles do not form a coherent flock. A flock is defined here as a coherent, ordered group of SPPs undergoing collective motion. When the average density $\bar{\rho} = \frac{N}{L^2}$ is sufficiently high and η_0 is sufficiently low (Fig. 1.1d), particles will spontaneously break rotational symmetry to align in a single direction. Once the rotational symmetry breaks and a flock forms, a change in direction is a rare event with a probability that is exponentially small in system size, unless external forces are added to cause the flock to turn.

The ability of a flock to form in the 2d Vicsek model is notable given its similarity to the 2d XY model, in which long-range order is forbidden. The Mermin-Wagner theorem [73] states that continuous symmetries (like the rotational symmetry of particle direction/spin) cannot be spontaneously broken at finite temperatures in one- or two-dimensional systems with short-range interactions. The key difference between the Vicsek and XY models is the motion of the particles in the Vicsek model, which allows the continuous symmetry to spontaneously break and enables long-range order to exist. The Vicsek model allows for a more efficient transfer of information than the XY model and hence long-range order can exist for dimensions $d > \frac{3}{2}$ [53, 107, 110].

The transition between the ordered and disordered states was initially assumed

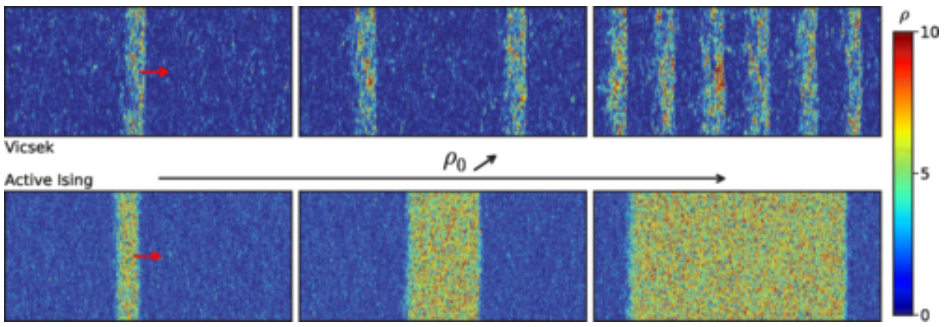

Figure 1.2 *Banding in a two-dimensional Vicsek model (top) and a two-dimensional active Ising model. The number of bands in the Vicsek model increases as the total density is increased and remains constant as they propagate through the system. Figure reproduced with permission from [104].*

to be continuous, i.e. second-order [116], akin to the ferromagnet-paramagnet phase transition [45]. Later works questioned whether this was the case [75], with Solon & Tailleur [19, 104, 106] proving that the transition is discontinuous and that systems phase separate into high-density, highly-ordered and low density, disordered regions, akin to a liquid-gas transition [2]. The highly ordered condensates are known as "bands", and the probability of a change in direction or size due to fluctuations within the band is exponentially small in the system size, though the number and size of the bands depends on the model choice and system size (see Fig. 1.2). Phase separation is observed in the Vicsek model regardless of whether intrinsic or extrinsic noise is used, provided the system size is sufficiently large [53].

The Vicsek model in higher dimensions

Equations (1.1, 1.2, 1.3) work well for systems with spatial dimension $d = 2$. For systems in higher dimensions, (1.2) must be tweaked. A common implementation [36] is to include stochasticity through a rotation matrix that takes the (normalised) local average velocity and rotates it through an angle of η about a randomly chosen axis perpendicular to the local average. Thus, the velocity of particles in a higher dimensional Vicsek model update as

$$\mathbf{v}_i^{t+1} = v_0 \mathcal{R}(\eta) \left(\frac{\sum_{j=1}^{N} n_{ij}^t \mathbf{v}_j^t}{\left| \sum_{j=1}^{N} n_{ij}^t \mathbf{v}_j^t \right|} \right) . \tag{1.7}$$

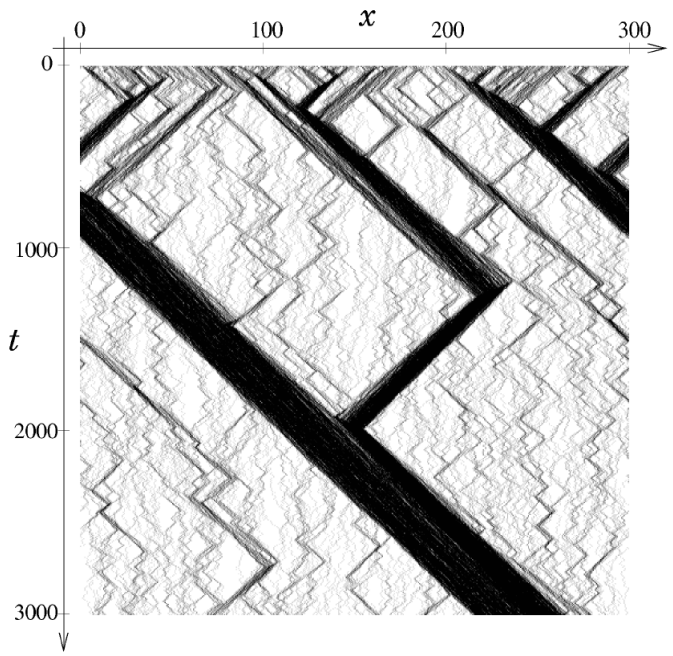

Figure 1.3 *The dynamics of a trajectory of the one-dimensional Vicsek SPP model with $L = 300$, $N = 600$ and $\eta_0 = 2.0$. The darker area represent regions of higher particle density, and time increases in the negative y direction. Particles undergo phase separation and clustering into condensates, with the condensate alternating direction stochastically. Note that η_0 here is much larger than for the ordered state of the two-dimensional SPP model [116]. Figure reproduced with permission from [35].*

An alternative approach [53] is to use extrinsic noise (1.6) again here. The equation for the implementation of extrinsic noise remains the same for two dimensions or greater, thus it can be useful for comparing results from Vicsek models across dimensions. As the results for Vicsek class models in two dimensions and greater are broadly similar, we will not consider systems with three spatial dimensions or greater any further in this work.

1.2.2 Agent-based flocking models in one dimension

While (1.7) works well for dimensions higher than two, a model of aligning SPPs in one dimension is more challenging due to the change from a continuous to a discrete rotational symmetry. Following the approach of Czirók *et al.* [35] wherein a particle's velocity no longer has a constant magnitude, the transition from a disordered to ordered state can be found in a continuous one-dimensional

space by using the following equations

$$r_i^{t+1} = r_i^t + \Delta t v_i^t, \tag{1.8}$$

$$v_i^{t+1} = v_0 \left[G\left(\left\langle v^t \right\rangle_i \right) + \eta_i^t \right], \tag{1.9}$$

where $\langle v^t \rangle_i$ is the average local velocity near particle i

$$\left\langle v^t \right\rangle_i = \frac{\sum_{j=1}^{N} n_{ij}^t v_j^t}{\sum_{j=1}^{N} n_{ij}^t}, \tag{1.10}$$

and $G(u)$ is an antisymmetric function incorporating the deterministic forces present in the system, defined as

$$G(u) = \begin{cases} \frac{u+1}{2}, & u > 0, \\ \frac{u-1}{2}, & u < 0. \end{cases} \tag{1.11}$$

For sufficiently high noise, the system is disordered, while in the absence of noise, the system tends towards a steady state where $|v_i| = 1$ and $P(r_i = x) = \frac{1}{L}$, although the direction of the steady state depends on the initial conditions of the system. Unlike in two dimensions, when the noise is small but non-zero, the system phase separates into high density, highly-ordered and low density disordered regions (see Fig. 1.3). Additionally, the direction of the highly-ordered regions (flocks) are not constant in time. Instead, they stochastically alternate direction [82, 119], which can be clearly observed in Fig. 1.3.

The existence of an alternating flock can be seen more clearly in the discretised model of O'Loan & Evans [82]. In this model, N particles lie on a lattice with L sites. Unlike the Vicsek model in one dimension (1.8, 1.9), particles in the discrete space model update their positions stochastically. Thus, while a particle will move a fixed distance with each move, they do not have a constant speed. Stochasticity is introduced in the form of a fixed "anti-alignment" probability, η, which is the probability that a particle will choose to move in the direction opposite to the local average. The behaviour of the discrete space model for different values of η can be seen in Fig. 1.4.

The size of the condensate's peak is extensive in system size [7], although the shape of the nose is independent of system size or time elapsed since the last reversal. Once formed, the condensate travels in a single direction for some time before reversing direction at semi-regular intervals, with the time between reversals $T \sim \mathcal{O}(\log L)$ [7, 82]. A reversal begins with particles in the

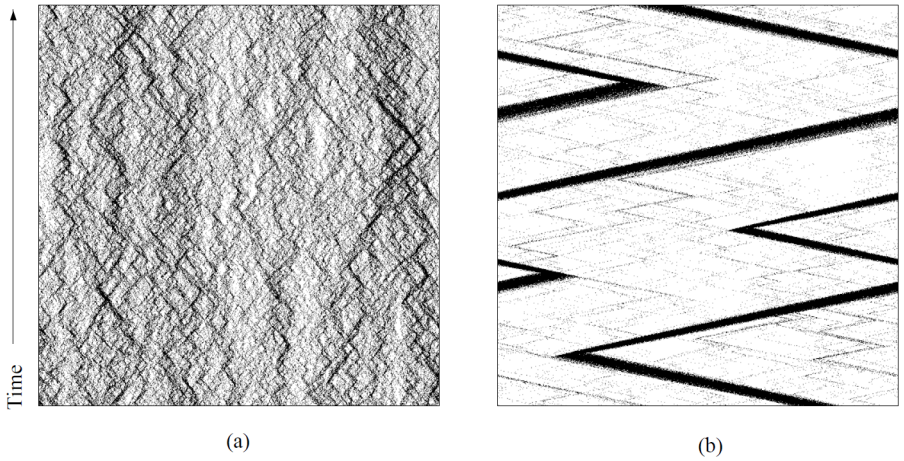

Figure 1.4 *The dynamics of a trajectory of a discrete space one-dimensional SPP model with $L = 1000$ and $N = 1000$. The darker area represent regions of higher particle density. (a) $\eta = 0.2$, time between snapshots $\Delta t = 1$. Particles change direction frequently and no ordered flock is observed. (b) $\eta = 0.02, \Delta t = 5$. Particles undergo phase separation and clustering into condensates, with the condensate alternating direction stochastically. Figure reproduced from [82].*

nose changing direction causing a wave akin to a shock to travel through the condensate, returning to its compact form once the shock has travelled through the condensate. Its width then increases with time, initially expanding diffusively in the co-moving frame, before becoming more diffuse at the front than at the rear [7].

While the discrete-space [82] and continuous space models (1.8, 1.9) [35] display similar asymptotic behaviour, they differ in their implementation. Stochasticity was introduced in the continuous model by removing the constraint that the particles' speed is fixed and adding fluctuations to the speed; the discrete model instead added an anti-alignment probability $\eta \in [0, 1]$. Additionally, the discrete model added some diffusion to the particle's motion by updating their positions stochastically instead of simultaneously. These details have little effect on the observed behaviour in the ordered state, and as such both models belong to the Vicsek-class of models.

O'Loan & Evans [82] showed that, if particles near the front (or "nose") of a flock change direction - either due to random perturbations or a collision with another flock - the remainder of the flock will also change direction. Thus, the question of how often the flock alternates can be reduced to the question of how

often perturbations form at the flock's nose. This highlights the important role of stochasticity in the existence of the phase-separated ordered alternating flock state in one dimension and suggests that successfully modelling a physical system requires an appropriate treatment of stochastic effects.

1.2.3 Reaction-diffusion models of aligning self-propelled particles

While the Vicsek model is a good basis for studying aligning SPPs, other choices exist. Some of these are expansions or modifications to the original Vicsek model, while others have a substantially different setup. Using multiple interaction types between particles diffusing through a system, each occurring at their own rate, reaction-diffusion equations seek to simulate SPPs as active versions of chemical reactions.

An example of the reaction-diffusion approach is the work of Dyson *et al.* [46] to model the motion of locusts in a ring-shaped arena, based on the experiments of Buhl *et al.* [15]. The model consist of N individuals, each of whom is facing clockwise or anti-clockwise. The size of the system is immaterial, as particles can interact with one another at any distance and the parameter of interest is the average velocity of the particles taken over the entire system.

In the model of [46], particles can interact with one another in six different ways. In the following, X_l denotes a left-facing (clockwise) particle, while X_r denotes a right-facing (anti-clockwise) particle.

$$X_l \xrightarrow{\hat{r}_1} X_r, \qquad X_r \xrightarrow{\hat{r}_1} X_l, \tag{1.12}$$

$$X_l + X_r \xrightarrow{\hat{r}_2} 2X_r, \qquad X_r + X_l \xrightarrow{\hat{r}_2} 2X_l, \tag{1.13}$$

$$X_l + 2X_r \xrightarrow{\hat{r}_3} 3X_r, \qquad X_r + 2X_l \xrightarrow{\hat{r}_3} 3X_l. \tag{1.14}$$

$\hat{r}_1$, $\hat{r}_2$ and $\hat{r}_3$ denote the rates for a one-, two- and three-body interaction occurring. The one-body interaction represents a stochastic switch in direction, akin to anti-alignment for particles on an otherwise empty site in the discrete-space one-dimensional model (1.8, 1.9). The two- and three-body interactions cause particle alignment, with three-body interactions being necessary for the drift and diffusion coefficients of the model system to match the experimental results.

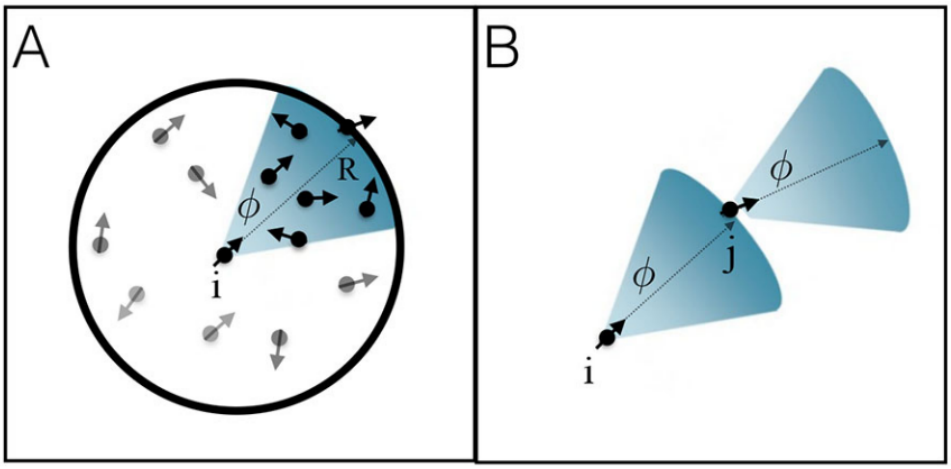

Figure 1.5 *(A) The neighbourhood of the i-th particle (shaded blue) in a limited field-of-view Vicsek model. Here, $n_{ij} = 1$ if the j-th particle lies within a sector of angle 2ϕ of a fixed radius circle centred on particle i. (B) An example of a non-reciprocal interaction. While $n_{ij} = 1$, $n_{ji} = 0$ due to the directional vision. Reproduced with permission from [44].*

The necessity of three-body interactions is expanded on by the work of Chatterjee & Goldenfeld [32]. Their work adds spatial diffusion to the model of Dyson *et al.* and demonstrates that, as $\hat{r}_3 \to 0$, the high density, highly-ordered flock (as in the one-dimensional continuous [35] and discrete [82] space models) is no longer present in the system.

1.2.4 Alternative neighbourhoods for a self-propelled particle model

A common modification of the original Vicsek model involves changing the criteria that particles must satisfy to be considered neighbours. Examples of such a modified neighbourhood are a sector of a fixed-radius circle (see Fig. 1.5) to better simulate a limited field of view, projection of the whole flock against the sky [86], or directional vision [44, 47], such as used in modelling pedestrian behaviour [85]; particles within a fixed radius whose direction differs from the central particle by no greater than a given amount [96]; or a scaling-invariant neighbourhood consisting of a fixed number of particles [20] or geometric Voronoi neighbours [54], motivated by the observation that the density of the flock does not determine whether order is observed in starling flocks [4] or pedestrian dynamics [77]. Models that use a scaling-invariant neighbourhood are typically referred to as

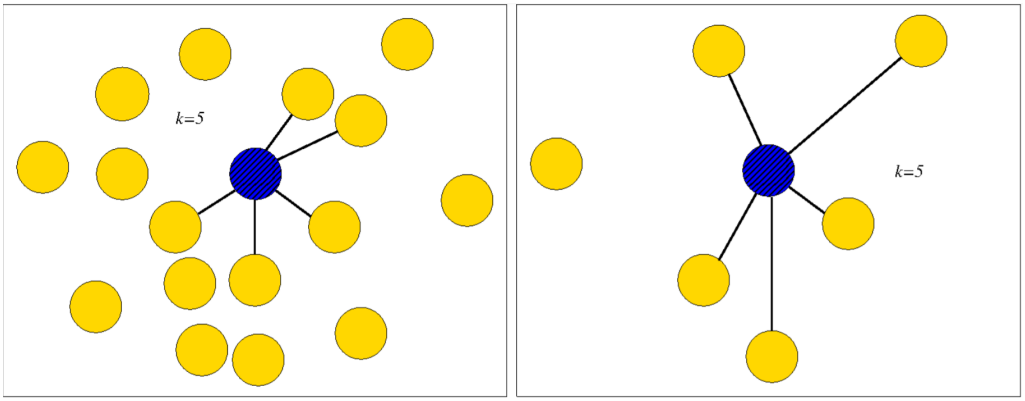

Figure 1.6 *An example of a non-metric neighbourhood where the $k = 5$ nearest particles are considered neighbours in a dense (a) and dilute (b) system. Reproduced from [55].*

"non-metric" or "topological" due to the focus on relative particle positions over a metric distance for determining neighbours (see Fig. 1.6).

Modifying the particle neighbourhood such that it no longer depends on the distance to neighbouring particles has a substantial effect on the dynamics of the ordered state of SPP systems. Ginelli & Chaté [54] demonstrated that by forcing particles to interact via a non-metric interaction as opposed to the usual metric interaction, bands in a two-dimensional system would no longer form. Instead, the phase transition from disordered to order is continuous, and no phase separation occurs [88]. Additionally, the flock stochastically changes its direction, something not observed in the metric Vicsek model in dimensions greater than one.

Much has been made of the ability of the flock to alternate directions in the topological Vicsek model. Solon *et al.* [104] showed that the high density, highly-ordered bands in the metric Vicsek model are stable to momentum fluctuations. In contrast, anti-symmetric [37] and more generally asymmetric [27] interactions in SPP models lead to an instability in the longitudinal diffusivity causing the ordered flock to turn. Cavagna *et al.* [27] suggested that asymmetric interactions and heterogeneity of the particle density may both be necessary for particle systems to exhibit a reorientation of the ordered flock in finite time, based on the propagation of the turning stimulus through the flock (see Fig. 1.7). In contrast, we demonstrate in Chapter 3 that non-symmetry is *not* a required feature for the presence of macroscopic turning in Vicsek-class models.

In the long wavelength limit, the Vicsek model is well described by the Toner-Tu equations [112], a phenomenological hydrodynamic approach to studying how

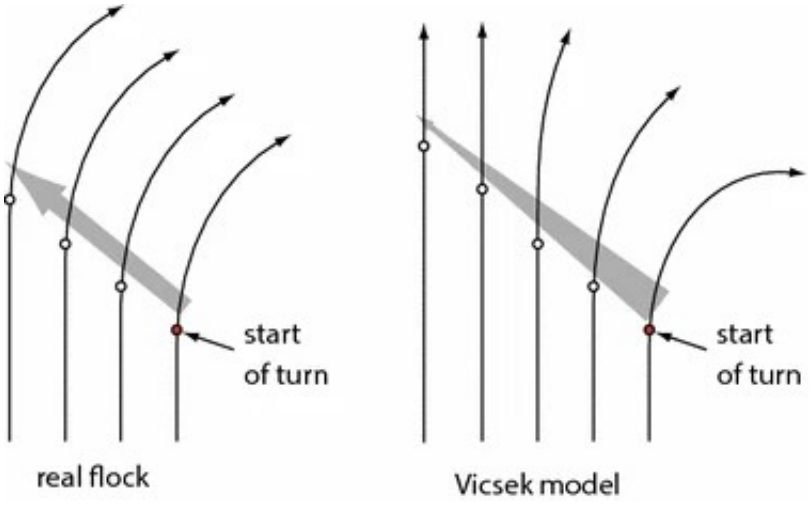

Figure 1.7 *Representation of the propagation of turning information in a real flock and a Vicsek model. (a) The turning information is undamped in a real flock, propagating throughout the system and causing a macroscopic turn. (b) In a Vicsek model, turning information is damped. Reproduced with permission from [23].*

the density and velocity of SPP systems evolve in time on a large scale. We now move on to discussing this approach and other continuum equation approaches to studying aligning active matter. The derivation of continuum equations for SPP systems will be the focus of much of this thesis, in particular Sections 2.2 and 4.1.

1.3 Active hydrodynamics

While simulations of agent-based models of SPPs can be used to determine how the system behaves with a specific set of particle interactions, they are unable to ascertain in advance whether the system will tend towards order or disorder or to explain how the order or disorder arises. It is more straightforward to comprehend how large-scale behaviours manifest in systems of aligning SPPs by focussing on coupled partial differential equations (PDEs) of macroscopic fields such as particle density or velocity. The equations governing particle dynamics are similar to the Navier-Stokes equations [108] for hydrodynamic systems due to similar terms existing in both, although the PDEs for aligning SPP systems are typically not momentum-conserving for "dry" systems (see Section 1.2) and may contain explicit stochastic effects not typically seen in hydrodynamic models.

1.3.1 Phenomenological equations

An early attempt to represent the dynamics of the Vicsek model as continuous fields came from the work of Toner & Tu [111, 112]. Their "top-down" approach [17] to generating field equations for the Vicsek model considered every relevant term in the equations not excluded by symmetries and conservation laws in the system. In this context, "relevant" means retaining only terms that are important at large length-scales; practically, higher order gradients are excluded. Under this approximation, the following equations for density and velocity fields ρ and $\mathbf{v}$ emerge, known as the Toner-Tu equations,

$$\partial_t \rho = \nabla \cdot (\rho \mathbf{v}), \tag{1.15}$$

$$\begin{aligned} \partial t \mathbf{v} + \lambda_1 (\mathbf{v} \cdot \nabla) \mathbf{v} + \lambda_2 (\nabla \cdot \mathbf{v}) \mathbf{v} + \lambda_3 \nabla |\mathbf{v}|^2 & \\ = \left(\alpha - \beta |\mathbf{v}^2|\right) \mathbf{v} - \nabla P(\rho) + D_B \nabla (\nabla \cdot \mathbf{v}) & \\ + D_T \nabla^2 \mathbf{v} + D_2 (\mathbf{v} \cdot \nabla)^2 \mathbf{v} + \mathbf{f}, & \end{aligned} \tag{1.16}$$

$$P(\rho) = \sum_{n=1}^{\infty} \sigma_n (\rho - \rho_0)^n, \tag{1.17}$$

where $P(\rho)$ is akin to the pressure term in a traditional hydrodynamic model, ρ_0 is the mean of the number density, σ_n are coefficients of the pressure expansion, β, D_B, D_T and D_2 are all positive, and $\alpha > 0$ gives an ordered state while $\alpha < 0$ leads to a disordered state. (1.15) is the usual equation of conservation of mass, as we have assumed that no particles are created or destroyed in the system and the time-scale is such that diffusion has a negligible effect on the dynamics.

The λ_1, λ_2 and λ_3 terms are the convective derivatives, with all three forms having non-zero prefactors due to the lack of Galilean invariance in the system. α and β give rise to the average velocity in the ordered state, where $\alpha > 0$ and $|\langle \mathbf{v} \rangle| = \sqrt{\frac{\alpha}{\beta}}$. The D_i's are diffusion constants, and $\mathbf{f}$ is a stochastic driving force, assumed to be Gaussian white noise with constant variance Δ (similar to ξ_i^t in (1.6)). At scales sufficiently large that (1.15, 1.16, 1.17) accurately describe the system, local fluctuations do not play a significant effect on the dynamics, and as such a simple additive noise suffices to ensure the system does not get trapped in an unstable fixed point of state space.

As reasoned above, (1.15, 1.16, 1.17) are useful equations for studying the large-scale properties of a Vicsek-class system, such as the long-range correlations of velocity (or orientation) fluctuations. These fluctuations were shown to be

"scale-free" [112] as a consequence of the spontaneous breaking of a continuous symmetry. This feature of model aligning SPP systems has also been observed experimentally [21]. However, it is not clear how the many macroscopic variables in the Toner-Tu equations relate to the microscopic variables in the agent-based Vicsek models such as particle speed, frequency of alignment, or particle interaction radius.

While it is possible to experimentally determine the value of the macroscopic variables for a particular agent-based model [113], a better comprehension of the way macroscopic variables depend on the microscopic parameters can be obtained through approaches that can generate PDEs from an agent-based system directly. In the next section, we introduce three key approaches to obtaining field equations in this "bottom-up" manner [17] and discuss the benefits and limitations of each approach.

1.3.2 Microscopic to Macroscopic

Boltzmann equation

An early attempt to identify the macroscopic variables with microscopic parameters utilised the Boltzmann equation [28], which describes the average forces acting on particles in a non-equilibrium stochastic system. The Boltzmann equation evolves the probability distribution of a single particle which can be changed through three processes: diffusion of the particle through the system, collision with other particles, and through the application of external forces. Given a one-particle probability distribution $f(\mathbf{r}, \theta, t)$ of particles with position vector $\mathbf{r}$ and angle of motion θ at time t, the evolution of this probability density obeys the following relation

$$\partial_t f + \mathbf{e}(\theta) \cdot \nabla f = I_{\text{diff}}[f] + I_{\text{coll}}[f] + I_{\text{ext}}[f], \tag{1.18}$$

where $\mathbf{e}(\theta)$ is the unit vector in the direction of θ, $I_{\text{diff}}[f]$ contains the forces due to self-diffusion, $I_{\text{coll}}[f]$ describes the effect of collisions with other particles, and $I_{\text{ext}}[f]$ describes the effect of any external forces.

Bertin *et al.* [9, 10] considered a dilute system of SPPs travelling through space with a fixed speed v_0, rotating diffusively, aligning through particle collisions and in the absence of external forces. The dilute nature of the system ensures

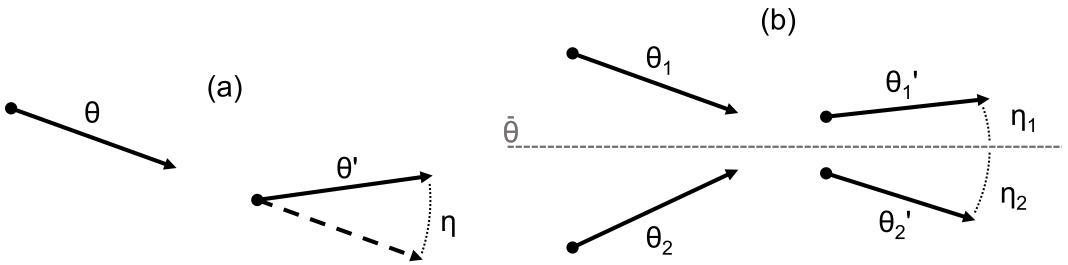

Figure 1.8 *(a) A typical rotational diffusive "kick", where a random angle η has been applied to a particle moving in a direction θ to give it a new velocity with angle θ'. (b) A typical collision between two particles with directions θ_1 and θ_2, where the average angle $\bar{\theta}$ (1.19) is given by the dashed line. After the collision, each particle assumes a new velocity that differs from $\bar{\theta}$ by a random noise η_1 and η_2 respectively.*

that collisions involving more than two particles were sufficiently rare as to be ignored, therefore the collision kernel $I_{\text{coll}}[f]$ could be simplified to consider binary collisions only.

Each particle moves ballistically until a "kick" occurs with rate λ, causing it to change orientation from angle θ to $\theta' = \theta + \eta$, where η is drawn from a Gaussian distribution $\mathcal{P}(\eta)$ with mean 0 and variance η_0^2. A collision occurs if two particles get within a distance d_0 of one another. When this occurs, both particles update their orientation from θ_1 and θ_2 to $\theta_1' = \bar{\theta} + \eta_1$ and $\theta_2' = \bar{\theta} + \eta_2$ (see Fig. 1.8b), where the η_i are also drawn from a Gaussian distribution $\mathcal{P}'(\eta)$ with mean zero and variance $\eta_0'^2$ (which need not be the same as η_0^2), and $\bar{\theta}$ is the average of θ_1 and θ_2, calculated as

$$\bar{\theta} = \text{Arg}\left[e^{i\theta_1} + e^{i\theta_2}\right]. \tag{1.19}$$

Under these conditions, I_{diff} and I_{coll} can be expressed as

$$I_{\text{diff}}[f] = -\lambda f + \lambda \int d\eta\ \mathcal{P}(\eta) \int d\theta'\ f(\mathbf{r}, \theta', t) \sum_n \delta\left(\theta - \theta' - \eta + 2n\pi\right), \tag{1.20}$$

$$\begin{aligned} I_{\text{coll}}[f] = &-2d_0 v_0 f(\mathbf{r}, \theta, t) \int d\theta'\ |\mathbf{e}(\theta) - \mathbf{e}(\theta')| f(\mathbf{r}, \theta', t) + 2d_0 v_0 \int d\eta\ \mathcal{P}'(\eta) \\ &\times \int d\theta_1 \int d\theta_2\ |\mathbf{e}(\theta_1) - \mathbf{e}(\theta_2)| f(\mathbf{r}, \theta_1, t) f(\mathbf{r}, \theta_2, t) \sum_n \delta\left(\theta - \bar{\theta} - \eta + 2n\pi\right). \end{aligned} \tag{1.21}$$

Note that while stochastic effects occur in the agent-based model, the Boltzmann equation is deterministic due to the stochasticity being integrated out. As the particle models are broadly similar and stochasticity does not feature prominently,

we expect the continuum equations should contain terms also found in the Toner-Tu equations (1.15, 1.16).

We can define density $\rho(\mathbf{r}, t)$ and velocity $\mathbf{u}(\mathbf{r}, t)$ fields by integrating the particle probability distribution f as

$$\rho(\mathbf{r}, t) = \int d\theta \; f(\mathbf{r}, \theta, t), \tag{1.22}$$

$$\mathbf{u}(\mathbf{r}, t) = \frac{1}{\rho(\mathbf{r}, t)} \int d\theta \; \mathbf{e}(\theta) f(\mathbf{r}, \theta, t). \tag{1.23}$$

It is more natural in this case to consider the evolution of the momentum field $\mathbf{w}(\mathbf{r}, t) = \rho(\mathbf{r}, t)\mathbf{u}(\mathbf{r}, t)$ instead of the velocity field $\mathbf{u}(\mathbf{r}, t)$. As such, subsequent equations will be written in terms of ρ and $\mathbf{w}$. As a result, any direct comparison with the Toner-Tu equations must first transform one set of equations to match the variables of the other.

Integrating (1.18) over θ directly gives the usual equation of mass conservation for compressible fluids

$$\partial_t \rho(\mathbf{r}, t) = -\nabla \cdot \mathbf{w}(\mathbf{r}, t). \tag{1.24}$$

Obtaining the evolution equation of $\mathbf{w}$ is more challenging. To simplify this, we introduce the Fourier transform of f,

$$\hat{f}_k(\mathbf{r}, t) = \int d\theta \; e^{ik\theta} f(\mathbf{r}, \theta, t). \tag{1.25}$$

Note that these Fourier components relate to the density and momentum fields as

$$\rho = \hat{f}_0 \qquad \text{and} \qquad \mathbf{w} = \begin{pmatrix} \Re[\hat{f}_1] \\ \Im[\hat{f}_1] \end{pmatrix}, \tag{1.26}$$

where $\Re[\hat{f}_1]$ and $\Im[\hat{f}_1]$ denote the real and imaginary components of $\hat{f}_1$ respectively. Thus, obtaining the equation of evolution of $\mathbf{w}$ is equivalent to finding the evolution of $\hat{f}_1$. By multiplying the Boltzmann equation (1.18) by $e^{ik\theta}$ and integrating over θ, an equation for $\hat{f}_k$ in terms of $\hat{f}_{k-1}$ and $\hat{f}_{k+1}$ can be obtained.

By the definition of the Fourier components $\hat{f}_k$ (1.25), $\hat{f}_k^* = \hat{f}_{-k}$. Thus, the system of equations can be solved if for some $k \geq 0$, $\partial_t \hat{f}_k$ does not depend on $\hat{f}_{k+1}$. Under the assumption that the average momentum is much smaller than the average density, $\hat{f}_2$ varies sufficiently slowly that $\partial_t \hat{f}_2 \approx 0$, and subsequent

terms $\hat{f}_k \approx 0$ for $k \geq 3$. This assumption thus truncates the infinite series of coupled equations, enabling an explicit solution for $\hat{f}_2$ to be found in terms of $\hat{f}_1$ and $\hat{f}_0$. Finally, the equations describing the system reduce to [10]

$$\partial_t \rho = -v_0 \nabla \cdot \mathbf{w}, \tag{1.27}$$

$$\begin{aligned}\partial_t \mathbf{w} + v_0 \gamma (\mathbf{w} \cdot \nabla)\mathbf{w} = &\left(\mu - \xi |\mathbf{w}|^2\right)\mathbf{w} - \frac{1}{2}\nabla\rho + \frac{\kappa}{2}\nabla\left(|\mathbf{w}|^2\right) - \kappa\left(\nabla\cdot\mathbf{w}\right)\mathbf{w} \\ &+ \nu\nabla^2\mathbf{w} + \nu'\nabla\rho\cdot\left(\nabla\mathbf{w} + \nabla\mathbf{w}^T\right) - \nu'\left(\nabla\cdot\mathbf{w}\right)\nabla\rho,\end{aligned} \tag{1.28}$$

where μ, ξ, κ, γ, ν and ν' depend on the microscopic parameters ρ, v_0, d_0, λ, η_0 and η_0' as

$$\mu = \frac{8 d_0 v_0 \rho}{\pi}\left(e^{-\frac{\eta_0^2}{2}} - \frac{2}{3}\right) - \lambda\left(1 - e^{-\frac{\eta_0'^2}{2}}\right), \tag{1.29}$$

$$\nu = \frac{v_0^2}{4}\left[\lambda\left(1 - e^{-\frac{\eta_0'^2}{2}}\right) + \frac{16 d_0 v_0 \rho}{3\pi}\left(\frac{7}{5} + e^{-\frac{\eta_0^2}{2}}\right)\right]^{-1}, \tag{1.30}$$

$$\nu' = \frac{\partial\nu}{\partial\rho} = \frac{64 d_0 \nu^2}{3 v_0}\left(\frac{7}{5} + e^{-\frac{\eta_0^2}{2}}\right), \tag{1.31}$$

$$\gamma = \frac{16\nu d_0}{\pi v_0}\left(\frac{16}{15} + 2e^{-2\eta_0^2} - e^{-\frac{\eta_0^2}{2}}\right), \tag{1.32}$$

$$\kappa = \frac{16\nu d_0}{\pi v_0}\left(\frac{4}{15} + 2e^{-2\eta_0^2} + e^{-\frac{\eta_0^2}{2}}\right), \tag{1.33}$$

$$\xi = \frac{256\nu d_0^2}{\pi^2 v_0^2}\left(e^{-\frac{\eta_0^2}{2}} - \frac{2}{5}\right)\left(\frac{1}{3} + e^{-2\eta_0^2}\right). \tag{1.34}$$

The first equation above (1.27) is the usual Navier-Stokes equation of mass conservation, as in the Toner-Tu equations (1.15). The second equation (1.28) is also similar to the Toner-Tu equation for velocity (1.16). Indeed, there is a one-to-one correspondence between some of the prefactors, mostly notably α and β from (1.16) are equivalent to μ and ξ from (1.28) respectively. Other variables are related, though are not directly one-to-one due to the change from velocity to momentum.

A similar set of equations was derived by Peshkov *et al.* [88] for a set of particles interacting through a topological interaction (see Sec. 1.2.4). The key change to the model is to the collision integral I_{coll} (1.21), though Peshkov *et al.* kept the assumption that binary collisions dominate. This is implemented through an aligning collision occurring with a rate α_0 per topological neighbour. The

resultant continuum equations are

$$\partial_t \rho = -\nabla \cdot \mathbf{w}, \tag{1.35}$$

$$\partial_t \mathbf{w} + \gamma_t(\mathbf{w}\cdot\nabla)\mathbf{w} = \left(\mu_t - \xi_t|\mathbf{w}|^2\right)\mathbf{w} - \frac{1}{2}\nabla\rho + \frac{\kappa_t}{2}\nabla\left(|\mathbf{w}|^2\right) + \nu_t\nabla^2\mathbf{w} - \kappa_t\left(\nabla\cdot\mathbf{w}\right)\mathbf{w}, \tag{1.36}$$

where $v_0 = \lambda = 1$ here. The equations above (1.35, 1.36) are functionally identical to the equations for the metric case (1.27, 1.28), although the dependence of the coefficients on density differs (and some higher order terms were dropped) and are instead represented by

$$\mu_t = \left(\frac{4\alpha}{\pi} + 1\right) e^{-\frac{\sigma^2}{2}} - (1+\alpha), \tag{1.37}$$

$$\nu_t = \frac{1}{4}\left[\alpha + 1 + e^{-2\sigma^2}\right]^{-1}, \tag{1.38}$$

$$\gamma_t = \frac{4\nu_t\alpha}{\rho}\left[e^{-2\sigma^2} - \frac{2}{3\pi}e^{-\frac{\sigma^2}{2}}\right], \tag{1.39}$$

$$\kappa_t = \frac{4\nu_t\alpha}{\rho}\left[e^{-2\sigma^2} + \frac{2}{3\pi}e^{-\frac{\sigma^2}{2}}\right], \tag{1.40}$$

$$\xi_t = \frac{16\nu_t\alpha^2}{3\pi\rho^2}e^{-\frac{5\sigma^2}{2}}, \tag{1.41}$$

where $\alpha = n\alpha_0$ is the average rate of binary collisions per particle and n is the average number of neighbours. When the density field varies slowly, the functional form of continuum equations describing SPP systems are not highly sensitive to whether particle interactions are metric or topological. As the magnitude of variables (1.29-1.34, 1.37-1.41) controls the behaviour of the continuum equations, their form is more important to predicting the behaviour we expect to see in trajectories of the system. We explore the similarities and differences between topological and metric continuous equations further in Chapter 4, based on agent-based models developed in Chapter 3.

The Boltzmann equation is clearly a powerful tool in obtaining the dependence of macroscopic variables on microscopic parameters. Due to the lack of stochasticity, however, the resulting equations are not suitable for generating trajectories that behave in a similar fashion to the agent-based models. As such, they fail to adequately predict or explain the existence of behaviours that rely on external or stochastic effects to occur, such as the macroscopic turning of the flock. We now turn to methods of deriving continuous hydrodynamic equations that include

stochastic effects explicitly.

Stochastic differential equations

The Toner-Tu (1.15, 1.16) and Boltzmann (1.27, 1.28) equations describe the mean dynamics of systems of SPPs at a large scale, with scaling exponents of the agent-based models well reproduced by these equations. For systems below the length scale where hydrodynamic considerations dominate, finite size effects and realisations of the noise play a significant role in the dynamics of the system [53]. An example of these finite size effects is that the bands described in Section 1.2.1 can't be observed in a 2d Vicsek system if the system size is too small. At these mesoscopic length scales, adding stochasticity to a system without regard for the structure of that term can alter fundamental properties such as the behaviour of the ordered state near the phase transition [72]. As such, a more complete understanding of the stochastic effects in a finite-sized system may require a more nuanced approach to stochasticity in continuum equations.

Starting from a set of Langevin equations describing N particles i interacting through a pairwise potential $V(x)$ and subject to a stochastic force $\boldsymbol{\eta}_i(t)$,

$$\frac{d\mathbf{X}_i}{dt} = -\sum_{j=1}^{N} \nabla V(\mathbf{X}_i(t) - \mathbf{X}_j(t)) + \boldsymbol{\eta}_i(t), \tag{1.42}$$

where $\boldsymbol{\eta}_i(t)$ is a Gaussian white noise with mean zero and variance η_0^2, Dean [38] derived a stochastic differential equation for the density ρ of particles. To begin, consider the single particle density $\rho_i(\mathbf{x}, t)$ defined by

$$\rho_i(\mathbf{x}, t) = \delta(\mathbf{X}_i(t) - \mathbf{x}), \tag{1.43}$$

and the total particle density $\rho(\mathbf{x}, t)$

$$\rho(\mathbf{x}, t) = \sum_{i=1}^{N} \rho_i(\mathbf{x}, t) = \sum_{i=1}^{N} \delta(\mathbf{X}_i(t) - \mathbf{x}). \tag{1.44}$$

For an arbitrary function $f(\mathbf{x})$ defined over the system, the properties of the Dirac delta function gives

$$f(\mathbf{X}_i(t)) = \int d\mathbf{x}\ \rho_i(\mathbf{x}, t) f(\mathbf{x}). \tag{1.45}$$

Taking the time derivative of (1.45), the integral becomes

$$\frac{df(\mathbf{X}_i(t))}{dt} = \int d\mathbf{x}\ \frac{\partial \rho_i(\mathbf{x},t)}{\partial t} f(\mathbf{x}). \tag{1.46}$$

However, the left hand side of (1.46) can also be expanded using Itô calculus [89], (1.42) and integration by parts to arrive at

$$\begin{aligned}\frac{df(\mathbf{X}_i(t))}{dt} = \int d\mathbf{x}\ f(\mathbf{x}) \Bigg[&-\nabla\rho_i(\mathbf{x},t)\cdot\boldsymbol{\eta}_i(t) + \frac{\eta_0^2}{2}\nabla^2\rho_i(\mathbf{x},t) \\ &+\nabla\rho_i(\mathbf{x},t)\cdot\sum_{j=1}^{N}\nabla V(\mathbf{X}_i(t)-\mathbf{X}_j(t))\Bigg].\end{aligned} \tag{1.47}$$

As f is an arbitrary function, the evolution of the single particle density ρ_i in time becomes

$$\partial_t\rho_i = -\nabla\rho_i\cdot\boldsymbol{\eta}_i(t) + \nabla\rho_i\cdot\sum_{j=1}^{N}\nabla V(\mathbf{X}_i(t)-\mathbf{X}_j(t)) + \frac{\eta_0^2}{2}\nabla^2\rho_i. \tag{1.48}$$

Finally, summing over all particles and by replacing the noise term with one that is statistically identical, a stochastic differential equation for the density is obtained as

$$\begin{aligned}\partial_t\rho(\mathbf{x},t) =&\nabla\cdot\left(\rho(\mathbf{x},t)\int d\mathbf{y}\ \rho(\mathbf{y},t)\nabla V(\mathbf{x}-\mathbf{y})\right) + \frac{\eta_0^2}{2}\nabla^2\rho(\mathbf{x},t) \\ &+\nabla\cdot\left(\sqrt{\rho(\mathbf{x},t)}\ \boldsymbol{\eta}(t)\right).\end{aligned} \tag{1.49}$$

The above equation (1.49) can be read as a modified continuity equation with diffusion and explicit stochasticity added. The entire right hand side can be written as the divergence of a vector, thus enforcing mass conservation. Crucially, the stochastic term is also expressed as the divergence of a Wiener process with a multiplicative density term. The divergence preserves mass conservation, while the multiplicative prefactor ensures that spontaneous particle creation cannot occur.

While (1.49) is an early example of deriving stochastic differential equations for SPP systems, its usefulness can be limited by the equations of motion of the particles in the system of interest. For example, if we wish to obtain continuum equations for the Vicsek model with intrinsic noise (1.1, 1.2), the particle velocity cannot be displayed in the Langevin form $\frac{dV_i}{dt} = f(X_i,V_i,t) + g(X_i,V_i,t)\eta(t)$ as

the stochasticity is present in the angular equation. Therefore, the Itô calculus used to obtain (1.47) cannot be used for the velocity or momentum field equation.

Another method of obtaining coupled PDEs is the Kramers-Moyal expansion [66, 78, 115]. While it requires more approximation than the approach above resulting in Eq. (1.49), the Kramers-Moyal expansion is a powerful tool for creating coupled PDEs to describe many systems, and we will use it in much of the main body of this thesis for that purpose.

The Kramers-Moyal expansion

While Dean's approach [38] started from a set of Langevin equations for particle positions, the Kramers-Moyal expansion typically begins with a master equation for the probability of a position in space-time having a given density and momentum. In a continuous space system, however, the master equation has an infinite number of states between which the system can travel. For this reason, it is often easier to use the Kramers-Moyal expansion in systems that sit on a spatial lattice (such as the one-dimensional O'Loan & Evans model [82] from Section 1.2). For sufficiently large systems, we do not expect discretisation will have a significant effect on the macroscopic behaviour.

Consider a master equation where the state of the system can be expressed in terms of state variables $\psi_1, ..., \psi_n$ and time t. These state variables could be the density and momentum values at each site in a lattice, for example. A state in this system is represented by a specific set of values $\{\psi_1, ..., \psi_n\}$ the state variables can take, and will be denoted by σ. The probability of the system being in a given state σ at time t evolves as follows

$$\frac{\partial P(\sigma, t)}{\partial t} = \sum_{\sigma'} T(\sigma' \to \sigma) P(\sigma', t) - T(\sigma \to \sigma') P(\sigma, t) \tag{1.50}$$

where $T(\sigma' \to \sigma)$ is the transition rate from the state σ' to a state σ.

The Kramers-Moyal expansion is a power series expansion in powers of $\nu = \sigma - \sigma'$. To this end, $T(\sigma' \to \sigma)$ is rewritten as $T(\sigma - \nu, \nu)$. The expansion can be written in the form [94, 115]

$$\partial_t P = \sum_{k=1}^{\infty} \frac{(-1)^k}{k!} \sum_{i_1,...,i_k=1}^{n} \left(\frac{\partial^k}{\partial \psi_{i_1} ... \partial \psi_{i_k}} \right) \left[a_{i_1,...,i_k}(\sigma) P(\sigma, t) \right] \tag{1.51}$$

where $a_{i_1,...,i_k}(\sigma)$ is the "k-th jump moment" of the process and is defined as

$$a_{i_1,...,i_k}(\sigma) = \sum_{\nu} v_{i_1}...v_{i_k} T(\sigma, \nu) \tag{1.52}$$

where $\nu = \{v_1, ..., v_n\}$. The expansion can often be truncated after the first or second term [84], i.e. $a_{i_1,...,i_k}(\sigma) \equiv 0$ for $k \geq 3$. Thus, the Kramers-Moyal expansion (1.51) becomes a Fokker-Planck equation

$$\frac{\partial P(\sigma, t)}{\partial t} = -\sum_{i=1}^{n} \frac{\partial}{\partial \psi_i} \left[a_i(\sigma) P(\sigma, t)\right] + \frac{1}{2} \sum_{i,j=1}^{n} \frac{\partial^2}{\partial \psi_i \partial \psi_j} \left[a_{i,j}(\sigma) P(\sigma, t)\right]. \tag{1.53}$$

If it cannot be truncated exactly, infinitely many terms are non-zero [94]. In this case, another approach must be considered to arrive at the Fokker-Planck equation above. This usually takes the form of a system size expansion [114], whereby the jump moments $a_{i_1,...,i_k}(\sigma)$ scale inversely with some large parameter N, usually proportional to N^{-k} [14]. In the large N limit and under an appropriate rescaling of time, $a_{i_1,...,i_k}(\sigma) \equiv 0$ for $k \geq 3$ as above. Thus, the Fokker-Planck equation is recovered.

The Fokker-Planck equation 1.53 can be transformed into a set of coupled Langevin equations in the Itô sense [8] to describe the evolution of a particular trajectory of the system,

$$\frac{d\psi_i}{dt} = -a_i(\sigma) + \sum_{j=1}^{n} b_{i,j}(\sigma) \xi_j(t), \tag{1.54}$$

where $b_{i,k}(\sigma)$ is a matrix satisfying the property $\sum_{k=1}^{n} b_{i,k} b_{j,k} = a_{i,j}$ and $\xi_j(t)$ is a delta-correlated random variable drawn from a Gaussian distribution with mean 0 and variance 1. In general, for a given $a_{i,j}$, the matrix $b_{i,k}$ is not unique, as a different representation can be created as $b'_{i,j} = \sum_{k=1}^{n} b_{i,k} c_{k,j}$ where $c_{i,j}$ is any orthogonal matrix. The usual choice for creating $b_{i,j}$ is to use Cholesky decomposition [67] which creates an upper triangular matrix.

The Langevin equations are useful as they allow us to simulate trajectories of the system that the original master equation (1.50) represents. In practice, this involves numerical integration, which is the process of evolving the field variables at discrete points in space and time, usually by discretising the spatial and temporal derivatives. A specific choice of discretising these derivatives is known as a "discretisation scheme". Numerical integration often comes with its

own challenges, such as finding a stable discretisation scheme; namely, one in which errors do not grow exponentially large as time increases.

An additional benefit to starting with a particle system based on a discrete spatial lattice is that the simple "forward time, centred space" (FTCS) difference schemes are stable. Under the FTCS scheme, the field variables $f(\mathbf{x}, t)$ are replaced by a discrete field $f^n_{i_1,...,i_d} = f(i_1\Delta x_1, ..., i_d\Delta x_d, n\Delta t)$ and derivatives are treated as

$$\partial_t f^n_{i_1,...,i_d} \longrightarrow \frac{f^{n+1}_{i_1,...,i_d} - f^n_{i_1,...,i_d}}{\Delta t}, \tag{1.55}$$

$$\nabla \cdot \mathbf{f}^n_{i_1,...,i_d} \longrightarrow \sum_{j=1}^{d} \frac{\mathbf{f}^{n+1}_{i_1,...,i_j+1,...,i_d} - \mathbf{f}^n_{i_1,...,i_j-1,...,i_d}}{2\Delta x} \cdot \mathbf{e}_j, \tag{1.56}$$

$$\nabla^2 f^n_{i_1,...,i_d} \longrightarrow \sum_{j=1}^{d} \frac{f^{n+1}_{i_1,...,i_j+1,...,i_d} - 2f^{n+1}_{i_1,...,i_j,...,i_d} + f^n_{i_1,...,i_j-1,...,i_d}}{\Delta x^2}, \tag{1.57}$$

where $\mathbf{e}_j$ are the unit vectors in the j-th direction. In Sections 2.3.2 and 4.4, we describe a numerical integration process to generate trajectories based on specific Langevin equations.

1.4 The structure of this thesis

In the remainder of this thesis, we examine coupled stochastic differential equations to identify the features required for an ordered flock to alternate direction stochastically. We generate these equations using the Kramers-Moyal approach detailed above, using numerical integration to demonstrate that the equations are a good representation of the agent-based system.

In Chapter 2, we introduce a one-dimensional system with SPPs on a lattice, interacting with one another through an alignment interaction. The model introduced is a simplified version of the O'Loan & Evans model described earlier in this chapter 1.2.2. We use the Kramers-Moyal expansion to generate a set of coupled stochastic differential equations for particle density and momentum and explain the assumptions used to justify truncating the expansion at second order and subsequently transforming the Fokker-Planck equation into a set of Langevin equations. Using numerical integration, we demonstrate the resulting equations exhibit the same behaviours as the particle system. We examine the requirements on the equations for trajectories to exhibit turning, and use those requirements to

obtain a minimal model for turning in one-dimensional aligning particle models.

Chapter 3 focuses on examining aligning active matter on a two-dimensional lattice. We expand our one-dimensional model from the previous chapter into two dimensions and examine the conditions under which stochastic macroscopic turning is present in the system. Contrasting our extended model with another lattice-based model, we explore model choices which do and do not affect the existence of macroscopic turning. We find that systems where particles align according to a topological rather than metric neighbourhood rule are not the only systems in which macroscopic turning can manifest. The existence of a metric model in which macroscopic turning can be observed provides an avenue for analytical comparison with more traditional flocking models.

We return to stochastic field equations in Chapter 4, where we use the Kramers-Moyal approximation to derive field equation representations of the models in Chapter 3. The differences between the equations generated for the two model choices highlight a potential reason for the discrepancy observed in the previous chapter. As the macroscopic turning of the ordered flock occurs as the growth of an instability, we conduct linear stability analysis on the two models. We demonstrate that the behaviour of the models due to the interaction neighbourhood differs greatly, with one model having no dependence on interaction type, while the other demonstrates different linear stability depending on the choice. We then conduct numerical analysis on the equations to compare trajectories of the system with the agent-based models from the previous chapter.

Finally, in Chapter 5, we gather and discuss the key findings of the previous chapters and suggest further routes of exploration in this field, along with detailing exploratory work to expand this approach to off-lattice models.

Chapter 2

Stochastic field equations for one-dimensional flocking

In Chapter 1, we saw how a Vicsek-class model of self-propelled particles (SPP) in one dimension (hereafter 1d) [35] can exhibit an aligning ordered collective motion (see Fig. 1.3). Unlike its traditional counterpart in higher dimensions [112, 116] where rotational symmetry is broken in the ordered state, the ordered flock in 1d has the capacity to alternate directions, a behaviour also observed in schools of fish [62]. This manifests as a macroscopic change in the direction of the flock (see Fig. 2.1). Additionally, the order is not present on all lattice sites for a finite number of particles; instead a condensate forms in the system, which phase separates into a high-density, highly ordered travelling flock and a low density, disordered region.

The main aim of this chapter is to obtain a continuum equation description of a model that exhibits this alternating flocking behaviour in 1d. Previous work with this aim by Raymond & Evans [92] used a mean-field approach to generate a set of deterministic partial differential equations for density and polarisation fields, in addition to adding in attraction and repulsion interactions as in other flocking models with non-local interactions [47, 50, 93]. While the equations generated through the mean-field approximation reproduced the position of the phase transition between the ordered and disordered states, the ordered state obtained in the trajectories of the mean-field model differed from the alternating flock observed in the agent-based model (hereafter ABM) by the absence of turning. The ability of the flock to turn was hypothesised to be the result of

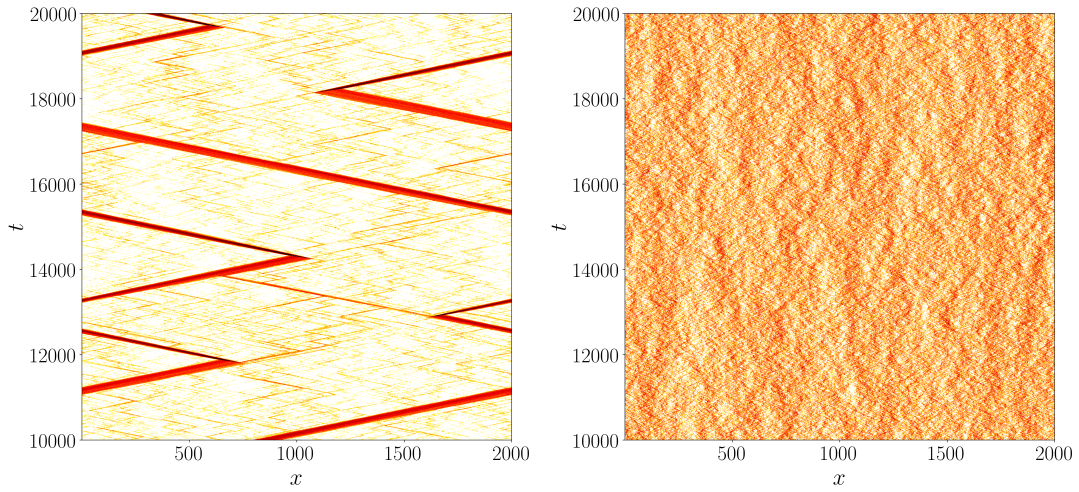

Figure 2.1 *Sample trajectories of the agent-based model at different values of the noise strength η. Points with darker colours have more particles on that site, with black denoting the most dense regions. Left: $\eta = 0.02$. Here, a condensed group (red) is moving through the lattice before stochastically alternating direction. Other than the large flock, the lattice is sparsely populated with a small number of travelling particles (yellow). Right: $\eta = 0.2$. The stochastic effects dominate here and no condensate forms. Particle density is approximately uniform and no coherent motion is observed. For both trajectories, $N = L = 2000$ and $\beta = 2.0$. For these plots, $\Delta x = 1$ and $\Delta t = 5$.*

stochastic fluctuations in the front, or "nose", of the flock, thus the mean-field approximation is unable to reproduce the alternating behaviour. We demonstrate conclusively later in this chapter that artificially inducing a fluctuation in the nose of a mean-field flock is sufficient to return the alternating flock behaviour.

We will start by describing a lattice-based model of aligning SPPs as a basis to compare our continuum equations to. Although the O'Loan & Evans model [82] is suitable for clearly demonstrating the alternating flock in an ABM, there are a number of choices in the model definition that do not translate easily to a continuum description. In Section 2.1, we define a model based on the one in [82], with modifications that facilitate an analytical understanding of the behaviour exhibited. In this way, the model contains only local terms and has an analytical form for the alignment that can be understood in terms of an average of sampling the majority direction.

In Section 2.2, we utilise the Kramers-Moyal approximation to generate a set of field equations for density and momentum. As described in Section 1.3.2, the Kramers-Moyal approximation is a method of generating stochastic differential equations (SDEs) from ABMs governed by a master equation. Given certain

assumptions, realisations of these SDEs can reproduce the behaviour of the ABM. We detail what assumptions are necessary to generate a set of Langevin equations that will exhibit the alternating flock observed in the ABM as described in Section 2.1. These assumptions include a particular choice of the stochastic variable in the system to avoid the issue of complicated correlations.

As with any numerical integration, the specifics of the discretisation can play a role in the behaviour of the system. Additionally, correctly approximating the Wiener process is crucial to achieve quantitative matching between the ABM and the continuum equations. We discuss in Section 2.3 the merits of different approaches to discretising the SDEs generated by the Kramers-Moyal approximation, including using non-Gaussian noise to eliminate a bias towards higher order due to non-zero time-steps. Sampling from a beta distribution with mean and variance equivalent to the Gaussian distribution in question gives quantitative agreement with the ABM, strong evidence that substituting a Gaussian distribution with beta-type noise can generate physically accurate equations.

Once we have a set of continuum equations that match the behaviour of the ABM, we reduce the complexity of the system to obtain minimal requirements for flocking to occur. We show in Section 2.5 that a linear interaction term is insufficient to allow a single ordered flock to emerge from a disordered system. A modified model that includes non-interacting motion in the form of run-and-tumble behaviour [109] is used to explain the lack of flocking with a linear interaction. Using a third-order local interaction instead is then shown to be sufficient for the alternating flock behaviour to be exhibited. This supports evidence that three-body interactions are required for flocking in 1d [32, 61].

Finally, in Section 2.6, we explore some variations on the ABM and observe the effect they have on the behaviour exhibited by the system. These variations focus primarily on different choices for particle neighbourhoods corresponding to alternative physical interactions such as sight-based interactions. We also examine the effect of a particle including itself in its definition of neighbours, highlighting the large effect this can have on the existence of an ordered flocking phase.

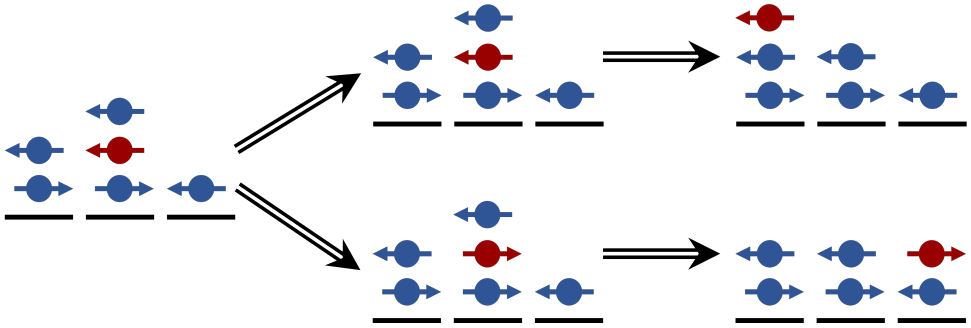

Figure 2.2 *Graphical representation of the update rules for a single time-step. Once a particle has been selected (red above), a new direction is chosen with probabilities given by (2.1), represented by the diverging paths. Once the particle has a new velocity, it travels one space in that direction, then the process repeats.*

2.1 Agent-based model

2.1.1 Model definition

The system described by O'Loan & Evans [82] consists of N polar particles (as defined in Section 1.2) on a one-dimensional (1d) periodic lattice of length L, where the sites have no maximum capacity. Each particle α has a position $x_\alpha \in \{1, ..., L\}$ and a velocity $v_\alpha \in \{-1, 1\}$. The agent-based description of the system is updated for a single time step δt according to the following rules.

1. A single particle α is chosen uniformly at random.
2. It obtains a new velocity $v_\alpha = \pm 1$ with probability $W_\alpha^\pm$ (defined below).
3. It moves a single site in the direction of its new velocity.
4. Repeat steps 1-3 with a new particle for a designated number of time steps.

With these rules, each particle will have moved on average one space on the lattice in N time steps. The probability of hopping right (+) or left(-) is given by

$$W_\alpha^\pm = \frac{1}{2}\left(1 \pm v(p_\alpha)\right), \tag{2.1}$$

where p_α is the polarisation of the site x_α and is defined as

$$p_\alpha = \frac{\sum_{\beta=1}^{N} v_\beta \delta(x_\alpha - x_\beta)}{\sum_{\beta=1}^{N} \delta(x_\alpha - x_\beta)}. \tag{2.2}$$

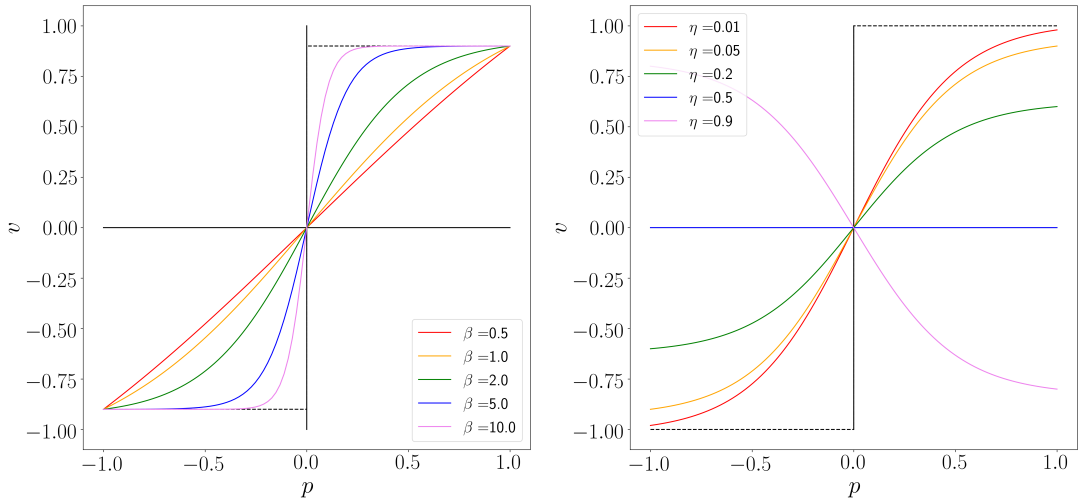

Figure 2.3 *Plot of the mean site velocity v as a function of the site polarisation p for (left) varying strengths of non-linear interactions β and (right) varying strengths of stochasticity η. Note that the $\beta \to \infty$ limit approaches a step function of height $2 - 4\eta$.*

From 2.2, we see that the polarisation must lie between -1 and 1. The mean velocity function, $v(p)$, is chosen here as

$$v(p) = (1 - 2\eta)\frac{\tanh(\beta p)}{\tanh(\beta)}, \tag{2.3}$$

where β represents the ability of the particles to identify the majority direction and η is the probability of a particle to anti-align with its neighbours. These can be thought of as the strength of the non-linear interactions and the strength of the stochasticity respectively. The effect of β and η on the structure of v can be seen in Fig. 2.3. The constraint on probability such that $W^{\pm} \geq 0$ and $W^{+} + W^{-} = 1$ forces $v \in [-1, 1]$ and hence $\eta \in [0, 1]$.

2.1.2 ABM behaviour

The main control parameter of this model is η, as there exists a non-zero critical value η_c such that the behaviour of the system switches from order to disorder as η increases across this threshold value (see Fig. 2.4). In the $\eta \to 0$ limit, all particles assume the same direction (depending on initial conditions) and a phase-separated condensate forms that diffuses until a uniform density over the lattice is reached (directional order). Hereafter, this condensate will be called a "flock", as it matches the definition in Chapter 1. For η larger than η_c, the system exists in a state of disorder as the particles change direction too often for the flock

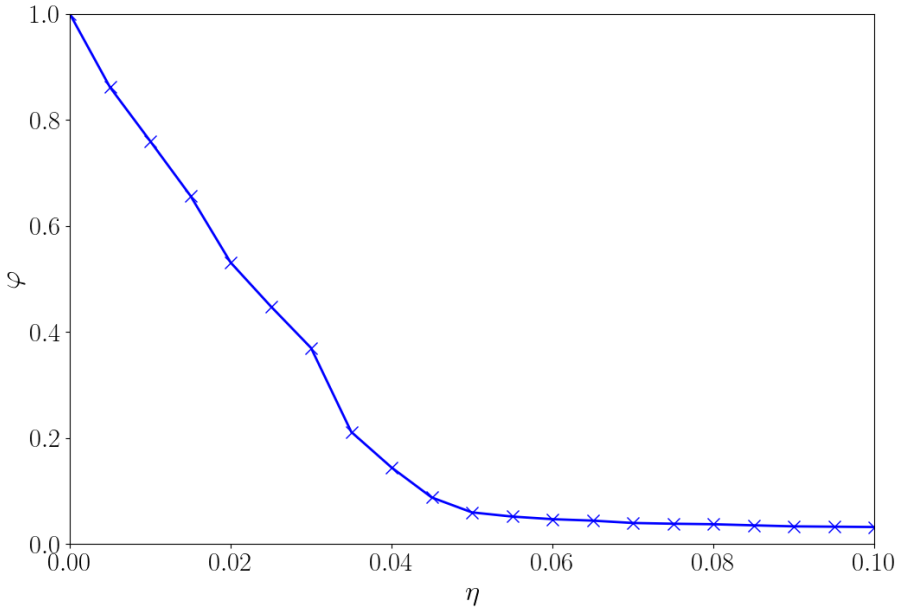

Figure 2.4 *Plot of a measure of order in the system as a function of the stochasticity η. Below the phase transition $\eta = \eta_c \approx 0.05$, the system exhibits order, while above the critical noise strength, no global order is observed.*

to be stable. Between these two extremes, there exists an ordered state with bi-directional order, where a flock propagates through the lattice, occasionally alternating its direction of propagation.

Order in this system at a given time is characterised by a non-zero value of the unsigned mean particle velocity, defined as

$$\bar{v}(t) = \left| \frac{1}{N} \sum_{\alpha=1}^{N} v_\alpha(t) \right|, \tag{2.4}$$

while the order parameter of the system for a given set of parameters is the average of this quantity, i.e.

$$\varphi = \langle \bar{v} \rangle \,. \tag{2.5}$$

As the particle interaction has no explicit time dependence, we expect that the average in (2.5) is identical whether it is taken over many realisations of the noise or over a sufficiently long time for a single trajectory. This property is known as ergodicity [115].

2.1.3 Differences from O'Loan model

The ABM above differs from the O'Loan & Evans model in two respects, both in the definition of $v(p)$ (2.3). The first is the reduction of the neighbourhood of each particle. While the original model evaluated the total magnetisation across the sites $i-1$, i and $i+1$, we have reduced our model to consider contributions at site i only. By comparing Fig. 2.1 to Fig. 1.4, we observe that the interaction in Eq. (2.3) does not change the qualitative behaviours in the ordered or disordered states, though it may affect the position of the phase transition.

The other change is the softening of the hard "majority-rules" update used by Raymond & Evans [92], which is the change to (2.3) from

$$v_{\mathrm{O'Loan}}(p) = (1-2\eta)\mathrm{sgn}(p) \tag{2.6}$$

where sgn is the "signum" function defined as

$$\mathrm{sgn}(x) = \begin{cases} 1 & \text{if } x > 0, \\ -1 & \text{if } x < 0. \end{cases} \tag{2.7}$$

The motivation behind the above change is to introduce a tuning parameter β acting as another source of noise, akin to a thermodynamic $\beta = (k_B T)^{-1}$. Raymond & Evans demonstrated a relationship between β and the maximum number of neighbours M sampled in the majority-rule interaction [92], showing that this source of noise acts in a similar way to an incomplete sample of the particles in the neighbourhood.

The above connection assists us in interpreting the small and large β limits. The $\beta \to 0$ limit is a linear interaction

$$v_{\beta\to 0}(p) = (1-2\eta)p, \tag{2.8}$$

akin to a simple voter-type interaction [41], where a single particle from the neighbourhood is chosen at random to be the preferred direction. In the other extreme, $\beta \to \infty$, the strict "majority-rule" is taken over the entire neighbourhood and $v \to v_{\mathrm{O'Loan}}$.

2.2 Kramers-Moyal approximation

We wish to gain a better understanding of the macroscopic behaviour of the agent-based system described in Section 2.1, in particular how stochasticity affects the steady states. To this end, it is useful to switch to a continuous model as in Section 1.3. As the dynamics of the ABM can be written in a master equation form, we use the Kramers-Moyal approximation to generate a coupled set of Langevin equations describing the dynamics of the system.

2.2.1 Arriving at a set of Langevin equations

We follow here the van Kampen system size expansion approach as in [115] and outlined in Section 1.3.2. In the O'Loan & Evans model, we can take the ψ_i as the set of density ρ_i and magnetisation m_i values at each site on the lattice (with $n = 2L$) which are defined as

$$\rho_i(t) = \frac{1}{N}\sum_{\alpha=1}^{N}\delta(x_i - x_\alpha(t)) \tag{2.9}$$

$$m_i(t) = \frac{1}{N}\sum_{\alpha=1}^{N} v_\alpha\delta(x_i - x_\alpha(t)). \tag{2.10}$$

This choice represents a natural set of variables to describe the behaviours of the system and aligns with those often studied in other field models of flocking. The polarisation field that was the study of early forays in the field [35, 112] is thus

$$p_i(t) = \frac{m_i(t)}{\rho_i(t)}. \tag{2.11}$$

Computationally simulating a trajectory of a system requires evolution equations for the variables of interest, so we would like to obtain a set of Langevin equations to describe this system. Following the approach laid out in Section 1.3.2, these have the following form in the Itô sense,

$$\frac{d\psi_i}{dt} = \frac{\langle\delta\psi_i\rangle}{\delta t} + \sum_{j=1}^{n} b_{ij}\xi_j(t), \tag{2.12}$$

where $\xi_j(t)$ is a Gaussian white noise with mean $\langle\xi_j(t)\rangle = 0$ and correlator

$\langle \xi_j(t)\xi_k(t')\rangle = \delta_{jk}\delta(t-t')$, and b_{ij} is a matrix that satisfies the relation

$$\left(bb^T\right)_{ij} = \sum_{k=1}^{n} b_{ik}b_{jk} = \frac{\langle \delta\psi_i \delta\psi_j\rangle}{\delta t}. \tag{2.13}$$

If the set of ψ_i are uncorrelated (i.e. $\langle \delta\psi_i\delta\psi_j\rangle = \delta_{ij}\langle \delta\psi_i^2\rangle$), b has a diagonal matrix representation and (2.12) can be expressed as

$$\frac{d\psi_i}{dt} = \frac{\langle \delta\psi_i\rangle}{\delta t} + \sqrt{\frac{\langle \delta\psi_i^2\rangle}{\delta t}}\xi_i(t). \tag{2.14}$$

2.2.2 The density equation

Now we have a structure for the Langevin equations of the evolution of ρ and w, we must find the jump moments for these variables. We start with the density ρ. In a single time-step δt where one particle undergoes a move as described in Section 2.1, the density at a site i can change in the following ways

$$\delta\rho_i(t) = \rho_i(t+\delta t) - \rho_i(t) = \begin{cases} \frac{1}{N} & \text{with probability } W_{i-1}^{+}\rho_{i-1} + W_{i+1}^{-}\rho_{i+1} \\ -\frac{1}{N} & \text{with probability } \rho_i \\ 0 & \text{otherwise} \end{cases} \tag{2.15}$$

Here, $W_i^{\pm}$ is the transition probability of a particle at site i moving one step in the $\pm$ x-direction. The jump moments are calculated by taking the mean and variance of (2.15) as

$$\langle \delta\rho_i\rangle = \frac{1}{2N}\left[\rho_{i+1} + \rho_{i-1} - 2\rho_i - v(p_{i+1})\rho_{i+1} + v(p_{i-1})\rho_{i-1}\right], \tag{2.16}$$

$$\left\langle \delta\rho_i^2\right\rangle = \frac{1}{2N^2}\left[\rho_{i+1} + \rho_{i-1} + 2\rho_i - v(p_{i+1})\rho_{i+1} + v(p_{i-1})\rho_{i-1}\right]. \tag{2.17}$$

The next step in the derivation is to take the $L\to\infty$ limit, keeping $\frac{N}{L}$ constant, by making the replacements $\rho_i \to \rho(x)$ and $p_i \to p(x)$, with $x = ia$ and Taylor expanding $\rho(x\pm a)$ to second order in a. Finally, space can be rescaled so that $a = 1$. Under the transformation to continuous space, (2.16, 2.17) become

$$\langle \delta\rho\rangle = \frac{1}{N}\left[-\frac{\partial\left(v(p)\rho\right)}{\partial x} + \frac{1}{2}\frac{\partial^2\rho}{\partial x^2}\right], \tag{2.18}$$

$$\left\langle \delta\rho^2\right\rangle = \frac{1}{N^2}\left[2\rho - \frac{\partial\left(v(p)\rho\right)}{\partial x} + \frac{1}{2}\frac{\partial^2\rho}{\partial x^2}\right]. \tag{2.19}$$

We next set the time-scale of the system so that $\delta t = \frac{1}{N}$ [14]. This results in a Langevin equation for the density evolution

$$\frac{\partial \rho}{\partial t} = -\frac{\partial \left(\rho v(p)\right)}{\partial x} + \frac{1}{2}\frac{\partial^2 \rho}{\partial x^2} + \sqrt{\frac{2}{N}}\sqrt{\rho - \frac{1}{2}\frac{\partial \left(\rho v(p)\right)}{\partial x} + \frac{1}{4}\frac{\partial^2 \rho}{\partial x^2}}\ \xi_\rho(x,t) \tag{2.20}$$

where $\xi_\rho(x,t)$ is delta-correlated in time and space.

The number of particles in the system is fixed, therefore we should expect (2.20) to have a conservation form, i.e.

$$\frac{\partial \rho}{\partial t} = -\frac{\partial F(\rho, p, x, t)}{\partial x} \tag{2.21}$$

for some function F. While the first two deterministic terms in (2.20) exhibit this behaviour, it is not seen in the stochastic term. The lack of a conservative form for the stochastic term is a consequence of the assumption that the densities on neighbouring sites are uncorrelated. One potential fix is to assume that the white noise function ξ_ρ does not have a delta-correlation in space. Introducing a non-delta-correlated noise function adds significant complexities to our equation, and finding a useful matrix solution to (2.13) is more difficult.

Another approach, and the one we take here, is to assume that the noise does not have a strong effect on the density through Eq. (2.20). In the $N \to \infty$ limit, the ratio $\frac{a^{(2)}_{\rho\rho}}{a^{(1)}_{\rho}} \sim N^{-1} \to 0$. Therefore, the second jump moment of density is negligible in the Fokker-Planck equation in the thermodynamic limit, and we ignore it in the Langevin equation also. Although the typical size for many flocks has $N = O(100)$, this will be sufficient for the stochastic term in (2.20) to be negligible compared to the deterministic term.

When the assumption that the stochastic term is negligible is included, we arrive at the following equation for the evolution of density in the system

$$\frac{\partial \rho}{\partial t} = -\frac{\partial \left(\rho v(p)\right)}{\partial x} + \frac{1}{2}\frac{\partial^2 \rho}{\partial x^2}. \tag{2.22}$$

Therefore, the density of our system evolves in time according to an advective term with variable velocity plus a diffusive term with constant diffusion. In order for a dense flock to form in the ordered state, the advection must overcome the constant diffusion of particles in some way. In the paper this model is based on, O'Loan and Evans [82] note this diffusive behaviour and that the flock is more compact after a change in direction, theorising that the changes in orientation

are responsible for maintaining the structural integrity of the flock.

2.2.3 The magnetisation equation

The derivation of the Langevin equation for the magnetisation is more challenging than for density. While we can assume here that the correlations between magnetisation on neighbouring sites is also negligible, the assumption that the magnetisation and density at the same site i are uncorrelated is highly unlikely to be justifiable as both depend on the number of particles on a site. Thus we are unable to use magnetisation as one of the variables in the Kramers-Moyal expansion as in Section 2.2.1.

Instead, we will use the polarisation, defined as in (2.11). The polarisation is a measure of the number of particles facing right vs left on a site, and has no direct dependence on the total number of particles on that site in the large N limit. We therefore assume, that the correlation between density and polarisation at a site is negligible.

As the polarisation is defined in terms of the density and magnetisation, these quantities can be used to obtain the jump moments of polarisation for this system. To begin with, we obtain the first two jump moments for the magnetisation. In a single time-step δt, the magnetisation updates as

$$\delta m_i(t) = m_i(t+\delta t) - m_i(t) \approx \begin{cases} \frac{1}{N} & \text{with probability } W^+_{i-1}\rho_{i-1} + \rho^-_i \\ -\frac{1}{N} & \text{with probability } W^-_{i+1}\rho_{i+1} + \rho^+_i \\ 0 & \text{otherwise} \end{cases} \tag{2.23}$$

where $W^\pm_i$ are defined as in (2.1) and ρ^+_i and ρ^-_i represent the densities of right- and left-facing particles respectively. These latter quantities relate to ρ_i and m_i as

$$\rho^\pm_i = \frac{\rho_i \pm m_i}{2}. \tag{2.24}$$

Following the same procedure as in Section 2.2.2, the first and second jump moments of magnetisation are

$$\langle \delta m_i \rangle = \frac{1}{2N}\left[\rho_{i-1} - \rho_{i+1} + v(p_{i+1})\rho_{i+1} + v(p_{i-1})\rho_{i-1} - 2m_i\right], \tag{2.25}$$

$$\left\langle \delta m_i^2 \right\rangle = \frac{1}{2N^2}\left[\rho_{i-1} + \rho_{i+1} - v(p_{i+1})\rho_{i+1} + v(p_{i-1})\rho_{i-1} + 2\rho_i\right], \tag{2.26}$$

which, in the continuous limit and keeping terms up to second order, become

$$\langle \delta m \rangle = \frac{1}{N}\left[\rho v(p) - m - \frac{\partial \rho}{\partial x} + \frac{1}{2}\frac{\partial^2 \left(\rho v(p)\right)}{\partial x^2}\right], \tag{2.27}$$

$$\left\langle \delta m^2 \right\rangle = \frac{2}{N^2}\left[\rho - \frac{1}{2}\frac{\partial \left(\rho v(p)\right)}{\partial x} + \frac{1}{4}\frac{\partial^2 \rho}{\partial x^2}\right] = \left\langle \delta \rho^2 \right\rangle. \tag{2.28}$$

Next, we examine how the jump moments of p change with m. The change in p in a single time-step is

$$\delta p = p(t+\delta t) - p(t) = \frac{m(t+\delta t)}{\rho(t+\delta t)} - \frac{m(t)}{\rho(t)} = \frac{m(t)+\delta m}{\rho(t)+\delta \rho} - \frac{m(t)}{\rho(t)}. \tag{2.29}$$

Assuming that δm and $\delta \rho$ are small compared to m and ρ respectively (true in the large N expansion), the first fraction can be expanded in powers of δm and $\delta \rho$ to get

$$\delta p = \frac{m}{\rho}\left[\frac{\delta m}{m} - \frac{\delta \rho}{\rho} + O\left(\left(\frac{\delta m}{m}\right)^2, \frac{\delta m \delta \rho}{m\rho}, \left(\frac{\delta \rho}{\rho}\right)^2\right)\right] \tag{2.30}$$

Dropping powers of $\frac{\delta m}{m}$ and $\frac{\delta \rho}{\rho}$ greater than one, the first two jump moments of p become (using the transformations $\delta m = \rho \delta p + p \delta \rho$ and $\langle \delta p \delta \rho \rangle = \langle \delta p \rangle \langle \delta \rho \rangle$ as we have assumed that p and ρ are uncorrelated)

$$\begin{aligned} \langle \delta p \rangle &= \frac{\langle \delta m \rangle - p \langle \delta \rho \rangle}{\rho} \\ &= \frac{1}{N}\left[v(p) - p - \frac{1}{\rho}\frac{\partial \rho}{\partial x} + \frac{1}{2\rho}\frac{\partial^2 (\rho v(p))}{\partial x^2} - \frac{p}{\rho}\left(-\frac{\partial \left(v(p)\rho\right)}{\partial x} + \frac{1}{2}\frac{\partial^2 \rho}{\partial x^2}\right)\right], \end{aligned} \tag{2.31}$$

$$\begin{aligned} \left\langle \delta p^2 \right\rangle &= \frac{\left\langle \delta m^2 \right\rangle - p \langle \delta m \delta \rho \rangle + p^2 \left\langle \delta \rho^2 \right\rangle}{\rho^2} \\ &= \frac{\left\langle \delta \rho^2 \right\rangle (1+p^2) - p\left(\rho \langle \delta p \delta \rho \rangle + p \left\langle \delta \rho^2 \right\rangle\right)}{\rho^2} \\ &= \left(1-p^2\right)\frac{\left\langle \delta \rho^2 \right\rangle}{\rho^2} - \frac{p}{\rho}\langle \delta p \rangle \langle \delta \rho \rangle \\ &= \frac{2}{N^2 \rho}\left(1-p^2\right) + O\left(\partial_x \rho, \partial_x p\right). \end{aligned} \tag{2.32}$$

In regions of the system where the prefactor in (2.32) is sufficiently large to contribute to $\frac{\partial p}{\partial t}$, the derivative terms are negligible compared to the density at

those sites. Thus, these terms do not contribute significantly to the dynamics of the system, and we choose to suppress them in the following equations.

The jump moments of p give a Langevin equation for the behaviour of p

$$\frac{\partial p}{\partial t} = v(p) - p - \frac{1}{\rho}\frac{\partial \rho}{\partial x} + \frac{1}{2\rho}\frac{\partial^2(\rho v(p))}{\partial x^2} - \frac{p}{\rho}\frac{\partial \rho}{\partial t} + \sqrt{\frac{2}{N\rho}}\sqrt{1-p^2}\,\xi_p(x,t). \quad (2.33)$$

Using Itô's lemma [89], we can transform this into an equation for the magnetisation as

$$\frac{\partial m}{\partial t} = \rho v(p) - m - \frac{\partial \rho}{\partial x} + \frac{1}{2}\frac{\partial^2(\rho v(p))}{\partial x^2} + \sqrt{\frac{2}{N\rho}}\sqrt{\rho^2 - m^2}\,\xi(x,t) \quad (2.34)$$

where $\xi(x,t) = \xi_p(x,t)$, but we have dropped the subscript in the noise function.

2.2.4 Choice of stochastic variable

One key assumption made in Section 2.2.3 is that the correlation between ρ and p on a single site is negligible. If instead, the correlation between ρ and m was negligible, what effect would this have? Following the same procedure for above using m as one of the stochastic variables, we get the following equation for the evolution of magnetisation,

$$\frac{\partial m}{\partial t} = \rho v - m - \frac{\partial \rho}{\partial x} + \frac{1}{2}\frac{\partial^2(v\rho)}{\partial x^2} + \sqrt{\frac{2\rho}{N}}\,\xi(x,t), \quad (2.35)$$

while the density evolution (2.22) remains the same, due to a lack of a stochastic term. Notice that although the deterministic term is identical to (2.34), the stochastic prefactor is missing a multiplicative term, $\sqrt{1-p^2}$. If there are any differences in behaviour between simulations of the two sets of equations, it will be due to this factor. A similar factor is seen in some voter models [1, 40, 41, 98] and reaction-diffusion processes [6].

To determine which of these is a more accurate description of the dynamics of the system, we must consider what happens in the ABM in a single time-step. We start by considering a single site i that has n particles on it with directions v_α for $\alpha \in \{1, ..., n\}$. Next, we choose a particle β at random to move from this site to a neighbouring site. If $v_\alpha = 1$ for all particles on site i, v_β must have the value 1 and the change in the magnetisation does not depend on which particle

is chosen, i.e. the change in the state of the system at that site is deterministic. The same argument can be made if $v_\alpha = -1$ for all particles on site i. This would indicate that, for sites where $|m_i| = \rho_i$, any change in m_i (and hence p_i) should be deterministic only.

Looking again at (2.34, 2.35), only the former is purely deterministic under this condition, while the latter has the same stochastic strength regardless of the magnitude of m. This would suggest that (2.35) does not accurately represent the dynamics of the system while (2.34) displays behaviour consistent with the ABM. This alone is not enough evidence to show that (2.22, 2.34) accurately translate the ABM to a set of continuum equations, something we can accomplish by direct numerical integration of these equations instead.

2.3 Numerical integration

To investigate the behaviour of the system described by the stochastic field equations (2.22) and (2.34), we numerically integrate them. In the deterministic terms, we follow the standard approach of replacing space and time derivatives with finite differences: throughout this work we use $\delta x = 1$ and $\delta t = 0.01$ (hence $N = 100$). The standard (Euler-Maruyama) method for handling the stochastic term, wherein one replaces the combination $\xi(x,t)\sqrt{\delta t}$ with a Gaussian random variable with zero mean and variance δt is not well adapted to the problem at hand. The issue with the Euler-Maruyama approach is that as $p \to \pm 1$, unphysical values of the polarization (i.e., $|p| > 1$) can be obtained with a sufficiently large random number.

2.3.1 Truncating the noise term

One method to prevent unphysical values of polarisation arising, used by Dickman [39] to numerically integrate trajectories of directed percolation equations, involves truncating the Gaussian noise term such that $|\xi(x,t)|$ never exceeds a given value ξ_{max}. This method also requires that the density and polarisation are discretised to integer numbers of ρ_{min} and p_{min} respectively. The value of p_{min} must satisfy $p_{min} = \frac{1}{n}$ for some integer n, while the value of ρ_{min} must be such

that the maximum stochastic jump can never cause $|p| > 1$. Calculating this, we arrive at a value of $\rho_{min} \geq \frac{2\xi^2_{max}(2-p_{min})\delta t}{Np_{min}}$.

The Dickman method often results in many time-steps that don't lead to a change in p that is an integer multiple of p_{min}. To overcome this, two new variables are introduced, ψ_ρ and ψ_p. Rather than integrating the discretised ρ and p directly, the Dickman approach involves integrating ψ_ρ and ψ_p and storing the integer multiples of ρ_{min} and p_{min} of these variables as ρ and p. While we expect this method to work for our system of equations (2.22, 2.34), we instead use a more efficient but less general method of removing the possibility of unphysical values of polarisation p

We first notice that the noise term is of the voter type i.e. $\propto \sqrt{1-p^2}$ [40, 41, 98] (also characteristic of the Wright-Fisher model [5, 34]), causing the noise to vanish at the boundary points $p = \pm 1$. A crucial feature of the dynamics is that p must be constrained to the interval $-1 \leq p \leq 1$ by the definition of p. Allowing p to have magnitude greater than 1 is both unphysical and is incompatible with the numerical scheme, as m at the following time-step would evaluate to a complex value.

In the following, we compare results using two strategies to remove the ability for unphysical values to appear. The first, and more straightforward strategy, is to truncate p to the physical range whenever it has greater magnitude than physically allowable. This approach is dangerous, as it may tend towards higher polarisation than seen in the ABM. The more sophisticated strategy, inspired by the approach of Michaud [74], is to replace the Gaussian random variable in the numerical integration scheme with a variable drawn from a distribution that is defined only over the physical range, and has the required mean and variance.

More precisely, this second approach involves integrating the stochastic and deterministic parts of the equation separately using Hamiltonian operator-splitting on the Fokker-Planck equation equivalent to (2.34) [42, 76]. If the Fokker-Planck equation is written in the following form

$$\partial_t P(w,t) = \mathcal{H} P(w,t) \Longrightarrow P(w,t) = e^{\mathcal{H}(t-t_0)} P(w,t_0), \tag{2.36}$$

where $\mathcal{H} = \mathcal{H}_{\text{det}} + \mathcal{H}_{\text{stoc}}$ is a Hamiltonian operator defined as the sum of a deterministic Hamiltonian and a stochastic Hamiltonian, then $\mathcal{H}$ can be split

across two exponential functions as

$$P(w,t) = e^{\mathcal{H}_{\rm det}(t-t_0)} e^{\mathcal{H}_{\rm stoc}(t-t_0)} P(w,t_0), \tag{2.37}$$

with corrections of order $[\mathcal{H}_{\rm det}, \mathcal{H}_{\rm stoc}](t-t_0)^2$ where $[A,B]$ is the commutator of the operators A and B (this is a consequence of the Baker–Campbell–Hausdorff formula [57]). This is equivalent to performing the operations sequentially, i.e. each time-step $\delta t = t - t_0$ is separated into two processes; the probability distribution is updated to consider only the stochastic contribution to the evolution of ρ and m, then the deterministic change in these variables is calculated based on the intermediate values obtained from the stochastic step, $\rho_{\rm int}$ and $m_{\rm int}$. In practice, $\rho_{\rm int} = \rho(t_0)$ as the stochastic contribution in (2.22) has been dropped.

The method above involves sampling an intermediate value of p, $p_{\rm int}$, from the probability distribution obtained by solving

$$\partial_t P(p,t) = \mathcal{H}_{\rm stoc} P = \frac{1}{N\rho} \partial_{pp} \left[(1-p^2) P \right]. \tag{2.38}$$

By transforming to another variable $y = \frac{1}{2}(1+p)$, (2.38) is shown to be equivalent to a Wright-Fisher equation [65] that has a known solution, an infinite series of hypergeometric functions,

$$\begin{aligned} P(y,t|y_0,t_0) &= y_0(1-y_0) \sum_{i=1}^{\infty} i(i+1)(2i+1) F(1-i, i+2, 2, y_0) \\ &\quad \times F(1-i, i+2, 2, y) e^{-\frac{i(i+1)}{N}(t-t_0)}. \end{aligned} \tag{2.39}$$

Unlike other forms of noise with a known distribution such as directed percolation [42], the beta distribution cannot be written in a form that allows it to be easily sampled. However, it can be shown (see Appendix B) that, given an initial condition y_0, the mean and variance of this distribution after a time δt are given by $\mu = y_0$ and

$$\sigma^2 = y_0(1-y_0) \left(1 - \exp\left[-\frac{2}{N\rho} \delta t \right] \right). \tag{2.40}$$

An appropriate distribution to sample y from is the Beta distribution, $P_{\alpha,\beta}(y) \propto y^{\alpha}(1-y)^{\beta}$ for $y \in [0,1]$ (see Fig. 2.5), with the parameters α and β taking the values

$$\alpha = \mu \left(\frac{\mu(1-\mu)}{\sigma^2} - 1 \right) = \frac{y_0}{\exp\left[\frac{2}{N\rho} \delta t \right] - 1}, \tag{2.41}$$

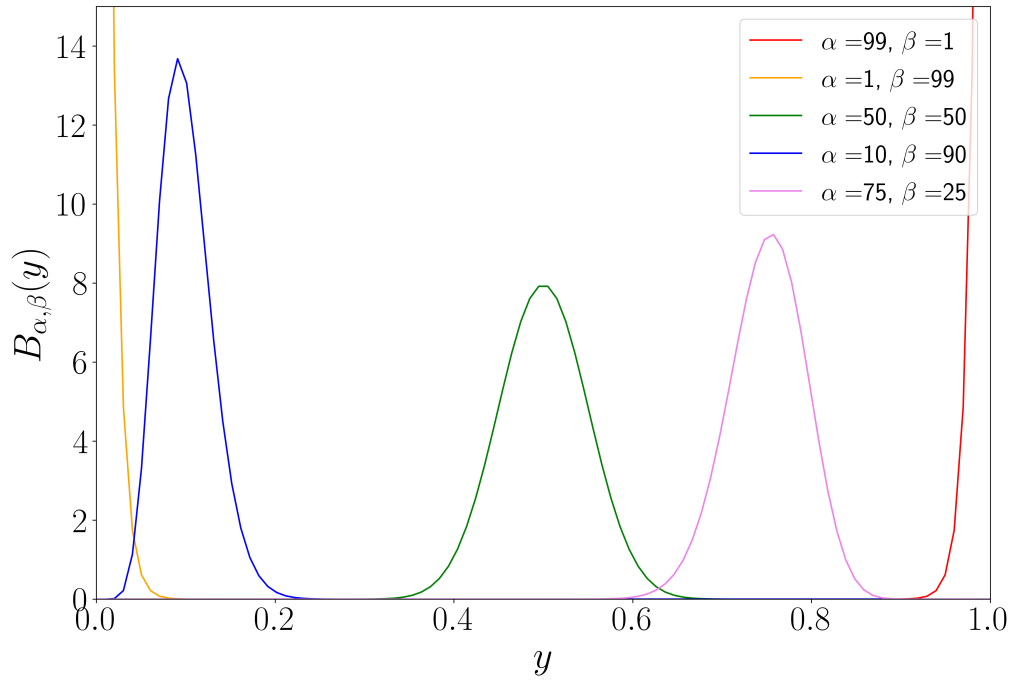

Figure 2.5 *Plots of $Beta_{\alpha,\beta}(y)$ for various α and β. We have kept $\alpha+\beta$ constant for comparison. This relates to a constant density (here, $\rho \approx \frac{2}{N}$).*

$$\beta = (1-\mu)\left(\frac{\mu(1-\mu)}{\sigma^2} - 1\right) = \frac{1-y_0}{\exp\left[\frac{2}{N\rho}\delta t\right] - 1}. \tag{2.42}$$

This is a natural distribution to choose because it is defined only for a finite interval and has an independent mean and variance. Since we have already truncated the Kramers-Moyal expansion at second order to obtain the stochastic field equations (2.22) and (2.34), we do not expect differences between the Beta and Gaussian distributions in the third and higher moments to be physically relevant for small δt. Once the intermediate value $p_{\text{int}} = (2y-1)$ is sampled, we then integrate the deterministic part of (2.34) numerically using this intermediate value in the usual Euler method with forward time and centred space derivatives, i.e.

$$\begin{aligned} m_i(t+\delta t) - m_i(t) \;=\; & \frac{\delta t}{2N}\left[(1+v(p_{i-1}(t)))(1-p_{\text{int}})\rho_{i-1}(t)\right. \\ & \left. -(1-v(p_{i+1}(t)))(1+p_{\text{int}})\rho_{i+1}(t)\right]. \end{aligned} \tag{2.43}$$

Note in the above equation the use of intermediate values of p for site i only, not including the intermediate values for neighbouring sites. This is a safe assumption to make if the values of p at neighbouring sites are uncorrelated. This assumption

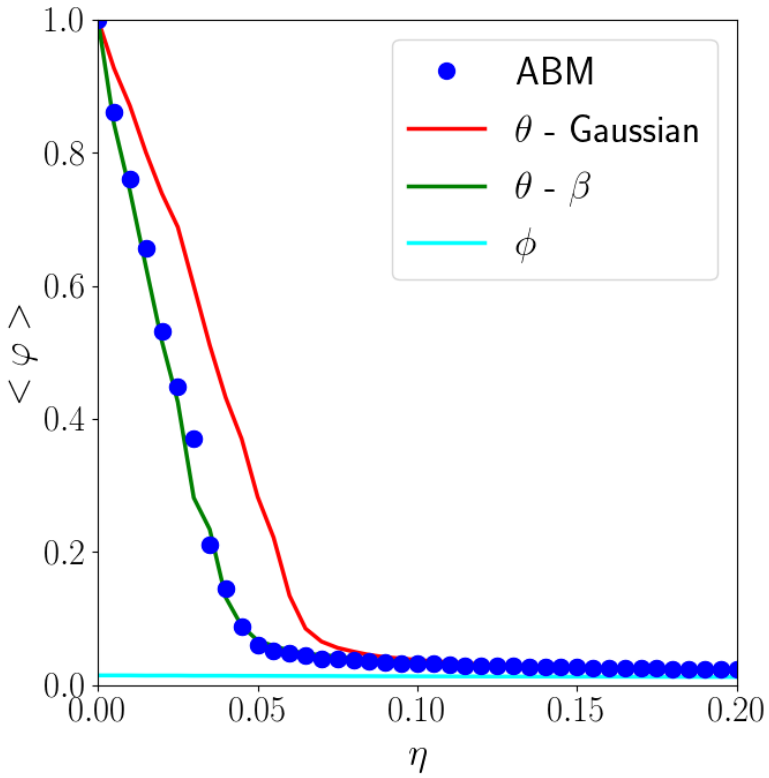

Figure 2.6 *The order parameter of the system φ vs the noise strength η for three different implementations of the continuum equations and compared with the ABM (dots). In all of these implementations, we had $N = L = 100$, $\beta = 2.0$, $\delta t = \frac{1}{N} = 0.01$, $T = 50000$.*

has already been made in the derivation of (2.34), so we make use of it again here to increase computational performance.

2.3.2 Comparison of continuum equations with agent-based model

In the preceding sections, we have made some claims about which numerical implementations of the continuum model give results that match the behaviour of the ABM and which will not. These claims are based on Fig. 2.6, which is a section of the phase diagram of the system in which we plot the order parameter of the system, φ (2.5), against the control parameter η. Three different numerical integrations of continuum equations are considered here against a single implementation of the ABM.

The first set of continuum equations are given by (2.22, 2.35) and the Euler-

Maruyama discretisation of the noise (beta-type noise will not work for this model as the multiplicative prefactor does not vanish for $\rho^2 = m^2$). As can be seen from Fig. 2.6 (light blue line, labelled ϕ), no significant order is observed for any value of η. This supports the assumption that correlations between ρ and m at the same site are not negligible, hence (2.22, 2.35) are a poor choice of continuum equations to describe the system in Section 2.1.

The implementations that do allow an ordered flock to exist in the low noise regime are both implementations of (2.22, 2.34), with the difference between them being the choice of discretisation of the stochastic term, as explained in Section 2.3. Within the margins of error, there is quantitative agreement between the behaviour of the ABM (blue dots) and the continuum equations with beta-type noise (green line, labelled $\theta - \beta$). We take this as strong support for the replacement of the white noise $\xi(x,t)$ with the operator splitting method involving sampling from a beta distribution.

The red line in Fig. 2.4 (labelled $\theta - Gaussian$) indicates the values of the order parameter if truncated white noise is used instead. The higher value of the order parameter than for the beta-type noise suggests that truncating out-of-bounds values to the closest physical value acts as a bias towards greater order. We expect that in the $\delta t \to 0$ limit, this discrepancy will vanish. Fig. 2.7 shows sample space-time trajectories for the system using a beta-type and truncated Gaussian noise (left and right panels respectively).

Another way to demonstrate that our SDEs (2.22, 2.34) accurately depict the ABM system in Section 2.1 would be by demonstrating that the polarisation correlations align between the two. These polarisation correlation functions are defined as

$$C_{ABM}(r) = \frac{1}{LT}\int_0^T dt \sum_{\alpha,\beta=1}^{N} \left[v_\alpha(t)v_\beta(t) - \bar{v}(t)^2\right] \delta\left(r - |r_\alpha - r_\beta|\right), \tag{2.44}$$

$$C_{SDE}(r) = \frac{1}{LT}\int_0^T dt \int_0^L \left[m(x,t)m(x+r,t) - \bar{m}(t)^2\right] dx, \tag{2.45}$$

where $\bar{v}(t)$ and $\bar{m}(t)$ are the mean velocity and mean magnetisation at time t respectively. We don't study these functions in detail in this chapter, as we have demonstrated the agreement between the ABM and SDE through the order

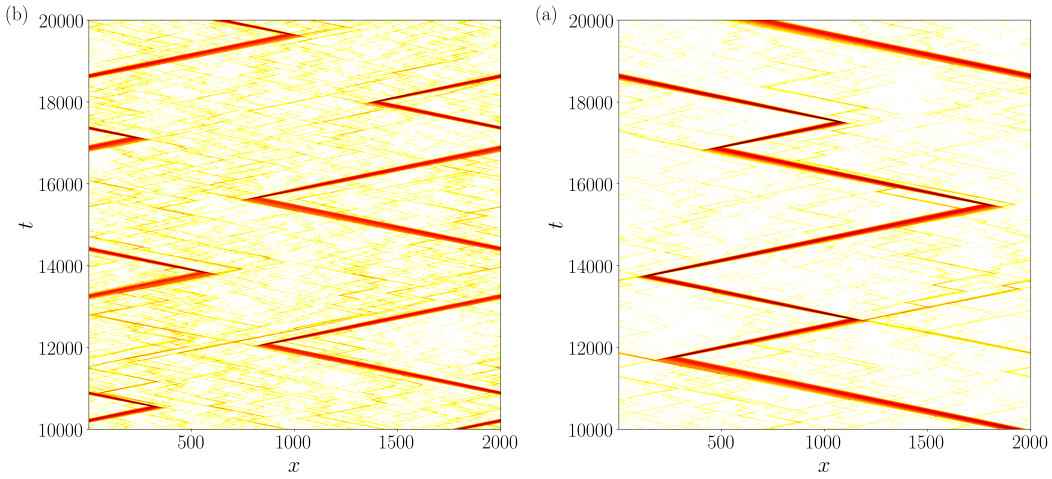

Figure 2.7 *Sample space-time trajectories for (2.22, 2.34) using beta noise (left) and truncated Gaussian noise (right). Both trajectories show the existence of a phase separated ordered flock. For the same system parameters ($N = L = 2000$, $\beta = 2$, $\eta = 0.02$), the flock in the truncated Gaussian model is more dense, suggesting this treatment of the noise gives rise to greater order. This can be seen more clearly in Fig. 2.6*

parameter, but examining the graphs of these functions against inter-particle distance r could be used to further demonstrate this agreement.

2.4 Interpretation of the continuum equations

To facilitate comparison of (2.22, 2.34) to other equations for similar systems both in 1d and higher dimensional analogues, we will discuss the physical interpretation of the terms in these equations.

2.4.1 Density equation

The most crucial thing to note about (2.22) is that, as previously mentioned, it satisfies global conservation of mass $\left(\int_0^L \rho(x,t)dx = 1\right)$, and hence has the form of a conservation equation with a particle current given by

$$J_\rho(x,t) = v\rho - \frac{1}{2}\partial_x\rho. \tag{2.46}$$

This was made possible by removing the stochastic term in Section 2.2.2. Given that the matrix decomposition of the second jump moments (2.12, 2.13) is not

unique, we cannot say for certain that a conservation form of the stochastic term cannot be found, in a method similar to that of Dean [38] described in Section 1.3.2. It is also possible that careful manipulation of the noise function $\xi_\rho(x,t)$, akin to a reversal of the process in [63], could generate a conserved noise term.

Additionally, the presence of a second order spatial derivative in (2.22) suggests that particle diffusion should be observed in the system. In Fig. 2.1, this diffusion can be seen in the ordered state (left image). The spatial dimensions of the flock grow with time, increasing the likelihood of a "flip", whereupon the flock alternates direction [82]. This diffusion separates (2.22) from the traditional Navier-Stokes continuity equation [108] or the Toner-Tu equations [112], both of which contain an advective term only. The presence of a diffusive term reflects the non-fixed speed of particles in the ABM, wherein particles may move more or less than a single lattice step in a time-step $\Delta t = 1$.

2.4.2 Magnetisation equation

Active matter systems generally involve an input of energy into the system, usually in the form of additional forces. These will affect the momentum $w = v\rho$, which in turn affects the magnetisation by altering the direction particles are facing. As expected, (2.34) cannot be written in the form of a conservation equation due to the presence of a non-differential deterministic term $v\rho - m$ and the presence of a non-zero non-differential stochastic term. Although it is feasible that the stochastic term could be written in conserved form by manipulating the noise function $\xi(x,t)$, the deterministic term cannot be rearranged into a spatial derivative of some current J_m provided $\eta, \beta \neq 0$.

The deterministic terms all linearly scale with density, as does the magnetisation itself. The first two terms reflect the local magnetisation updating by the change due to the momentum and is non-linear in m provided $\beta \neq 0$. The third term is a density gradient, which represents a pressure term similar to that seen in other hydrodynamic equations [23, 112]. The fourth deterministic term is momentum diffusion and is included for the same reasons as the diffusion term in the density equation (2.22).

The key to replicating the flocking behaviour in stochastic differential equations comes through the stochastic prefactor in (2.34), $\sqrt{\frac{2}{N\rho}(\rho^2 - m^2)}$. Unlike the deterministic terms that scale linearly with ρ, this term scales as $\rho^{\frac{1}{2}}$. On sparsely

populated sites, such as those in the disordered state or outside the flock in the ordered state, the stochastic and deterministic terms of (2.34) are of similar magnitude. However, for densely populated sites where $\rho \gg \frac{1}{N}$, such as those near the centre of the flock in the ordered state, only the deterministic terms play a role in the time evolution of the polarisation due to the $N^{-\frac{1}{2}}$ prefactor in the stochastic term.

The continuum equations (2.22, 2.34) work together to display the alternating state behaviour observed in the trajectories of the ABM. As the flock propagates, it diffuses, spreading out slowly. This decreases the density throughout the flock, especially at the nose and tail. When density decreases, the stochastic effects in the nose and tail cause particles to change direction. In the tail, this results in a decrease in total flock density as particles leave the condensate to join the diffuse disorder in the rest of the system.

The change in direction in the nose, on the other hand, is responsible for the existence of the alternating state. Once sufficient particles have turned around in the sparse nose of the flock, the remainder of the flock becomes unstable to a change in direction. Fig. 2.8 shows an implementation of the continuum model (2.22, 2.34) where the stochastic effects have been removed. A small pulse (equivalent to a single particle) starts on the right hand side of the system at $t = 3000$ travelling left. When it impacts on the flock, it is sufficient to cause the flock to flip through deterministic effects only. This suggests that a single particle in the nose of the flock stochastically changing direction and persisting in that new direction for long enough is sufficient to cause a macroscopic change in direction in the flock.

2.5 Minimal model

Now that a set of stochastic differential equations have been derived for this system, one can ask how much of this structure is necessary for the desired behaviour to be observed and why. We have previously noted that the $\beta \to \infty$ limit has been studied [82], which can be thought of as the non-linear limit of the interactions. Instead, let's examine the $\beta \to 0$ limit.

Fig 2.9 shows that when $\beta = 0$, the order parameter is small for all values of the noise strength η, showing that no flocking is possible in this limit. The $\beta \to 0$ limit

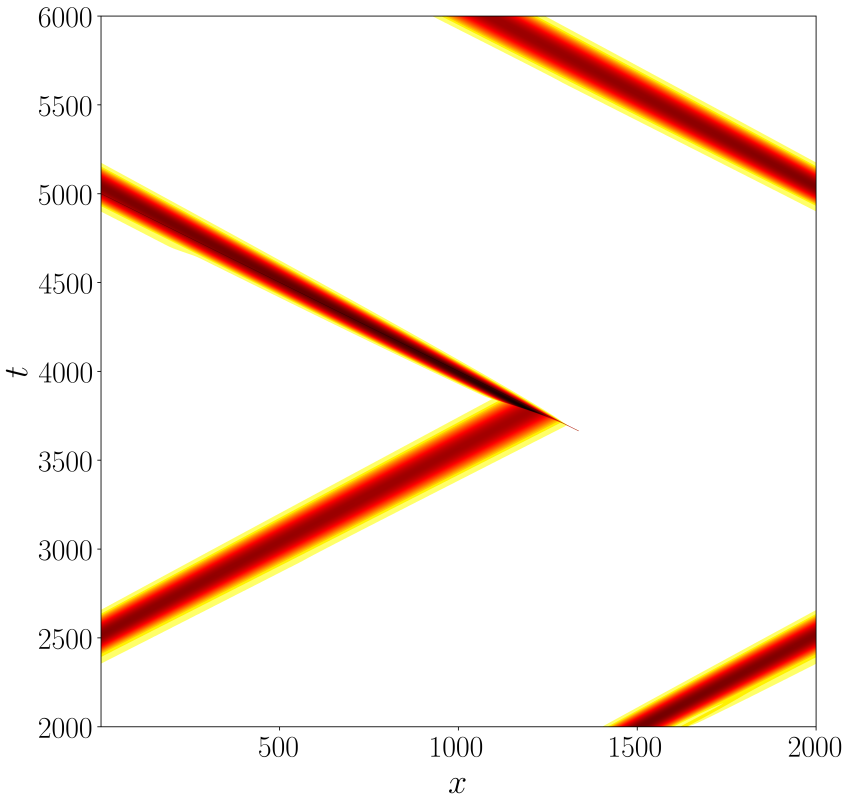

Figure 2.8 *A purely deterministic version of the agent-based model with a small pulse sent in from the right. This pulse is enough to turn the flock around, demonstrating that the flock is unstable to a sufficiently persistent fluctuation in the nose.*

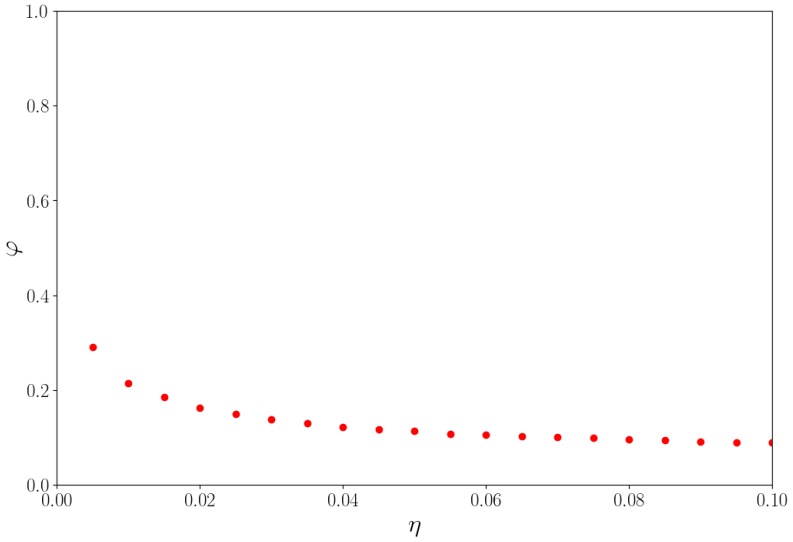

Figure 2.9 *When $\beta = 0$, all values of η have low order parameter φ. Other parameters: $N = L = 1000$, $T = 90000$.*

is equivalent to the particle choosing its preferred direction based on a random sample of a single other particle in its neighbourhood, akin to a simple voter model [40, 41]. To understand why flocking cannot occur in the system in this limit, we consider how the model with non-zero β changes when an additional interaction is added to the system.

We add in a "run-and-tumble" behaviour [70, 99, 102] with tumble rate η to the ABM defined in Section 2.1. At each time-step a particle either undergoes run-and-tumble behaviour with probability r or alignment with probability $1-r$. In a system with no maximum site occupancy, tumbling particles do not spontaneously order [18]. Therefore, we expect that the $r \to 1$ limit gives a disordered system under any non-zero value of η. The resulting equations using the Kramers-Moyal approximation are found to be identical to (2.22, 2.34), with one minor change to the exact form of the mean velocity $v(p)$ (the derivation may be found in Appendix C). The updated $v(p)$ is now

$$\tilde{v}(p) = (1 - 2\eta)\left[(1 - r)\frac{\tanh \beta p}{\tanh \beta} + rp\right]. \tag{2.47}$$

In the $r \to 1$ limit, v has become linear with the same form as the $\beta \to 0$ limit. Therefore, the stochastic equations resulting from a non-flocking interaction (run-and-tumble) are the same as those for a linear form of the alignment interaction or a simple voter-type interaction.

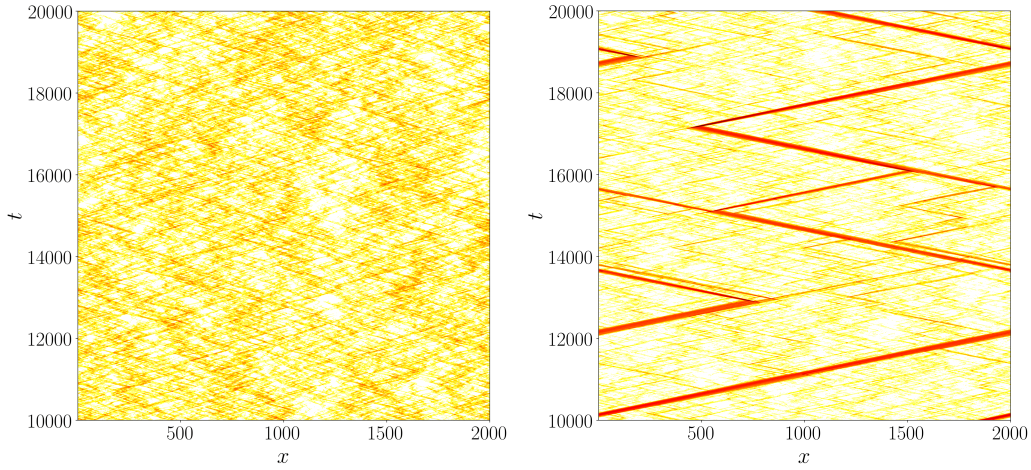

Figure 2.10 *Space-time trajectories of the field equations (2.22, 2.34) for a linear interaction (left) (2.47) and a third order interaction (right) (2.48). Parameters are* $N = L = 2000$, $\beta = 2$, $\eta = 0.02$, $r = 1$.

Including the next order term in the expansion of tanh and rescaling appropriately is sufficient for the flocking to occur (see Fig. 2.10), i.e.

$$v_{min}(p) = \frac{3}{2}(1 - 2\eta)\left(p - \frac{p^3}{3}\right). \tag{2.48}$$

The form of (2.48) matches the expression needed for a particle sampling a random set of three neighbours to determine the preferred direction [92]. This supports the findings of Chatterjee *et al.* [32], where is it shown that one- and two-body interactions are insufficient for an ordered flocking state to occur in 1d. Run-and-tumble without volume exclusion is a one-body interaction, while a simple voter-type interaction is a two-body interaction.

2.6 Modifications to the alignment rule

We return to the agent-based model for a discussion of the alignment rule. The continuum equations describing the system (2.22, 2.34) were derived with no assumptions made about the nature of the alignment function v, other than the densities and polarisations on neighbouring sites were uncorrelated. Therefore, it stands to reason that modifications to this function should produce the same set of equations, whose behaviour we can expect to match the behaviour in their corresponding ABM. In this section, we discuss a number of alterations to v that reflect certain physical systems and observe their effects on the ABM.

Raymond & Evans [92] included repulsive and attractive effects in v, based on work by Reynolds [93] that proposed that such effects should be included to observe the breadth of movements observed in flocks of birds. While these may be necessary for the existence of coherent flocking in higher dimensional systems that Reynolds' work focussed on (in particular in keeping the flocks from diffusing throughout the system), there are no indications that they are needed in 1d. However, they would be straightforward to include by modifying the form of v. Raymond & Evans work is a comprehensive study of the new behaviours observed when these factors are included, so we will not explore it further here.

2.6.1 Particle self-interaction - persistence or uncertainty

One major question with ABMs such as the one in this work is how particles should behave in the absence of neighbours with whom to interact. In the model from this chapter, for example, if a particle has no other particles on its site, it will consider the direction it is moving to be the preferred direction for its move. We can conceive of a more uncertain particle that, in the absence of other particles with whom to align, performs an unbiased random walk, hoping to meet another particle in doing so. This behaviour can be extended such that the particle will always exclude itself from its own neighbourhood. We refer to particles with this quality as "uncertain", while particles that always include themselves in their neighbourhood are termed "persistent".

The change from a persistent to uncertain particle is straightforward to implement in the ABM where particles can be distinguished easily. In the continuum equations, implementing this change is more challenging. If we are not including the particle in its own neighbourhood, we must consider different transition probabilities for particles facing right and left, denoted

$$W_\alpha^{\pm,r,l} = \frac{1}{2}\left(1 \pm v_{r,l}(p_\alpha, \rho_\alpha)\right), \tag{2.49}$$

where, if we use the minimal velocity function from Section 2.5, the right/left-facing mean velocity is

$$v_{r,l}(p,\rho) = \frac{3(1-2\eta)}{2}\left(p_{r,l}(p,\rho) - \frac{p_{r,l}(p,\rho)^3}{3}\right) \tag{2.50}$$

with an effective polarisation given by

$$p_{r,l}(p,\rho) = \frac{Np\rho - r + l}{N\rho - 1}\Theta\left(N\rho - 1\right) \tag{2.51}$$

where $r, l = 1$ for particles facing right or left respectively and are zero otherwise. This changes the transition rates as

$$W_i^{\pm}\rho_i = W_i^{\pm,r}\rho_i^{+} + W_i^{\pm,l}\rho_i^{-} = \rho_i\frac{1}{2}\left[1 \pm v_{\text{uncertain}}(p_i,\rho_i)\right] \tag{2.52}$$

with the effective uncertain mean velocity becoming

$$v_{\text{uncertain}}(p,\rho) = (1-2\eta)p\left(1 + \frac{1-p^2}{2}\Delta(\rho)\right)\Theta\left(N\rho - 1\right) \tag{2.53}$$

with $\Delta(\rho) = \frac{\rho^2(\rho - \frac{3}{N})}{(\rho - \frac{1}{N})^3}$ as the change due to increased uncertainty for $N\rho > 1$ and whose form can be seen in Fig 2.11. For $\rho > \frac{5}{N}$, $\Delta \sim 1$ and the uncertain particle's behaviour approaches that of the persistent particle. On sites where $\frac{1}{N} < \rho < \frac{3}{N}$, uncertainty actively opposes the polarisation to arrive at the expected velocity. As the turning of the flock is determined by the flipping rate of particles at the nose (where particle density is comparatively low), and uncertainty decreases the mean velocity compared to persistence, we expect uncertainty to lead to lower order or perhaps only a disordered state.

This choice of particle persistence or uncertainty can be combined with different definitions of what constitutes a particle's neighbourhood to give rise to multiple models. Regardless of the details of these neighbourhood definitions, we expect uncertain particles to exhibit lesser order than their persistent counterparts.

2.6.2 Alternative neighbourhood definitions

While two particles α and β are considered neighbours in the model in this chapter only if they are on the same lattice site, previous works from O'Loan & Evans [82] and Raymond & Evans [92] included particles as neighbours if the distance between them was no larger than a single lattice site. Although the same qualitative behaviour is observed in those models as in the ABM from Section 2.1, it is worth examining what effects, if any, the changes to the neighbourhood definition have on the order in the system. Examples of other changes to the neighbourhood are discussed in Section 1.2.4.

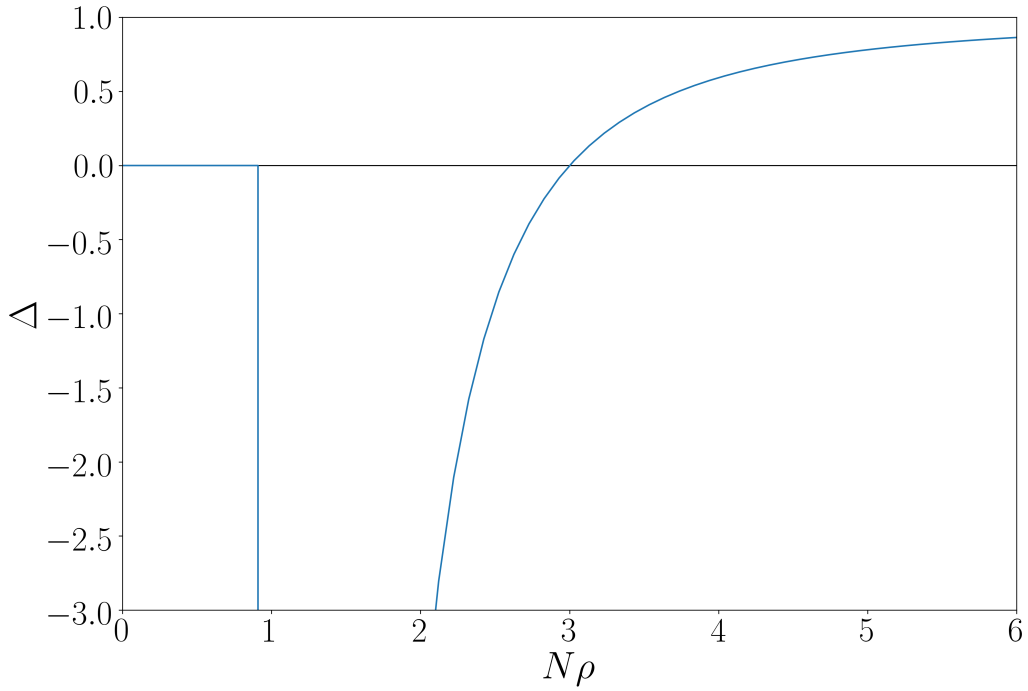

Figure 2.11 *The multiplicative change in p due to uncertainty instead of directional persistence. No difference is made when $\Delta = 1$, thus the low density regime $N\rho < 5$ has a large change in the mean velocity v due to particle uncertainty.*

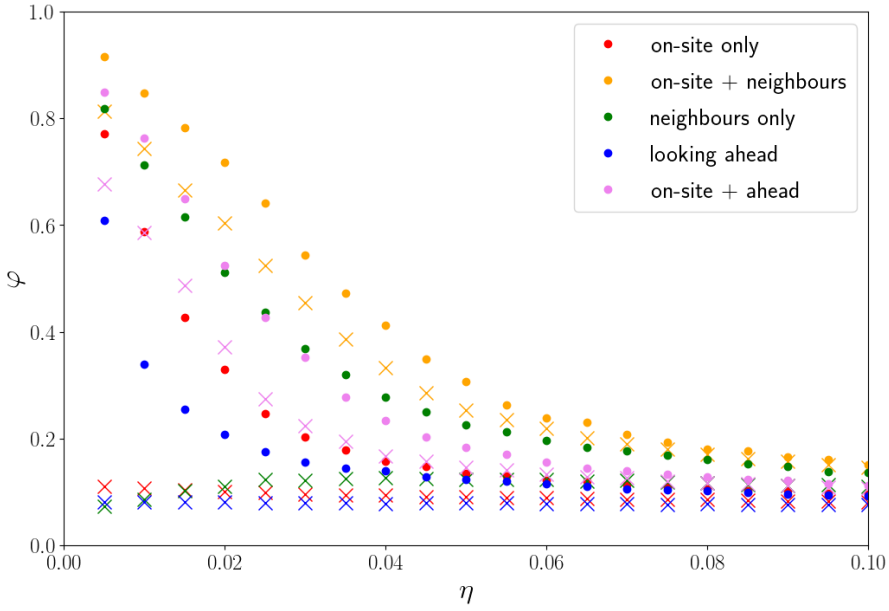

Figure 2.12 *A measure of the order parameter φ (2.5) against noise strength η for various neighbourhood definitions. The dots denote models where particles count themselves as their own neighbour, even if they would not normally meet the criteria for inclusion, while the crosses are for models where particles exclude themselves from their own neighbourhood, even if they would normally meet the criteria for inclusion.*

In Fig. 2.12, the order parameter φ (2.5) is plotted against noise strength η for a variety of neighbourhood definitions. Different coloured points denote a different neighbourhood for the particles, while dots denote models with persistent particles and crosses denote those with uncertain particles (as in Section 2.6.1). In this figure, persistence and uncertainty trumps the usual neighbourhood definition, i.e. if an uncertain particle has a property that would usually count it among its own neighbours, it does not, while if a persistent particle does not have such a property, it includes itself nevertheless (e.g. An uncertain particle will not count itself for the "on-site" interaction and a persistent particle will count itself for the "neighbours only' interaction).

The neighbourhood definitions are defined as follows: "on-site" is the neighbourhood definition for much of this chapter, where a particle on site i uses the polarisation on site i (including or excluding themselves) to determine the preferred direction; "neighbours" is where a particle on site i uses polarisation on sites $i-1$ and $i+1$ according to (2.54); and "looking ahead" is where a particle on site i will look at polarisation on site $i+v_\alpha$, where v_α is its direction at the start of the time-step. This last neighbourhood is equivalent to a "sight"-type interaction, where the range of a particle's sight is a single lattice site.

The other neighbourhood definitions in Fig. 2.12 are combinations of those in the previous paragraph. The polarisation for neighbourhoods spanning multiple sites is given by ratio of total magnetisation to total density in the neighbourhood, i.e.

$$p = \frac{\sum_{i\in\text{neighbourhood}} m_i}{\sum_{i\in\text{neighbourhood}} \rho_i}. \tag{2.54}$$

Fig. 2.12 shows the behaviour of multiple models, as denoted in the legend. This figure tells us a few things, with the key results summarised in Table 2.1. Crucially, all the models that include explicit persistence will exhibit order to some degree for sufficiently low η. Additionally, those neighbourhoods that span multiple sites including the particle's own site will exhibit order even if particles are uncertain. These data suggest the degree of order for persistent models may depend on the number of sites sampled over, although the data does not exist to demonstrate this conclusively.

	Persisting	Uncertain
On-site	Flocking observed	No flocking observed
On-site + neighbours	Flocking observed	Flocking observed
Neighbours only	Flocking observed	No flocking observed
Ahead only	Flocking observed	No flocking observed
On-site + Ahead	Flocking observed	Flocking observed

Table 2.1 *Summarised behaviour of different ABMs according to Fig. 2.12.*

2.7 Summary

In this chapter, we have explored a family of one-dimensional lattice-based agent-based models of self-propelled particles undergoing collective motion and equivalent continuum equation models. We derived the continuum models by using the Kramers-Moyal approximation [66, 78, 115] on the master equation describing the agent-based model and truncating the expansion at second-order. This gave a set of Langevin equations that generated trajectories of density and polarisation matching the flocking behaviour observed in the agent-based model.

A key assumption in the derivation was that density and polarisation are weakly correlated in space and with one another. This assumption allowed us to diagonalise the diffusion matrix in the Fokker-Planck equation obtained by the Kramers-Moyal approximation. We showed that assuming a different set of variables were uncorrelated gave a different Langevin equation, which, when numerically integrated, did not allow for a coherent flock to form. In this way, we showed that the choice of stochastic variable used in the Kramers-Moyal expansion can greatly change the final behaviour of the continuum equations. We also explored alternative methods of numerically integrating continuum equations of this form to accurately replicate the behaviour of the agent-based models.

Given a general set of continuum equations for a class of one-dimensional lattice-based agent-based models, we then examined other members of that class by altering the inter-particle interaction function. By comparing these interactive particle models with non-interactive particle models, we obtained the minimal interaction necessary for collective motion to exist in these systems. We finished by discussing additional interactions based on physical processes and how they could be incorporated into these models.

Chapter 3

Agent-based flocking in two dimensions on a lattice

In Section 1.2.1, we introduced the Vicsek class of self-propelled particle (SPP) agent-based models (ABMs). Vicsek-class models in two dimensions (hereafter 2d) have been studied extensively, from SPPs aligning to their neighbourhood average direction [31, 116], to particles acting as moving Ising spins [106], to particles aligning their velocity to their internal orientation or "spin" [26]. Much focus in recent years has been on the presence or absence of "banding" [104–106] in continuous space (off-lattice) systems, which refers to regions of high density and high polarisation ("bands") travelling through the system, typically parallel to one of the system boundaries (see Fig. 1.2). These may exist as a single large band or as many individual bands, depending on the interaction type, but the key features are phase-separation between highly ordered, high density and low order, low density regions, and the lack of a macroscopic change in the direction of the band as time increases. Although individual particles may change direction within the band, the structure of the band and overall direction of motion are linearly stable to these fluctuations [104].

The fixed-radius interaction zone used by Vicsek *et al.* [116] will typically lead to bands forming in the ordered state of 2d systems [31], but macroscopic turning of a flock in continuous space can be introduced by changing the definition of a particle's neighbours. In Section 1.2.4, we introduced a variable interaction radius such that each particle has a fixed number of neighbours and showed that it can enable an ordered and directional group of particles (hereafter, flock)

travelling in a continuous space 2d system to turn [4, 16, 88]. This is known as a "topological" or "metric-free" measure of particle neighbourhoods, as the neighbourhood network is unchanged if the system is scaled up or down, changing the mean distance between particles. This does not imply that the system behaviour will be identical for two different densities, as there remains an inherent length-scale in the particle velocity which has not been removed. However, unless the velocity or time between reorientations are sufficiently large that the neighbourhood network changes often, similar qualitative behaviour should be observed in topological systems with the same density but different sizes.

It is unclear, however, if macroscopic turning can be introduced in the same way in a system on a 2d lattice, or if a topological interaction is the only way to obtain a flock capable of turning in such a system. Our aim in this chapter is to obtain a clearer understanding of the factors that can give rise to a flock being able to undergo a macroscopic turn in the absence of external forces. To this end, we explore the behaviour of a number of related SPP ABMs in 2d, primarily varying the method used by particles to reorient towards their neighbours.

In Section 3.1, we introduce two lattice-based models of interacting SPPs on a 2d lattice. One model is a simplification of a lattice-gas cellular automata (LGCA) model, while the other is an extension of our model from Section 2.1 into 2d. To facilitate comparison, these models differ only through the probability a particle will turn based on the direction of the local "magnetisation" field. We show that this difference is sufficient for different behaviours to be observed in the ordered state. Demonstrating the existence of turning in a model with a metric interaction disproves an assumption in the literature that asymmetric interactions between particles are required for this turning to occur (see Section 1.2.4 for more details).

We next replace the metric neighbourhood definition with a topological one as described above to both models and observe how this change affects the behaviour in the ordered state of both models in Section 3.2. We demonstrate that one of our models is incapable of turning with a metric neighbourhood and is capable of turning in a topological neighbourhood, while the other model exhibits turning behaviour regardless of the neighbourhood definition.

Finally, we inspect the behaviour of each of these models in the ordered state and explore the robustness of their behaviours in Section 3.3. We demonstrate in this section that the qualitative behaviours of our lattice-based models should not differ from the more traditional models explored in Section 1.2 as a result of

the lattice or the implementation of stochastic uncertainty. As these models differ very slightly in their implementation and demonstrate behaviour that is robust to changes to the implementation of these models, we are led towards analysing the stochastic differential equations associated with each model to understand this difference, which is the topic of Chapter 4.

3.1 Agent-based models

We begin by introducing two lattice-based models for SPPs in 2d. The first, based on the lattice-gas cellular automata (LGCA) family of models [58, 59, 79], exhibits banding in the ordered phase, while the second, based on a 2d version of the model from Chapter 2, produces an ordered phase that undergoes macroscopic turning. These models differ only in the update rule for the velocity of particles, where the probability is an exponential function of the local magnetisation field for the first model and is a linear function of the local magnetisation field for the second model. Hence, we term these models "exponentially-aligning" (EA) and "linearly-aligning" (LA) respectively.

3.1.1 Exponentially aligning model (lattice-gas cellular automata)

LGCA models typically consist of a spatial lattice of sites where each site has a number of states with a given maximum occupancy (see Fig. 3.1). As some of these states have an associated direction and each typically has a maximum occupancy, we refer to them here as spin states as an analogy with quantum systems. Each site usually consists of one spin state for each of the cardinal directions of the lattice plus a fixed number of spin-zero states representing particles with no velocity, termed "idle" states. The system evolves in time by stochastically rearranging which spins particles have in each site, then particles deterministically either move one lattice site in the direction of their spin, or they remain stationary in the idle states if their spin is zero. The method used to determine which spin state the particles move to is the key variable affecting the behaviour of the system as a whole.

We focus here on a version of an LGCA model where the particles attempt to align with one another, i.e. occupy corresponding spin states across different sites. Our

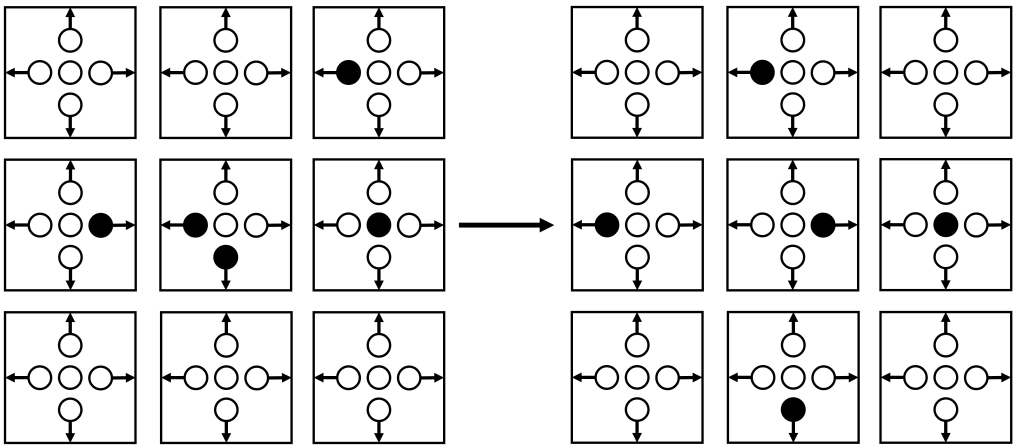

Figure 3.1 *Particles moving on a section of a lattice in an LGCA model. Note that the direction of motion is determined by the spin state particles occupy on the lattice site, with particles sitting in the centre spin states remaining stationary. Sites can contain multiple particles, while spin states within sites typically have a maximum occupancy of 1.*

model consists of N particles constrained to a square lattice with $L_x \times L_y$ sites, lattice spacing a, and periodic boundary conditions. There are no idle states, and the cardinal spin states (and hence sites) have no maximum occupancy. Although the cardinal states in an LGCA model typically have maximum occupancy of 1, for a sufficiently low density of particles we expect the probability that a spin state has occupancy greater than one to be negligible.

Particles in our lattice-based LGCA model have an average velocity v_0 and take discrete angular values $\theta_\alpha = \frac{n\pi}{2}$ with $n \in \{0, ..., 3\}$. The direction a particle faces is equivalent to it sitting on the corresponding cardinal spin state. At a given time t, each particle $\alpha \in \{1, ..., N\}$ has a position (site) $\mathbf{r}_\alpha(t)$ and an orientation (spin) $\mathbf{v}_\alpha(t) = a\cos\theta_\alpha(t)\hat{\mathbf{x}} + a\sin\theta_\alpha(t)\hat{\mathbf{y}}$. In what follows, we rescale the space and time variables such that $a = v_0 = 1$.

At each time-step $\delta t = \frac{1}{N}$, a single particle α is chosen. It then reorients (i.e. chooses a new spin state within a lattice site, which may be the same spin it previously had) and moves (i.e. changes site) in the direction of its updated direction. The probability $P(\mathbf{v}|\mathbf{M}_\alpha(t))$ that α will select a spin in the direction $\mathbf{v}$ is a function of the total magnetisation $\mathbf{M}_\alpha(t)$ in the neighbourhood of particle α. The neighbourhood is the usual metric definition whereby particles within a fixed radius R of particle α are considered to be its neighbours. Mathematically,

the probability can be expressed as

$$P(\mathbf{v}|\mathbf{M}_\alpha(t)) = \frac{1}{\mathcal{Z}_\alpha(t)} \exp\left[\beta \mathbf{v} \cdot \mathbf{M}_\alpha(t)\right] \delta\left(|\mathbf{v}| - 1\right). \tag{3.1}$$

where β is a positive finite number proportional to the strength of the alignment interaction and $\mathcal{Z}_\alpha(t)$ is the partition function for particle α at time t, given by

$$\begin{aligned} \mathcal{Z}_\alpha(t) &= \sum_{\mathbf{v}} \exp\left[\beta \mathbf{v} \cdot \mathbf{M}_\alpha(t)\right] \delta\left(|\mathbf{v}| - 1\right) \\ &= 2\cosh \beta M_{\alpha,x}(t) + 2\cosh \beta M_{\alpha,y}(t). \end{aligned} \tag{3.2}$$

Due to the form of the probability equation, we call this model "exponentially-aligning" (EA).

The total magnetisation of the neighbourhood of particle α, $\mathbf{M}_\alpha(t)$, is both a measure of the alignment strength near the chosen particle and an indication of the flock's preferred direction of motion near this point, and is given mathematically as

$$\mathbf{M}_\alpha(t) = \mathbf{R}\left(\eta_\alpha(t)\right) \sum_{\gamma=1}^{N} n_{\alpha\gamma} \mathbf{v}_\gamma(t) \tag{3.3}$$

where $\mathbf{R}\left(\eta_\alpha(t)\right)$ is a 2×2 rotation matrix with angle η_α drawn from a uniform distribution $\eta_\alpha \in [-\eta_0\pi, \eta_0\pi]$ $(0 \leq \eta_0 < 1)$. $\eta_\alpha(t)$ represents the error α has in calculating the preferred direction at time t, i.e. it is an intrinsic noise as defined in Section 1.2.1. $n_{\alpha\gamma}$ in Equation (3.3) is the neighbourhood matrix whose entries are 1 if particles α and γ are neighbours, and are 0 otherwise. For the metric neighbourhood in our EA model, $n_{\alpha\gamma}$ can be simplified to

$$n_{\alpha\gamma} = \Theta\left(R - |\mathbf{r}_\alpha(t) - \mathbf{r}_\gamma(t)|\right), \tag{3.4}$$

where $\Theta(x)$ is the Heaviside function.

As $\beta \to 0$, the system tends towards disorder and as $\beta \to \infty$, the system tends towards perfect alignment. Therefore, it is comparable to the inverse temperature β of equilibrium statistical physics. As β acts as a control parameter for the system, the intrinsic noise η is not strictly necessary here and we will set $\eta_0 = 0$ in our EA model for the rest of this chapter.

3.1.2 Linearly aligning model

We next turn to our other main model. To facilitate comparison between models, the model in this section is similar in most respects to our EA model in Section 3.1.1. We consider N polar particles confined to an $L_x \times L_y$ square lattice with spacing $a = 1$ and periodic boundary conditions. Each particle α has a position $\mathbf{r}_\alpha(t)$ and a direction $\mathbf{v}_\alpha(t) = a\cos\theta_\alpha(t)\hat{\mathbf{x}} + a\sin\theta_\alpha(t)\hat{\mathbf{y}}$. Akin to the ABM from Section 2.1, the direction and position of a single particle α are updated in a single time-step $\delta t = \frac{1}{N}$. The key difference between this alternative model and the LGCA-based model comes through the probability $P(\mathbf{v}|\mathbf{M}_\alpha(\mathbf{r},t))$ of α choosing a new velocity $\mathbf{v}$. Here, $P(\mathbf{v}|\mathbf{M}_\alpha(\mathbf{r},t))$ takes the form

$$P(\mathbf{v}|\mathbf{M}_\alpha(t)) = \frac{1}{\mathcal{Z}_\alpha(t)} \max\left\{\mathbf{v}\cdot\mathbf{M}_\alpha(t), 0\right\} \delta\left(|\mathbf{v}| - 1\right) \tag{3.5}$$

where the partition function $\mathcal{Z}$ becomes

$$\mathcal{Z}_\alpha(t) = |M_{\alpha,x}(t)| + |M_{\alpha,y}(t)|. \tag{3.6}$$

$\mathbf{M}_\alpha(t)$ again is the total magnetisation in the neighbourhood as defined in 3.3, with the neighbourhood again defined by the disc of radius R about particle α. Due to the form of the probability (3.5), we will refer to this model as our "linearly-aligning" (LA) model.

Note that in the LA model, there is no prefactor β multiplying $\mathbf{M}_\alpha(t)$. While we could include one in the definition of $P(\mathbf{v}|\mathbf{M}_\alpha(\mathbf{r},t))$, it would divide out due to the partition function. Thus, we cannot set the intrinsic noise strength η_0 to 0 here as in the EA model, as doing so would leave the system without a tunable source of noise.

The probability $P(\mathbf{v}|\mathbf{M}_\alpha(\mathbf{r},t))$ remaining unchanged when the magnetisation $\mathbf{M}_\alpha(\mathbf{r},t)$ is rescaled has an additional effect; the probability for each direction is unchanged by a change in the number of particles in the neighbourhood or the magnitude of the neighbourhood magnetisation, provided the angle of the magnetisation is unchanged. As in the 1d model of Section 2.1 and unlike the 2d EA model of Section 3.1.1, the probability of a particle choosing a new direction depends only on the total neighbourhood polarisation angle, not on the density of particles or their magnetisation. This is not a metric-free interaction, however, as if the system is sufficiently dilute or the interaction radius R sufficiently small

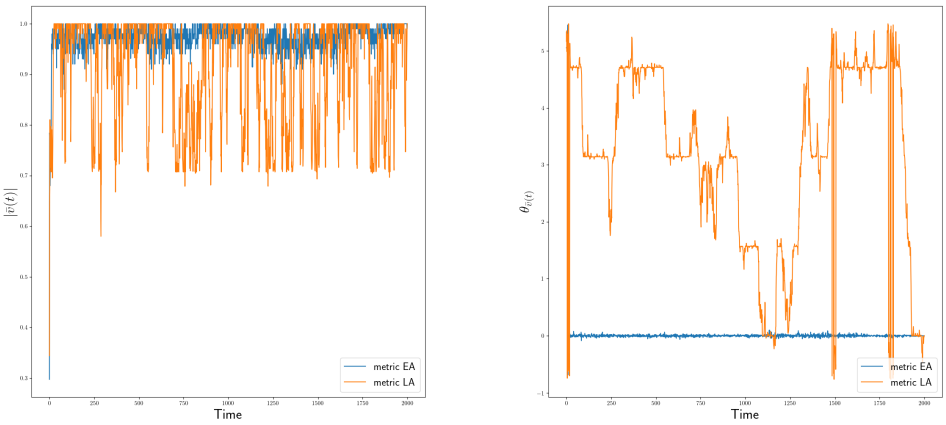

Figure 3.2 *Order parameter of selected trajectories of the ABM models. Order is present in each trajectory, as evidenced by the magnitude of the order parameter being close to 1. The LA model with metric interactions exhibits a change in orientation of the ordered flock, while the EA model does not. The average magnitude of the order parameter is lower for the LA model than the EA model.* $N = L_x = L_y = 100$, $\beta = 0.75$, $\eta = 0.02$.

that the probability of two particles interacting is rare, the system tends towards a system of non-interacting persistent random walkers on a lattice and global order does not emerge.

3.1.3 Ordered phase behaviour

To study the degree of order in the ABMs above, we examine the mean velocity of the particles, defined as

$$\varphi = |\langle \bar{\mathbf{v}}(t) \rangle| = \left| \left\langle \frac{1}{N} \sum_{\alpha=1}^{N} \mathbf{v}_\alpha(t) \right\rangle \right|, \tag{3.7}$$

where $\bar{\mathbf{v}}$ is the mean velocity at time t and the average $\langle\rangle$ is taken over multiple realisations of the noise. We cannot assume that $\bar{\mathbf{v}}$ itself is ergodic (i.e. the average over time will match the average over realisations of the noise [115]) as the ordered flock does not change direction if banding is present. As φ is invariant under a rotation of the system, we assume φ is ergodic, i.e. averaging over time and noise realisation will be the same given enough data.

Fig. 3.2 displays the mean velocity $\bar{\mathbf{v}}$ (magnitude on the left, orientation on the

right) for sample trajectories of the EA and LA models as a function of time. Beyond an initial transient state wherein the system transitions to the ordered state from the disordered state, the magnitude of $\bar{\mathbf{v}}$ is typically close to 1 for both models. The orientation, however, remains constant after the transition for the EA model, but it varies for the LA model as the flock changes direction.

Note that, as the metric interaction is by definition symmetric (i.e. $n_{ij} = n_{ji}$ for all particle pairs i, j), non-symmetry of the particle interaction is not strictly necessary for a system to exhibit a stable flock that can stochastically change direction. This finding partially contradicts the conclusions of Cavagna *et al.* [27], although we demonstrate in the next section that asymmetric interactions can lead to turning in a system where a symmetric interaction does not.

3.2 Topological interaction

As we discussed in Section 1.2.4, off-lattice agent-based models in 2d with topological interactions have been shown to exhibit an ordered flock capable of turning. While these models involve particles moving in a continuous 2d space, the behaviour of our LA model with a metric neighbourhood definition demonstrate that macroscopic turning on a 2d lattice is possible (see Fig. 3.2). In this section, we change the ABMs from Section 3.1 to a topological neighbourhood definition to determine whether flocks under the EA model are also capable of macroscopically turning and observe how the topological LA model varies from the metric model.

3.2.1 Definition of the neighbourhood

While there are multiple methods of implementing a topological interaction in agent-based models [20, 54, 68], the qualitative behaviour of the systems in the ordered state do not vary significantly between models. For that reason, we select an implementation that differs from our metric model as little as possible. We alter the definition of a particle's neighbours to those lying within a varying radius $R_\alpha(t)$ surrounding each particle, chosen to be the minimum radius needed to ensure each particle has the same (fixed) number of neighbours c. Mathematically, $R_\alpha(t)$ is defined as the radius of the smallest circular area around particle α

containing c particles, i.e. the minimum radius R that satisfies the equation

$$\sum_{\gamma=1}^{N} \Theta\left(R - |\mathbf{r}_\alpha(t) - \mathbf{r}_\gamma(t)|\right) = c. \tag{3.8}$$

With the above assumptions, the neighbourhood matrix in 3.4 can be written as

$$n_{\alpha\gamma}(t) = \begin{cases} \Theta\left(R_0 - |\mathbf{r}_\alpha(t) - \mathbf{r}_\gamma(t)|\right) & \text{metric interaction} \\ \Theta\left(R_\alpha(t) - |\mathbf{r}_\alpha(t) - \mathbf{r}_\gamma(t)|\right) & \text{topological interaction} \end{cases} \tag{3.9}$$

where $\Theta(r)$ is the Heaviside function and R_0 is a fixed parameter of the metric models. Note that under the above definitions for the neighbourhood matrix, α will be a neighbour of itself. This choice is akin to giving the particle some persistence, allowing local fluctuations in the flock's direction to last longer. We demonstrated in Section 2.6.1 that, in a 1d system with interactions similar to the metric LA, persistence leads to higher order (see Fig. 2.12). It is reasonable to assume that in metric systems, persistence leads to higher stability of the flock, although this may not also hold for topological flocks. Nevertheless, allowing persistence makes deriving the stochastic differential equations simpler, so we choose to keep it in our ABMs to better facilitate comparison later.

3.2.2 Changes to the ordered state

When the interaction neighbourhood is defined topologically instead of through a fixed distance, we expect to see changes to the observed behaviour of the ordered state in the ABM. As a reminder, the ordered state for the EA model displayed banding while the LA displayed a macroscopically turning flock in the ordered state.

Fig. 3.3 shows the mean velocity of a sample trajectory of the EA and LA models with a topological interaction. Note that, while the frequency of changes in the orientation of the order parameter varies between the two models, the flock is capable of turning in both. As expected from off-lattice models, changing the EA model from a metric to a topological interaction enables the flock to macroscopically turn and removes the banding previously present. Little has changed for the LA model, suggesting that the neighbourhood choice does not determine the dynamics of the ordered state of this model.

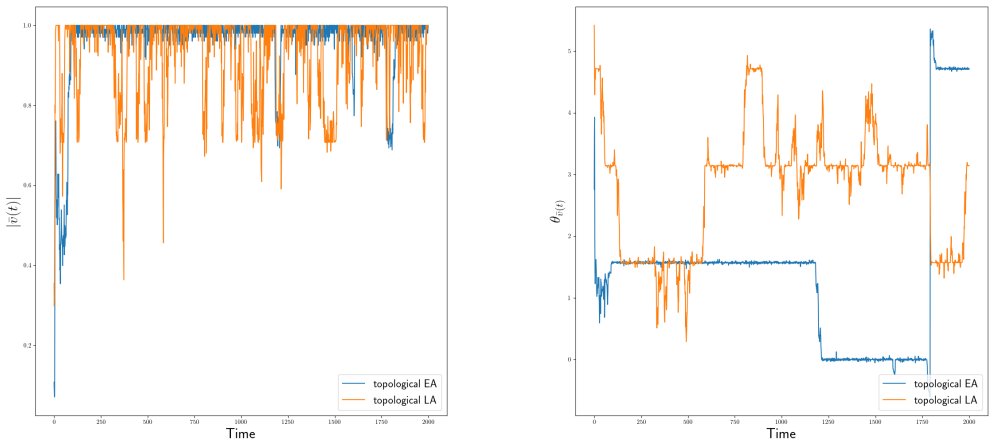

Figure 3.3 *Mean velocity of selected trajectories of topological neighbourhood ABMs. Order is present in each trajectory, evidenced by the magnitude of the order parameter (left plot) being close to 1. Unlike for metric neighbourhood ABMs, both the EA and LA models exhibit macroscopic turning here, as evidenced by the non-constant angle of the mean velocity (right plot). Parameters were* $N = L_x = L_y = 100$, $\beta = 0.75$, $\eta = 0.02$.

We now have three lattice-based ABMs (metric LA, topological EA, topological LA) with an ordered state consisting of a flock capable of macroscopically turning and one lattice-based ABM (metric EA) with an ordered state consisting of a flock that forms into stable directional bands. We can create two pairs of models from the four above that result in different macroscopic behaviours, yet differ in their implementation in one place only (metric EA and metric LA differ in the probability of choosing a new direction given a neighbourhood magnetisation; metric EA and topological EA differ in the determination of that neighbourhood). By examining how the effects of these changes are manifested in our model pairs, we may begin to understand what factors play a role in how aligning SPP systems form bands or change direction.

Before we begin to examine the whys of the different behaviours observed in our various EA and LA models, we must ensure that the behaviours observed are robust to changes to the implementation of simulations of the above models. If a change in implementation does not cause the ability of the ordered flock to turn to vanish or appear, we can be confident that the presence or lack of turning is indeed caused by the physics of the model and can begin to examine that physics in greater detail.

3.3 Robustness of the ordered phase behaviour to model changes

If we wish to determine if the behaviours exhibited by flocks in our ABMs are a result of a simulation choice or compare those behaviours with the literature, we must understand how changes in the model implementation can affect the order parameter of our systems. In this section, we explore the effects of changing from a lattice-based to an off-lattice model, from an intrinsic (scalar) to an extrinsic (vectorial) stochastic term, and from a stochastic particle update rule to a simultaneous update rule.

3.3.1 Constraining particles to a lattice

By definition, models where particles are constrained to lie along a lattice permit movement of particles between lattice sites only. In our EA and LA models above, this is further restricted to prohibit particles from moving to a site that is further than one lattice spacing away (i.e. moves are possible between nearest neighbours only). On a square lattice, a particle can only move in cardinal directions (up, down, left, right), a substantial restriction from the relative freedom of movement in 2d off-lattice systems.

Nava-Sedeno *et al.* [80] demonstrated that key qualitative features of an off-lattice model can be replicated with a comparable lattice-based model [79]. Although this analysis was performed with a specific model with a metric neighbourhood, it demonstrates that confining a system to a lattice need not remove its key behaviours. Their analysis did not determine whether the same was true for a model with a topological neighbourhood.

While removing the ability for a particle to turn diffusively could have an impact on the flock's ability to turn, we demonstrated with the metric LA model in Fig 3.2 and both topological models in Fig. 3.3 that an ordered flock *can* undergo macroscopic turning on a lattice given the right model. Meanwhile, the metric EA model demonstrates in Fig 3.2 that turning need not always be present in the system. As such, it is likely that any effect of the lattice affects the magnitude of the order parameter φ (3.7) or the position of the phase transition of the system, not whether the flock is capable of turning stochastically or not.

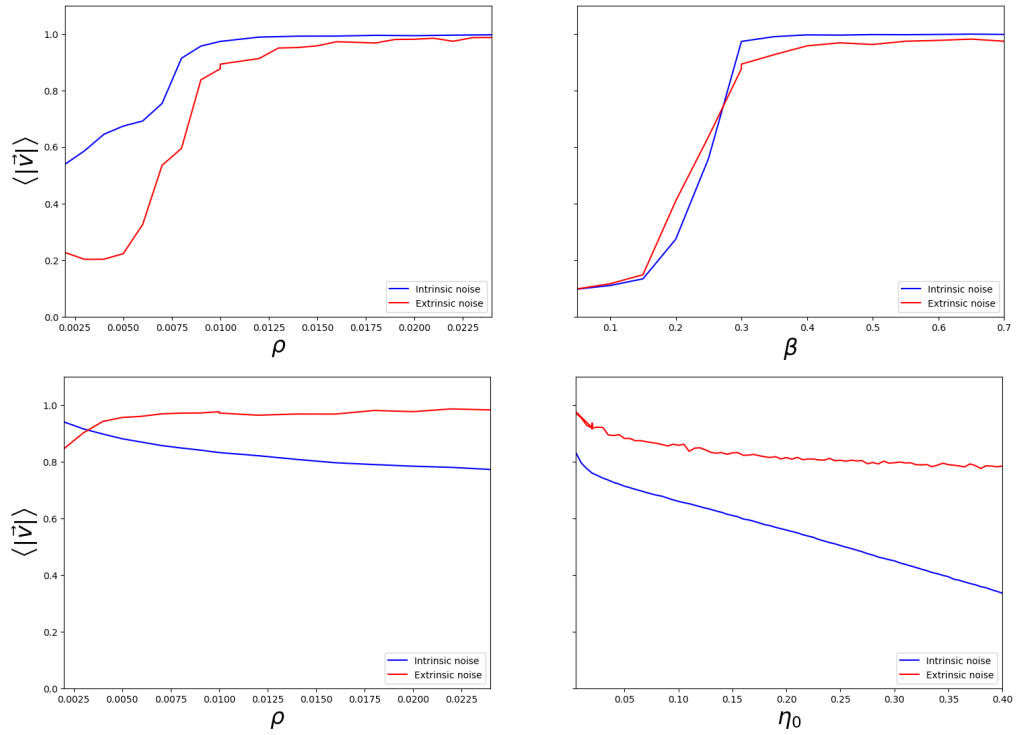

Figure 3.4 *Top: The order parameter in the metric EA model above as a function of system density using either intrinsic or extrinsic noise as a function of ρ or β. Bottom: The order parameter in the metric LA model above as a function of system density using either intrinsic or extrinsic noise as a function of ρ or η. The behaviour of the order parameter in the ordered state is similar between the two noise types, although it is closer quantitatively in the EA model than the LA model. $L_x = L_y = 100$, $R = 16$, $\beta = 0.3$ (top left), $\eta_0 = 0.005$ (bottom left), $\rho_0 = 0.01$ (top right and bottom right).*

3.3.2 Implementation of stochastic uncertainty

We discussed in Section 1.2.1 how a stochastic term can be added to models to simulate uncertainty. In both models above, we have used intrinsic (scalar) noise. While there should be no difference in the behaviour observed in systems with an intrinsic or extrinsic noise in the limit of infinite system size (with finite and non-zero mean density $\rho_0 = \frac{N}{L_x L_y}$) [53], we expect that the finite system size may affect the behaviour of the ordered state [105], although not significantly enough to alter whether or not macroscopic turning is possible.

From Fig. 3.4, we observe that the behaviour of the ordered state of the metric EA with extrinsic noise is very similar to the intrinsic noise model. However, the magnitude of the time-averaged mean velocity in the extrinsic noise metric LA model is significantly greater than in the intrinsic noise model. While η does

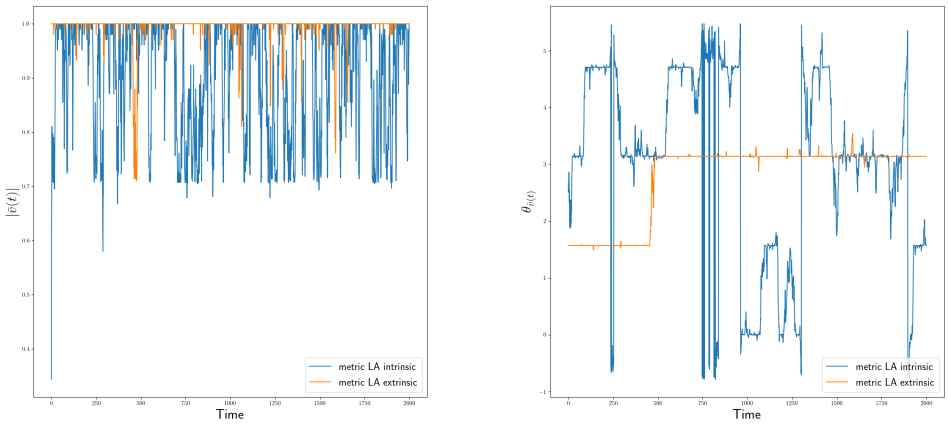

Figure 3.5 *Order parameter of selected trajectories of the ABM models. Order is present in each trajectory, as evidenced by the magnitude of the order parameter being close to 1. Changes in direction occur more frequently in the metric LA model with intrinsic noise than the metric LA model with extrinsic noise.* $N = L_x = L_y = 100$, $\eta = 0.02$.

represent a noise strength in both the intrinsic and extrinsic LA models, it is not implemented in the same manner. In the intrinsic model, η is added to the angle of the mean velocity (equivalent to η_i^t in Eq 1.3), while η is the magnitude of a random vector added to the mean velocity in the extrinsic model (equivalent to ξ_i^t in Eq. 1.6). Therefore comparisons should focus on the shape of the bottom plots in Fig. 3.4 rather than comparing quantitative behaviour for a given value of η.

Examining sample trajectories of the extrinsic model (Fig. 3.5) demonstrates that changes in direction are more frequent in the intrinsic metric LA model than in the extrinsic model for the same value of η, and the magnitude of the mean velocity decreases while the system is undergoing a change in direction. We conclude therefore that, while extrinsic noise may produce different behaviour in the ordered state in our finite-size systems, the qualitative behaviour (namely whether or not turning is possible in the ordered state) is unaffected by which noise type is used.

3.3.3 Removing the "fixed-speed" assumption

One limit of using models to simulate physical systems is that discretisation must be applied to the system. For modelling physical objects moving at a constant speed such as birds in flight, models typically use a discretisation of time where all particles update their positions simultaneously [26, 29, 71]. This preserves the constant speed of particles, though a delay of order δt is typically introduced between the position and velocity updates.

Another option is the stochastic update rule used in Chapter 2 for our 1d aligning SPP ABM. This rule does not preserve the constant speed of particles, although the average speed over all particles will be constant. However, we expect that in a sufficiently large system, we should observe no significant difference in the order parameter between these update rules. We set out the implementation of our choices of update rule below and explore how they affect the order parameter of our finite system.

Simultaneous update

The simultaneous update rule updates each particle in a single time-step δt_{sim} as

$$\mathbf{r}_\alpha(t+\delta t_{sim}) = \mathbf{r}_\alpha(t) + \delta t_{sim}\mathbf{v}_\alpha(t+\delta t_{sim}), \tag{3.10}$$

$$\mathbf{v}_\alpha(t+\delta t_{sim}) = \mathbf{V}\left(\mathbf{r}_\alpha(t), \{\mathbf{r}_{\alpha'}(t), v_{\alpha'}(t)\}\right), \tag{3.11}$$

where $\mathbf{V}$ is some function of the positions and velocities of all the other particles. In the models in Section 3.1 above, $\mathbf{V}$ is the new direction chosen randomly with weights given by $P\left(\mathbf{V}|\mathbf{M}(\mathbf{r},t)\right)$ (3.1, 3.5). Therefore, (3.11) can better be expressed as

$$\mathbf{v}_\alpha(t+\delta t_{sim}) = \begin{cases} \hat{\mathbf{x}} & \text{with prob. } P(\hat{\mathbf{x}}|\mathbf{M}_\alpha(t)) \\ \hat{\mathbf{y}} & \text{with prob. } P(\hat{\mathbf{y}}|\mathbf{M}_\alpha(t)) \\ -\hat{\mathbf{x}} & \text{with prob. } P(-\hat{\mathbf{x}}|\mathbf{M}_\alpha(t)) \\ -\hat{\mathbf{y}} & \text{with prob. } P(-\hat{\mathbf{y}}|\mathbf{M}_\alpha(t)) \end{cases} \tag{3.12}$$

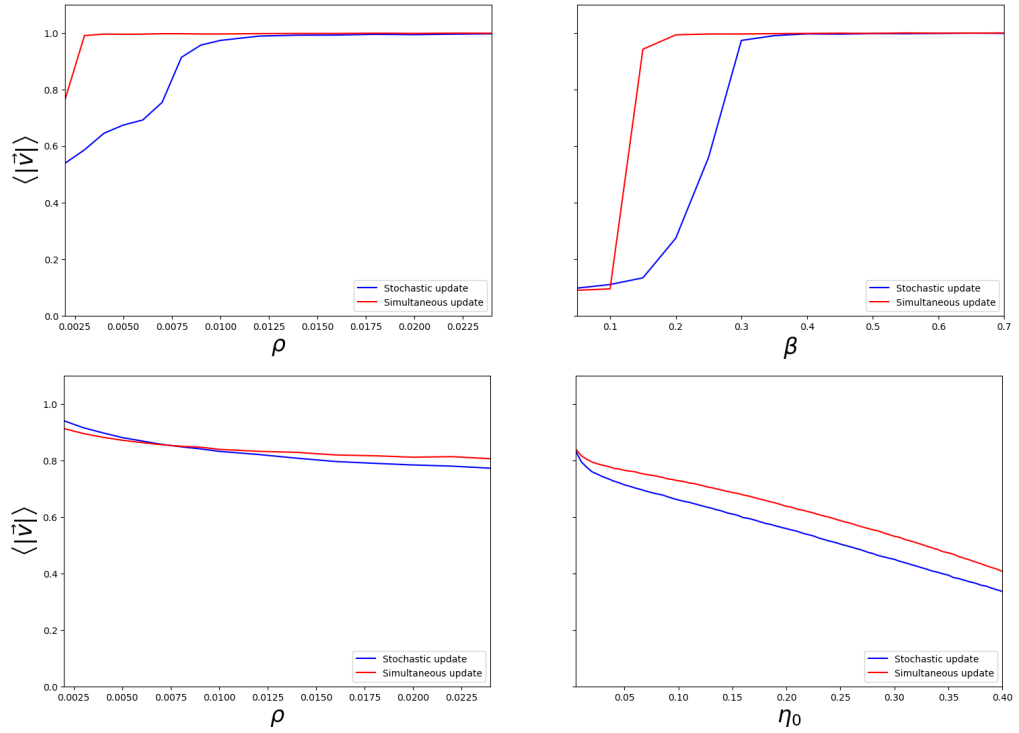

Figure 3.6 *Top: The order parameter in the metric EA model above using either a stochastic or simultaneous update rule as a function of ρ or β. Bottom: The order parameter in the metric LA model above using either a stochastic or simultaneous update rule as a function of ρ or η. While the position of the phase transition may differ between the two selections, the overall behaviour remains similar between the two update types. $N = L_x = L_y = 100$, $R = 16$, $\beta = 0.3$ (top left), $\eta_0 = 0.005$ (bottom left), $\rho = 0.01$ (top right and bottom right).*

Stochastic update

An alternative approach is to use a stochastic update, as in the 1d model in Chapter 2. Under this scheme, a single particle chosen at random takes a movement step in a time-step δt_{stoc}. In order to ensure the mean particle velocity remains constant between the two update rules, δt_{stoc} must be related to δt_{sim} by the relation

$$\delta t_{sim} = N \delta t_{stoc}. \tag{3.13}$$

The equations for how $\mathbf{r}_\alpha$ and $\mathbf{v}_\alpha$ are updated are the same as (3.10, 3.12), though δt_{sim} is replaced by δt_{stoc} and only a single particle is updated in each time-step.

Comparison

Although both update rules use the same equations, additional diffusion is present in the stochastic update due to the additional particle fluctuations introduced by particles moving at different speeds. The presence of additional diffusion suggests that care must be taken when directly comparing between equations derived from ABMs with equations of motion from other sources to properly account for any added diffusion due to the update rule.

Indeed, Fig. 3.6 demonstrates that, although the order parameter $\varphi = \langle |\mathbf{v}| \rangle$ is broadly similar for both update types, the lines do not fully overlap. Under most combinations of system variables, the stochastic rule leads to lower order including changing the position of the phase transition in our EA model.

3.4 Summary

In this chapter, we explored some variations in agent-based models in two dimensions, with a focus on identifying models that facilitated an ordered state capable of turning while remaining ordered. We introduced a baseline lattice-based model, based on the lattice-gas cellular automata family of models, to compare broadly with off-lattice models. This model, which we termed "exponentially-aligning" (EA), typically exhibits banding, a phase separation observed in many 2d models that exceed certain spatial dimensions [53], as described in Section 1.2.1.

We contrasted the EA model with a "linearly-aligning" (LA) model based on the 1d ABM in Chapter 2, in which banding is not present and the ordered state of the system is capable of changing its direction more akin to a real flock. To facilitate this comparison, the EA and LA models were designed to have few differences between then. We also introduced an alternative ("topological") neighbourhood definition, based on the observation that physical flocks utilise a topological neighbourhood [4, 20]. Turning was present in the ordered state of both the topological EA and LA models, leading to another avenue for comparison between our 4 models.

The key results in this chapter were obtained from simulations on a lattice with an intrinsic noise type and a stochastic update rule. To ensure the robustness of these results, we examined changing our simulations to an off-lattice system, to an extrinsic noise, or to a simultaneous update rule in turn. We demonstrated that our choice to use a lattice, intrinsic noise and a stochastic update did not cause the turning behaviour either to manifest or become suppressed and was instead due to differences in the model definition (and hence underlying physics). While there were differences in the order parameter between the choices we made and the alternatives, it is likely that many of these are finite size effects and would decrease or disappear in a larger system.

One change not examined in this section was how robust the behaviours in the ABMs are to changes in system size. While we expect that turning should be observed in large systems in the topological EA model and not in the metric EA model given its similarity to other SPP models in 2d [80, 104], we can be less certain the presence of turning in both LA models is robust to system size changes. In particular, if we wished to rigorously demonstrate that the presence of turning in the metric LA model is not a finite-size effect, an examination of how the order parameter changes with system size should be conducted. As we are more concerned in this thesis with replicating the behaviours in the ABMs using SDEs, the existence of a potential finite size effect here is not a great concern.

From our 4 models, we identified two model choices that either allowed or suppressed turning: the metric neighbourhood suppresses turning in the EA, while the topological neighbourhood allows it; and the probability of choosing a new direction in the metric EA also suppresses turning while the probability in the metric LA allows it. In the next chapter, we use the Kramers-Moyal approximation again to derive and compare stochastic differential equations for the 4 models explored in this chapter to identify how different model choices

enable or prohibit macroscopic turning in a physical context.

Chapter 4

Continuous space flocking in two dimensions

In the previous chapter, we introduced four related agent-based self-propelled particle models. Three of these models generate trajectories of ordered flocks undergoing macroscopic turning, while one resulted in an ordered flock continuing to travel in a single direction. In this chapter, we explore whether using the Kramers-Moyal approximation to generate stochastic differential equations can allow us to determine the cause of this turning behaviour.

In Section 1.3, we discussed a number of models consisting of PDEs describing the time evolution of SPPs and discussed methods of obtaining such equations, either phenomenologically from the symmetries of the system (Section 1.3.1) or by summation (or integration) over the microscopic dynamics of the particles involved (Section 1.3.2). Having a set of equations for macroscopic system variables allows for analytical analysis of the model, including the stability of the ordered state to macroscopic turning [3, 25].

We begin in Section 4.1 by deriving stochastic Langevin equations for the exponentially-aligning (EA) and linearly-aligning (LA) models using the Kramers-Moyal approximation as in Chapter 2. As we wish to compare the behaviour of multiple different models directly, we derive the field equations for a general set of interactions. This would also enable us to compare and contrast our equations with deterministic equations derived from other sources [10, 51, 101], although we do not make these comparisons here.

Unlike the 1d ABM examined for much of Chapter 2, the 2d ABMs in Chapter 3 use non-local interactions. We substitute these specific interactions into the general field equations in Section 4.2, where we examine how the particle current and directional density differ between model choices and discuss how the turning vs non-turning behaviour could arise as a result of these differences. In Section 4.3, we conduct linear stability analysis on our field equations and obtain dispersion relations, providing a quantitative measure of whether an ordered flock is or is not stable to fluctuations causing it to turn. While we cannot demonstrate conclusively that linear stability alone can determine whether or not turning is possible, we are able to identify when different alignment rules and different neighbourhood definitions play a role in enabled or suppressing turning in our four ABMs.

We next perform numerical integration and compare the resulting trajectories with the agent-based models to understand if the Kramers-Moyal approximation produces stochastic differential equations that replicate the behaviour exhibited by the ABMs. Based on our findings from Section 2.3.2 that a beta-type noise caused the ordered parameter of the numerically integrated trajectories and the agent-based models to match, we use this approach again here. We then examine the results and compare the resulting trajectories with the agent-based model to determine if the Langevin equations are an accurate representation of the ABM. While the stochastic differential equations we obtained do not match the behaviour observed in the ABMs, it remains possible that fewer approximations in the Kramers-Moyal expansion could yet yield accurate equations.

We finally summarise the key findings from this chapter, identifying the successes and failures of the Kramers-Moyal approximation for our two-dimensional models, highlighting the approximations that lead to these results, and suggesting ways in which the equations obtained might be improved.

4.1 Continuous equation derivation

We begin with a Kramers-Moyal expansion as in Chapter 2 of the ABMs in Chapter 3. As before, we use the density ρ (2.9) and magnetisation $\mathbf{m}$ (2.10) as our final stochastic variables of interest, although we continue to use the polarisation $\mathbf{p}$ (2.11) instead of magnetisation as our Kramers-Moyal variable for the same reason as in 1d: the assumption that correlations between magnetisation

and density are not negligible. Note that the magnetisation and polarisation are now vector quantities, thus the definitions should be altered slightly to accommodate the shift to 2d.

As we are discussing the differences between a number of models, the form of our continuous equations will be kept general as long as possible. In the following, we define the probability of a particle at position $\mathbf{x}$ and time t selecting a new direction $\mathbf{v}$ with fixed magnitude a as

$$\mathcal{P}(\mathbf{r}, \mathbf{v}, t) = P\left(\mathbf{v}|\mathbf{M}(\mathbf{r}, t)\right) \tag{4.1}$$

where $P\left(\mathbf{v}|\mathbf{M}(\mathbf{r}, t)\right)$ is the probability of an individual particle choosing a direction $\mathbf{v}$ when the preferred direction is $\mathbf{M}(\mathbf{r}, t)$ (3.1, 3.5) and

$$\mathbf{M}(\mathbf{r}, t) = \mathcal{R}\left(\eta(\mathbf{r}, t)\right) \int d\mathbf{r}' \; N \; \mathbf{m}(\mathbf{r}', t) \; n(\mathbf{r}, \mathbf{r}', t) \tag{4.2}$$

is a continuous space version of the total neighbourhood magnetisation (3.3) from Chapter 3. Recall that N was the number of particles in the ABM system, and the neighbourhood magnetisation was defined such that changing N would not change $\mathbf{M}$.

The stochastic rotation matrix $\mathcal{R}(\eta_i(t))$ of random angle $\eta_i(t)$ also has a continuous stochastic angle function $\eta(\mathbf{r}, t)$ and the neighbourhood matrix $n_{\alpha\gamma}(t)$ (3.9) has been replaced by a neighbourhood function $n(\mathbf{r}, \mathbf{r}', t)$ whose definition depends on the choice of particle interaction. For the metric interaction defined in Section 3.1, it takes the form

$$n_{\text{met}}(\mathbf{r}, \mathbf{r}', t) = \Theta\left(R_0 - |\mathbf{r}' - \mathbf{r}|\right), \tag{4.3}$$

where R_0 is the constant interaction radius and a parameter of the metric model, and $\Theta(y)$ is the Heaviside function. For the topological interaction in Section 3.2, it takes the form

$$n_{\text{top}}(\mathbf{r}, \mathbf{r}', t) = \Theta\left(R(\mathbf{r}, t) - |\mathbf{r}' - \mathbf{r}|\right), \tag{4.4}$$

where $R(\mathbf{r}, t)$ is the variable interaction radius (equivalent to (3.8)), defined implicitly by the relation

$$N \int d\mathbf{r}' \; \rho(\mathbf{r} + \mathbf{r}', t)\Theta(R(\mathbf{r}, t) - |\mathbf{r}|) = c \tag{4.5}$$

where c is the fixed number of neighbours that each particle in the topological

ABM interacts with. In a steady system with $|\nabla^k \rho| \ll \rho$ for $k \geq 1$, we can approximately solve Equation (4.5) to get

$$R(\mathbf{r}, t) \approx \sqrt{\frac{c}{\pi \rho(\mathbf{r}, t) N}} + O\left(\frac{\nabla^2 \rho}{N^{\frac{3}{2}} \rho^{\frac{5}{2}}}\right). \tag{4.6}$$

4.1.1 Jump moments of probability density

To reduce the complexity of the master equation for density and magnetisation, we introduce an intermediate quantity, the probability density u, defined as

$$u(\mathbf{r}, \mathbf{v}, t) = \frac{1}{N} \sum_{\alpha=1}^{N} \delta\left(\mathbf{r} - \mathbf{r}_\alpha(t)\right) \delta\left(\mathbf{v} - \mathbf{v}_\alpha(t)\right). \tag{4.7}$$

From this quantity, the particle density ρ and magnetisation $\mathbf{m}$ can be easily found as

$$\rho(\mathbf{r}, t) = \int u(\mathbf{r}, \mathbf{v}, t)\ d\mathbf{v} \qquad \text{and} \qquad \mathbf{m}(\mathbf{r}, t) = \int \frac{\mathbf{v}}{a} u(\mathbf{r}, \mathbf{v}, t)\ d\mathbf{v}, \tag{4.8}$$

where a is the lattice spacing. On a lattice, the above integrals become sums over the possible directions. For a square lattice in 2d, $\mathbf{v} \in \{a\hat{\mathbf{x}}, a\hat{\mathbf{y}}, -a\hat{\mathbf{x}}, -a\hat{\mathbf{y}}\}$. As ρ and $\mathbf{m}$ are linear functions of u, the jump moments of ρ and $\mathbf{m}$ can also be obtained by summing over the jump moments of u. Thus, finding the jump moments of u will lead to the desired Langevin equations.

In a single time-step, one particle will reorient itself and move in the direction of its new orientation, as described in Section 3.1. This changes u on a given site according to

$$\delta u(\mathbf{r}, \mathbf{v}, t) = \begin{cases} \frac{1}{N} & \text{with probability } \mathcal{P}(\mathbf{r} - \mathbf{v}, \mathbf{v}, t)\rho(\mathbf{r} - \mathbf{v}, t) \\ -\frac{1}{N} & \text{with probability } u(\mathbf{r}, \mathbf{v}, t) \\ 0 & \text{otherwise} \end{cases} \tag{4.9}$$

where $\mathcal{P}(\mathbf{r} - \mathbf{v}, \mathbf{v}, t)\rho(\mathbf{r} - \mathbf{v}, t)$ is the probability that a particle on site $\mathbf{r} - \mathbf{v}$ changes its velocity to $\mathbf{v}$ and moves one site in that direction, $u(\mathbf{r}, \mathbf{v}, t)$ is the probability that a particle on site $\mathbf{r}$ chooses any new velocity and moves away, and there are no changes to $u(\mathbf{r}, \mathbf{v}, t)$ otherwise.

We expand the position variable of $\mathcal{P}$ and ρ in powers of $\mathbf{v}$ and truncate after the

third term. Thus, the first two jump moments of u are

$$\langle \delta u \rangle = \frac{1}{N}\left[\left(1 - \mathbf{v}\cdot\nabla + \frac{1}{2}\left(\mathbf{v}\cdot\nabla\right)^2\right)\left(\mathcal{P}\rho\right) - u\right] + O\left(\left(\mathbf{v}\cdot\nabla\right)^3\left(\mathcal{P}\rho\right)\right), \quad (4.10)$$

$$\left\langle \delta u^2 \right\rangle = \frac{1}{N^2}\left[\left(1 - \mathbf{v}\cdot\nabla + \frac{1}{2}\left(\mathbf{v}\cdot\nabla\right)^2\right)\left(\mathcal{P}\rho\right) + u\right] + O\left(\left(\mathbf{v}\cdot\nabla\right)^3\left(\mathcal{P}\rho\right)\right), \quad (4.11)$$

where a lack of arguments in the functions above and hereafter indicate that they are evaluated at position $\mathbf{r}$ and time t (and orientation vector $\mathbf{v}$ where relevant).

4.1.2 Field equation for particle density

Once we have found the jump moments of the probability density u, we can find the jump moments of the density ρ from (4.8). Summing over the possible values of $\mathbf{v}$, the first moment of the density becomes

$$\begin{aligned}
\langle \delta\rho(\mathbf{r},t)\rangle &= \sum_{\mathbf{v}} \langle \delta u(\mathbf{r},\mathbf{v},t)\rangle \\
&= \frac{1}{N}\sum_{\mathbf{v}}\left[\left(1 - \mathbf{v}\cdot\nabla + \frac{1}{2}(\mathbf{v}\cdot\nabla)^2\right)\left[\rho(\mathbf{r},t)\mathcal{P}(\mathbf{r},\mathbf{v},t)\right] - u(\mathbf{r},\mathbf{v},t)\right] + O\left(\nabla^3\right) \\
&= \frac{\rho}{N}\left[\mathcal{P}(\mathbf{r},a\hat{\mathbf{x}},t) + \mathcal{P}(\mathbf{r},-a\hat{\mathbf{x}},t) + \mathcal{P}(\mathbf{r},a\hat{\mathbf{y}},t) + \mathcal{P}(\mathbf{r},-a\hat{\mathbf{y}},\mathbf{r},t) - 1\right] \\
&\quad -\frac{a}{N}\left[\partial_x\left[\left(\mathcal{P}(\mathbf{r},a\hat{\mathbf{x}},t) - \mathcal{P}(\mathbf{r},-a\hat{\mathbf{x}},t)\right)\rho\right] + \partial_y\left[\left(\mathcal{P}(\mathbf{r},a\hat{\mathbf{y}},t) - \mathcal{P}(\mathbf{r},-a\hat{\mathbf{y}},t)\right)\rho\right]\right] \\
&\quad +\frac{a^2}{2N}\partial_{xx}\left[\left(\mathcal{P}(\mathbf{r},a\hat{\mathbf{x}},t) + \mathcal{P}(\mathbf{r},-a\hat{\mathbf{x}},t)\right)\rho\right] \\
&\quad +\frac{a^2}{2N}\partial_{yy}\left[\left(\mathcal{P}(\mathbf{r},a\hat{\mathbf{y}},t) + \mathcal{P}(\mathbf{r},-a\hat{\mathbf{y}},t)\right)\rho\right] + O\left(\nabla^3\right) \\
&= -\frac{a}{N}\nabla\cdot\mathbf{J} + \frac{a^2}{2N}\left[\partial_{xx}\rho_x + \partial_{yy}\rho_y\right] + O\left(\nabla^3\right), \qquad (4.12)
\end{aligned}$$

where $\mathbf{J}(\mathbf{r},t) = J_x\hat{\mathbf{x}} + J_y\hat{\mathbf{y}}$ is the particle flux defined by

$$J_x(\mathbf{r},t) = \rho(\mathbf{r},t)\left[\mathcal{P}\left(\mathbf{r},a\hat{\mathbf{x}},t\right) - \mathcal{P}\left(\mathbf{r},-a\hat{\mathbf{x}},t\right)\right] \quad (4.13)$$

$$J_y(\mathbf{r},t) = \rho(\mathbf{r},t)\left[\mathcal{P}\left(\mathbf{r},a\hat{\mathbf{y}},t\right) - \mathcal{P}\left(\mathbf{r},-a\hat{\mathbf{y}},t\right)\right] \quad (4.14)$$

and ρ_x and ρ_y are the directional particle densities,

$$\rho_x(\mathbf{r},t) = \rho(\mathbf{r},t)\left[\mathcal{P}\left(\mathbf{r},a\hat{\mathbf{x}},t\right) + \mathcal{P}\left(\mathbf{r},-a\hat{\mathbf{x}},t\right)\right], \quad (4.15)$$

$$\rho_y(\mathbf{r},t) = \rho(\mathbf{r},t)\left[\mathcal{P}\left(\mathbf{r},a\hat{\mathbf{y}},t\right) + \mathcal{P}\left(\mathbf{r},-a\hat{\mathbf{y}},t\right)\right], \quad (4.16)$$

Their definitions depend on the model choice through $\mathcal{P}$, as laid out in Chapter 3. For now, they will be kept general.

Assuming that $u(\mathbf{r}, \mathbf{v}, t)$ and $u(\mathbf{r}, \mathbf{v}', t)$ are weakly correlated for $\mathbf{v} \neq \mathbf{v}'$,

$$\begin{aligned}
\left\langle \delta\rho(\mathbf{r}, t)^2 \right\rangle &= \sum_{\mathbf{v}} \sum_{\mathbf{v}'} \langle \delta u(\mathbf{r}, \mathbf{v}, t) \delta u(\mathbf{r}, \mathbf{v}', t) \rangle \\
&= \sum_{\mathbf{v}} \left\langle \delta u(\mathbf{r}, \mathbf{v}, t)^2 \right\rangle + \sum_{\mathbf{v} \neq \mathbf{v}'} \langle \delta u(\mathbf{r}, \mathbf{v}, t) \delta u(\mathbf{r}, \mathbf{v}', t) \rangle \\
&= \frac{1}{N^2} \sum_{\mathbf{v}} \left[\mathcal{P}(\mathbf{r}, \mathbf{v}, t) \rho(\mathbf{r}, t) + u(\mathbf{r}, \mathbf{v}, t) + O\left(\mathbf{v} \cdot \nabla(\rho \mathcal{P})\right) \right] \\
&\quad + \sum_{\mathbf{v} \neq \mathbf{v}'} \langle \delta u(\mathbf{r}, \mathbf{v}, t) \rangle \langle \delta u(\mathbf{r}, \mathbf{v}', t) \rangle \\
&= \frac{2\rho}{N^2} + \frac{1}{N^2} O\left(\nabla \cdot \mathbf{J}\right). \qquad (4.17)
\end{aligned}$$

The derivative terms in Equation (4.17) are negligible compared to the leading term for systems in the ordered phase. Thus, we truncate the second jump moment of ρ at the first order term.

Taking $\delta t = \frac{1}{N}$ and $a = 1$, the stochastic equation for ρ is

$$\begin{aligned}
\partial_t \rho &= -\nabla \cdot \mathbf{J} + \frac{1}{2} \left[\partial_{xx} \rho_x + \partial_{yy} \rho_y \right] + \sqrt{\frac{2\rho}{N}}\, \xi_\rho(\mathbf{r}, t) \\
&\approx -\nabla \cdot \mathbf{J} + \frac{1}{2} \left[\partial_{xx} \rho_x + \partial_{yy} \rho_y \right], \qquad (4.18)
\end{aligned}$$

where we have neglected the stochastic term again here as in (2.22), due to density conservation and its small magnitude compared to the deterministic term. Note that when motion is confined to a single axis, (4.18) matches the equation for density evolution in 1d (2.22). We have kept the diffusive terms here as they were found in 1d to have been necessary and sufficient to replicate the quantitative behaviour observed in the 1d ABM.

4.1.3 Field equation for magnetisation

Next, we obtain the first two jump moments of the magnetisation by summing over possible velocities as in the definition of the magnetisation field (4.8), where we assume again that $u(\mathbf{r}, \mathbf{v}, t)$ and $u(\mathbf{r}, \mathbf{v}', t)$ are weakly correlated for $\mathbf{v} \neq \mathbf{v}'$. Under this assumption and using the equations for the moments of u (4.10, 4.11),

the first two moments of $\mathbf{m}$ are given by

$$\begin{aligned}\langle \delta\mathbf{m}(\mathbf{r},t)\rangle &= \sum_{\mathbf{v}} \mathbf{v}\,\langle \delta u(\mathbf{r},\mathbf{v},t)\rangle \\ &= \frac{1}{N}\sum_{\mathbf{v}}\left[\mathbf{v}\left(1-\mathbf{v}\cdot\nabla+\frac{1}{2}(\mathbf{v}\cdot\nabla)^2\right)[\mathcal{P}\rho]-\mathbf{v}u\right]+O\left(\nabla^3\right) \\ &= \frac{1}{N}\left[\mathbf{J}-\mathbf{m}\right]-\frac{1}{N}\left[\partial_x\rho_x\hat{\mathbf{x}}+\partial_y\rho_y\hat{\mathbf{y}}\right]+\frac{1}{2N}\left[\partial_{xx}J_x\hat{\mathbf{x}}+\partial_{yy}J_y\hat{\mathbf{y}}\right]+O\left(\nabla^3\right), \end{aligned} \tag{4.19}$$

and

$$\begin{aligned}\left\langle \delta m(\mathbf{r},t)^2\right\rangle &= \left\langle\left(\sum_{\mathbf{v}}\mathbf{v}\delta u(\mathbf{r},\mathbf{v},t)\right)^2\right\rangle \\ &= \sum_{\mathbf{v}}\left\langle\delta u(\mathbf{r},\mathbf{v},t)^2\right\rangle+\sum_{\mathbf{v}\neq\mathbf{v}'}\mathbf{v}\cdot\mathbf{v}'\,\langle\delta u(\mathbf{r},\mathbf{v},t)\delta u(\mathbf{r},\mathbf{v}',t)\rangle \\ &= \frac{2\rho}{N^2}+\sum_{\mathbf{v}\neq\mathbf{v}'}\mathbf{v}\cdot\mathbf{v}'\,\langle\delta u(\mathbf{r},\mathbf{v},t)\rangle\,\langle\delta u(\mathbf{r},\mathbf{v}',t)\rangle+O\left(\frac{\nabla}{N^2}\right) \\ &= \frac{2\rho}{N^2}+O\left(\frac{\nabla}{N^2}\right)\approx\left\langle\delta\rho(\mathbf{r},t)^2\right\rangle, \end{aligned} \tag{4.20}$$

where $a=1$ as before and we truncate the second moment of $\mathbf{m}$ to include only constant terms as in the second moment of density (4.12). Note that, as in the 1d system, $\langle\delta m(\mathbf{r},t)^2\rangle\approx\langle\delta\rho(\mathbf{r},t)^2\rangle$ to $O\left(\frac{\nabla\cdot\mathbf{J}}{N^2},\frac{\partial_j\rho_j}{N^2}\right)$.

However, as in 1d, we cannot assume that correlations between $\rho(\mathbf{r},t)$ and $\mathbf{m}(\mathbf{r},t)$ are negligible and therefore cannot assume the Fokker-Planck diffusion matrix is approximately diagonal. Thus, we must find the jump moments for the polarisation $\mathbf{p}$ to perform the Kramers-Moyal expansion. These can be obtained from $\langle\delta\rho\rangle$, $\langle\delta\mathbf{m}\rangle$, $\langle\delta\rho^2\rangle$ and $\langle\delta m^2\rangle$ as in 1d (2.31, 2.32) through

$$\delta\mathbf{p}=\frac{\delta\mathbf{m}-\mathbf{p}\delta\rho}{\rho}+\frac{\delta\rho}{\rho^2}O\left(\delta\rho,\delta\mathbf{m}\right), \tag{4.21}$$

$$\begin{aligned}\langle\delta\mathbf{p}\rangle=&\frac{1}{N\rho}\mathbf{J}-\frac{1}{N}\mathbf{p}-\frac{\partial_x\rho_x\hat{\mathbf{x}}+\partial_y\rho_y\hat{\mathbf{y}}}{N\rho}+\frac{\partial_{xx}J_x\hat{\mathbf{x}}+\partial_{yy}J_y\hat{\mathbf{y}}}{2N\rho} \\ &-\frac{\mathbf{p}}{N\rho}\left[-\nabla\cdot\mathbf{J}+\frac{\partial_{xx}\rho_x+\partial_{yy}\rho_y}{2}\right]+O\left(\partial_j^3,N^{-2}\right), \end{aligned} \tag{4.22}$$

$$\left\langle\delta p^2\right\rangle=\frac{2}{N^2\rho}\left(1-p^2\right)+O\left(\partial_j\right). \tag{4.23}$$

We obtain an equation for the evolution of $\mathbf{p}$ through the above equations

(4.224.23) and the Kramers-Moyal approximation (2.14). The presence of the density ρ in the denominator of $\langle \delta \mathbf{p} \rangle$ suggests that, while $\mathbf{p}$ is the correct variable to use in the Kramers-Moyal expansion, it is not a natural variable to describe the system. Using the Itô transformation [89] again on the Langevin equation for polarisation gives us our equation for magnetisation, taking $\delta t = \frac{1}{N}$ as

$$\begin{aligned} \partial_t \mathbf{m} &= \mathbf{J} - \mathbf{m} - \partial_x \rho_x \hat{\mathbf{x}} - \partial_y \rho_y \hat{\mathbf{y}} + \frac{1}{2}\partial_{xx} J_x \hat{\mathbf{x}} + \frac{1}{2}\partial_{yy} J_y \hat{\mathbf{y}} \\ &\quad + \sqrt{\frac{2}{N\rho}\left(\rho^2 - m^2\right)}\, \boldsymbol{\xi}(\mathbf{r}, t), \end{aligned} \tag{4.24}$$

where $\boldsymbol{\xi}(\mathbf{r}, t)$ is a two-component vector whose components are drawn from a Gaussian white noise distribution and satisfy the relations

$$\langle \xi_i(\mathbf{r}, t) \rangle = 0 \qquad \text{and} \qquad \langle \xi_i(\mathbf{r}, t) \xi_j(\mathbf{r}', t') \rangle = \delta_{ij} \delta(\mathbf{r} - \mathbf{r}') \delta(t - t'). \tag{4.25}$$

When confined to a single dimension, (4.24) also reduces to our 1d equation for magnetisation (2.34).

4.1.4 Review of key assumptions

Before we begin to examine these equations in greater detail, we should review the assumptions made in their derivation. It is important that we do not make more assumptions than are required, nor make assumptions that cannot be justified.

Recall that, in Section 2.2, we demonstrated that the 1d Langevin equations (2.22, 2.34) obtained from the Kramer-Moyal approximation quantitatively matched the behaviour of the ABM (see Fig. 2.4). These equations, and the 2d Langevin equations above (4.18, 4.24), were truncated at second order in both the Kramers-Moyal approximation and the spatial expansion from a discrete lattice to continuous space.

The Kramers-Moyal truncation can be assumed provided the fluctuations are small and their derivatives become decreasingly small with increasing number of derivatives (see [14] for an example of this method). Without the approximation of the Kramers-Moyal expansion, a Fokker-Planck equation cannot be obtained, hence no Langevin equations and we are unable to directly simulate trajectories of the system. As such, truncating the Kramers-Moyal expansion to second order is necessary for the rest of the analysis.

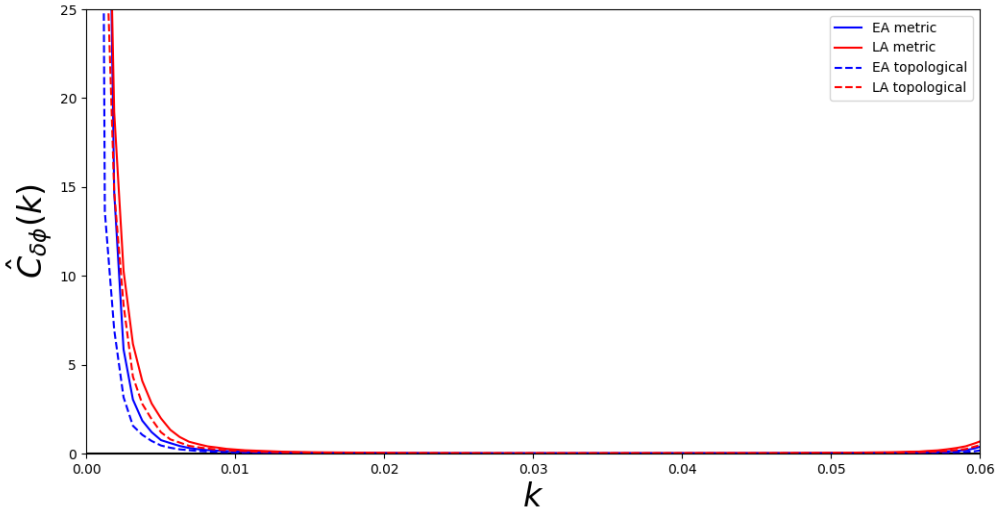

Figure 4.1 *The real values of the Fourier-transformed spatial correlation function of fluctuations in particle direction in our ABMs. The fluctuations are shown to be long-range, as indicated by the rapid decrease as k increases. Rising values for large k are due to the periodicity of the lattice. $N = L_x = L_y = 100$, $\beta = 0.75$, $\eta = 0.02$.*

The truncation of the spatial expansion in going from a lattice to continuous space is suitable for systems where any sufficiently large fluctuations are long-ranged (and hence, high order derivatives of such fluctuations rapidly die off). Typical fluctuations in the ordered state of the ABM systems in Chapter 3 are long-ranged (see Fig. 4.1), thus we are confident that truncation to second-order in the spatial expansion are justified here.

To ensure that the global density is conserved while also assuming that the density fluctuations are decoupled, the stochastic term of our density equation (4.18) must be negligible compared to the deterministic term and need not be included. We previously assumed in the 1d Langevin equation for density (2.22) that excluding the stochastic term led to a system of equations that matched the ABM, therefore we exclude the stochastic term in the 2d Langevin equation (4.18) as the details of particle motion have not changed significantly in our 2d ABMs from our 1d ABM and N is still sufficiently large that $N^{-2} \ll N^{-1}$.

The final key assumption, also made in the 1d equations, is that the diffusion matrix in the Fokker-Planck equation is diagonal, allowing for a straightforward matrix decomposition (2.13). This assumption relies on the density and polarisation on neighbouring sites being decoupled, and hence their correlators are negligible compared to the self-correlations in the large N limit. The reasoning

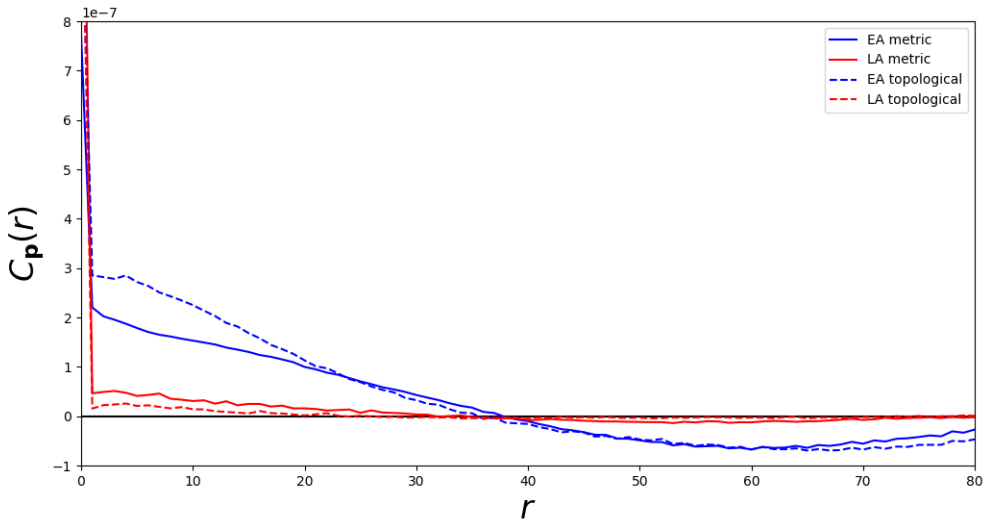

Figure 4.2 *Autocorrelation function of polarisation (4.26) within our ABMs. The correlation function drops sharply for $r \neq 0$, therefore correlations between neighbouring sites are significantly smaller than self-correlations.$N = L_x = L_y = 100$, $\beta = 0.75$, $\eta = 0.02$.*

behind the above assumption are clear in the 1d system, where the polarisation changes on a site were dependent on the polarisation of other particles on that site only.

In the 2d systems in Chapter 3, the polarisation on a site i depends on particles that sit within a fixed radius R or the nearest c particles, where c is fixed. In general, these neighbouring particles will not lie on the same lattice site, thus it is less clear that the correlations between polarisation on neighbouring sites should be negligible. Indeed, real-life flocks often have long-range correlations [11, 22]. However, we can see from Fig. 4.2 that the spatial auto-correlation function,

$$C(\mathbf{r}) = \frac{1}{L_x L_y T} \int_0^T dt \int d\mathbf{r}' \ \langle (\mathbf{p}(\mathbf{r}', t) - \bar{\mathbf{p}}(t)) \cdot (\mathbf{p}(\mathbf{r}' + \mathbf{r}, t) - \bar{\mathbf{p}}(t)) \rangle \,, \qquad (4.26)$$

drops off sharply for $|\mathbf{r}| > 0$, hence we have made the same assumption here as in the 1d equations. In the above, $\bar{\mathbf{p}}(t)$ is the mean polarisation at time t.

4.2 Comparison between interaction types

We now turn to how the different ABMs from Chapter 3 are implemented in these equations. We focus here on how $\mathbf{J}$ and $\rho_{x,y}$ differ between the linearly-aligning

(LA) and the exponentially-aligning (EA) models, and how the neighbourhood definition affects the total neighbourhood magnetisation field $\mathbf{M}(\mathbf{r}, t)$. As a reminder, the probability that a particle α in the ABM with position $\mathbf{r}_\alpha$ and velocity $\mathbf{v}_\alpha$ at time t will take a new velocity $\mathbf{v}'_\alpha$ is denoted by $P(\mathbf{v}'_\alpha|\mathbf{M}(\mathbf{r}_\alpha, t))$, where the function P depends on the model choice. This has been extended to continuous space through Equation (4.1).

4.2.1 EA model

In the EA model as set out in Chapter 3, the directional probability function P is given by Equation (3.5). A continuous version of this probability can be expressed as

$$\mathcal{P}(\mathbf{r}, \mathbf{v}, t) = \frac{e^{\beta \mathbf{v}\cdot\mathbf{M}(\mathbf{r},t)}}{2\cosh\beta M_x(\mathbf{r}, t) + 2\cosh\beta M_y(\mathbf{r}, t)}. \tag{4.27}$$

Therefore, the particle flux $\mathbf{J}$ (4.13, 4.14) and directional density $\rho_{x,y}$ (4.15, 4.16) for the EA model become

$$J_x(\mathbf{r}, t) = \frac{\rho(\mathbf{r}, t)\sinh\beta M_x(\mathbf{r}, t)}{\cosh\beta M_x(\mathbf{r}, t) + \cosh\beta M_y(\mathbf{r}, t)}, \tag{4.28}$$

$$J_y(\mathbf{r}, t) = \frac{\rho(\mathbf{r}, t)\sinh\beta M_y(\mathbf{r}, t)}{\cosh\beta M_x(\mathbf{r}, t) + \cosh\beta M_y(\mathbf{r}, t)}, \tag{4.29}$$

and

$$\rho_x(\mathbf{r}, t) = \frac{\rho(\mathbf{r}, t)\cosh\beta M_x(\mathbf{r}, t)}{\cosh\beta M_x(\mathbf{r}, t) + \cosh\beta M_y(\mathbf{r}, t)}, \tag{4.30}$$

$$\rho_y(\mathbf{r}, t) = \frac{\rho(\mathbf{r}, t)\cosh\beta M_y(\mathbf{r}, t)}{\cosh\beta M_x(\mathbf{r}, t) + \cosh\beta M_y(\mathbf{r}, t)}. \tag{4.31}$$

The above equations are highly dependent on the magnitude of $\mathbf{M}(\mathbf{r}, t)$, as increasing the neighbourhood magnetisation by a multiplicative factor κ (e.g. by multiplying the number of particles in that neighbourhood by κ) is equivalent to multiplying β by κ. β acts here similar to inverse temperature in equilibrium statistical mechanics. As such, anything that increases $\mathbf{M}$ by $\kappa > 1$ is equivalent to multiplying the "temperature" by the reciprocal of κ, leading to a higher degree of order.

4.2.2 LA model

In the LA, the directional probability function P is given by Equation (3.5). A continuous version of this probability can be expressed as

$$\mathcal{P}(\mathbf{r}, \mathbf{v}, t) = \frac{\max\{\mathbf{v} \cdot \mathbf{M}(\mathbf{r}, t), 0\}}{|M_x(\mathbf{r}, t)| + |M_y(\mathbf{r}, t)|}. \tag{4.32}$$

Therefore, for the LA model, $\mathbf{J}$ and $\rho_{x,y}$ become

$$J_x(\mathbf{r}, t) = \frac{\rho(\mathbf{r}, t)\mathbf{M}(\mathbf{r}, t)}{|M_x(\mathbf{r}, t)| + |M_y(\mathbf{r}, t)|},, \tag{4.33}$$

$$J_y(\mathbf{r}, t) = \frac{\rho(\mathbf{r}, t)\mathbf{M}(\mathbf{r}, t)}{|M_x(\mathbf{r}, t)| + |M_y(\mathbf{r}, t)|},, \tag{4.34}$$

and

$$\rho_x(\mathbf{r}, t) = \frac{\rho(\mathbf{r}, t)|M_x(\mathbf{r}, t)|}{|M_x(\mathbf{r}, t)| + |M_y(\mathbf{r}, t)|}, \tag{4.35}$$

$$\rho_y(\mathbf{r}, t) = \frac{\rho(\mathbf{r}, t)|M_y(\mathbf{r}, t)|}{|M_x(\mathbf{r}, t)| + |M_y(\mathbf{r}, t)|}. \tag{4.36}$$

As we observed when we introduced the LA in Section 3.1.2, the probability of a particular direction being chosen is unchanged by a rescaling of the neighbourhood magnetisation $\mathbf{M}$. We note here that, as the field equations depend on the particle flux $\mathbf{J}$ and directional densities $\rho_{x,y}$ and their derivatives, the behaviour of the density and magnetisation fields also should not depend on the magnitude of $\mathbf{M}$.

A consequence of the lack of dependence of the field variables on the magnitude of $\mathbf{M}$ is that the density and magnetisation fluctuations can be rescaled such that the deterministic terms in our Langevin equations (4.18, 4.24) are independent of the mean density $\rho_0 = \frac{1}{NL_xL_y}$. Although the model uses a metric interaction neighbourhood, as described in Section 3.1.2, robustness to system-size scaling is a feature typically associated with topological interactions [4]. As topological interactions in polar SPP systems lead to the ability to macroscopically turn, we suspect this robustness contributes to the LA flocks turning.

4.3 Stability analysis

To better understand the deterministic and stochastic effects of the two models, we first examine the stability of the ordered flock to an infinitesimal perturbation. We expect that, for a stable flock to exist, the magnitude of $\mathbf{p}$ should change very little in time, while the angle $\phi = \arctan\frac{p_y}{p_x} = \arctan\frac{m_y}{m_x}$ will be either stable or unstable to a sufficiently large fluctuation for non-turning and turning models respectively. To quantify the stability of the system to fluctuations introduced by the stochastic terms of our equations, we consider how small fluctuations of ρ and $\mathbf{m}$ about a fixed steady state behave under our equations of motion.

Under the assumption that fluctuations in our field variables are sufficiently small, ρ and $\mathbf{m}$ can be represented by

$$\rho(\mathbf{r},t) = \rho_0 + \delta\rho(\mathbf{r},t) \tag{4.37}$$

and

$$\mathbf{m}(\mathbf{r},t) = \mathbf{m}_0 + \delta\mathbf{m}(\mathbf{r},t) = (m_0 + \delta m)\begin{pmatrix}\cos(\phi_0+\delta\phi)\\ \sin(\phi_0+\delta\phi)\end{pmatrix}, \tag{4.38}$$

where the fluctuations $|\delta\rho| \ll \rho_0$, $|\delta m| \ll m_0$ and $|\delta\phi| \ll 1$. These definitions also lead to the polarisation field taking the form

$$\mathbf{p}(\mathbf{r},t) = \mathbf{p}_0 + \delta\mathbf{p}(\mathbf{r},t) = \frac{\mathbf{m}_0}{\rho_0} + \frac{\rho_0\delta\mathbf{m} - \mathbf{m}_0\delta\rho}{\rho_0^2} + O\left(\frac{\delta\rho\delta\mathbf{m}}{\rho_0^2}, \frac{\mathbf{m}_0\delta\rho^2}{\rho_0^3}\right). \tag{4.39}$$

We keep only terms that are linear in a small term (i.e. $\frac{\delta\rho}{\rho_0}$, $\frac{\delta m}{|m_0|}$ or $\delta\phi$) to observe the dominant behaviour near the ordered steady state (where $\delta\rho = \delta\mathbf{m} = 0$).

4.3.1 Fluctuations to the neighbourhood magnetisation M

To observe the behaviour near the steady state, we examine how the fluctuations affect (4.18, 4.24). We start by exploring how $R(\mathbf{r},t)$ changes. Recall from Sections 1.2.4 and 3.2, the metric and topological interactions have a fixed and varying radius of interaction respectively. Thus, $R(\mathbf{r},t)$ can be expanded to linear order as

$$R(\mathbf{r},t) = \begin{cases} R_0 + \delta R & \text{topological interaction} \\ R_0 & \text{metric interaction} \end{cases} \tag{4.40}$$

where

$$R_0 = \sqrt{\frac{c}{\pi\rho_0 N}} \qquad \text{and} \qquad \delta R \approx -\sqrt{\frac{c}{4\pi\rho_0^3 N}}\delta\rho = -\frac{R_0}{2\rho_0}\delta\rho, \tag{4.41}$$

with corrections to δR of order $\frac{R_0}{\rho_0^2}\nabla^2\delta\rho$. We subsequently generalise (4.40) by defining topological and metric radius fluctuations as $\delta R_{\rm t} = \delta R$ and $\delta R_{\rm m} = 0$ respectively.

We next derive the behaviour of the neighbourhood magnetisation $\mathbf{M}(\mathbf{r},t)$. We assume without loss of generality that $\phi_0 = 0$, i.e. the mean direction of motion is along the $\hat{\mathbf{x}}$-axis, giving $\mathbf{m}_0 = m_0\hat{\mathbf{x}}$. To linear order, the change in magnetisation $\mathbf{m}$ can be expressed in component form as

$$\mathbf{m}(\mathbf{r},t) = (m_0 + \delta m(\mathbf{r},t))\,\hat{\mathbf{x}} + m_0\delta\phi(\mathbf{r},t)\hat{\mathbf{y}}. \tag{4.42}$$

Hence, the neighbourhood magnetisation $\mathbf{M}(\mathbf{r},t)$ (4.2) can be expressed as

$$\begin{aligned}
\mathbf{M}(\mathbf{r},t) &\approx \mathcal{R}(\eta)\Bigg[\pi N m_0 R_0^2\hat{\mathbf{x}} + 2\pi N m_0 R_0\delta R(\mathbf{r},t)\hat{\mathbf{x}} + \sum_{\mathbf{r}'} N\delta m(\mathbf{r}+\mathbf{r}',t)\Theta(R_0 - |\mathbf{r}'|)\hat{\mathbf{x}} \\
&\quad + N m_0 \sum_{\mathbf{r}'} \delta\phi(\mathbf{r}+\mathbf{r}',t)\Theta(R_0 - |\mathbf{r}'|)\hat{\mathbf{y}}\Bigg] \\
&= [\cos\eta\,(M_0 + \delta M(\mathbf{r},t)) - m_0\sin\eta\;\delta\Phi(\mathbf{r},t)]\,\hat{\mathbf{x}} \\
&\quad + [m_0\cos\eta\;\delta\Phi(\mathbf{r},t) + \sin\eta\,(M_0 + \delta M(\mathbf{r},t))]\,\hat{\mathbf{y}},
\end{aligned} \tag{4.43}$$

where δM and $\delta\Phi$ are the neighbourhood magnetisation fluctuations in magnitude (including due to density fluctuations) and angle respectively. Note that we have removed the dependence on δR in the neighbourhood fluctuations, as any effects it would have involve higher order powers of small terms. As we are concerned with understanding the system's behaviour in the ordered state where $\eta \ll 1$, we next expand the rotation matrix in powers of η, dropping terms of $O(\eta^2)$ and $O(\eta\;\delta m, \eta\;\delta\phi)$. Thus (4.43) becomes

$$\mathbf{M}(\mathbf{r},t) = [M_0 + \delta M(\mathbf{r},t)]\,\hat{\mathbf{x}} + [M_0\eta(\mathbf{r},t) + m_0\delta\Phi(\mathbf{r},t)]\,\hat{\mathbf{y}}. \tag{4.44}$$

Recall that in Section 3.1, we kept η as the stochastic control parameter for the LA and set it to zero for the EA (in which we use thermodynamic β as the control parameter instead).

In the absence of noise (where $\mathcal{R}(\eta) = \mathcal{I}_2$), the fluctuations in the interaction

radius R due to the density only affect the neighbourhood magnetisation in the mean direction of propagation (i.e. the direction of $\mathbf{m}_0$). The inverse is also true, namely that the switch from a metric to topological interaction in a low rotational noise system should primarily affect the magnitude, not the orientation, of $\mathbf{M}$ at linear order. Therefore, any terms in our Langevin equations (4.18, 4.24) that depend on the orientation of $\mathbf{M}$ should not cause any difference in the behaviour observed due to a different interaction neighbourhood definition.

4.3.2 Fluctuations to particle flux and directional density

The next step in obtaining linearised field equations for the density and magnetisation is to examine the linearised forms of $\mathbf{J}$ and $\rho_{x,y}$. This is highly model dependent, and as such, we must discuss each interaction type separately here.

LA model

Recall the exact definition of $\mathbf{J}(\mathbf{r},t)$ (4.33, 4.34) and $\rho_{x,y}(\mathbf{r},t)$ (4.35, 4.36) for this model. Making the substitutions $\rho = \rho_0 + \delta\rho$, $M_x = M_0 + \delta M_x$ and $M_y = \delta M_y$ in those equations, noting that $M_0 \gg |\delta M_x| > 0$ and keeping terms up to linear order in $\delta\rho$, δM_x and δM_y, these become

$$J_x(\mathbf{r},t) = \rho_0 + \delta\rho - \frac{\rho_0|\delta M_y|}{M_0}, \qquad J_y(\mathbf{r},t) = \frac{\rho_0 \delta M_y}{M_0}, \tag{4.45}$$

$$\rho_x(\mathbf{r},t) = \rho_0 + \delta\rho - \frac{\rho_0|\delta M_y|}{M_0}, \qquad \rho_y(\mathbf{r},t) = \frac{\rho_0|\delta M_y|}{M_0}. \tag{4.46}$$

There are two main things to note here. Firstly, $M_0 > |\delta M_x| \implies |M_x| = M_x$ and hence $\rho_x = J_x$. In physical terms, there are no particles moving directly against the flow in the ordered state. The second, and more important thing, to notice is that none of the terms above depend on δM_x, and hence δR, to linear order. As we reasoned above, this suggests that a change from a metric to a topological interaction should have no effect on the behaviour of the ordered state at the linear level. Indeed, this is observed in the LA ABM, as demonstrated in Chapter 3.

EA model

Recall the exact definition of $\mathbf{J}(\mathbf{r},t)$ (4.28, 4.29) and $\rho_{x,y}(\mathbf{r},t)$ (4.30, 4.31) for this model. Making the substitutions $\rho = \rho_0 + \delta\rho$, $M_x = M_0 + \delta M$ and $M_y = \delta M_y$ in those equations, noting that $M_0 \gg |\delta M_x| > 0$ and keeping terms up to linear order in $\delta\rho$, δM_x and δM_y, these become

$$J_x(\mathbf{r},t) = (\rho_0 + \delta\rho)\tanh\left(\frac{\beta M_0}{2}\right) + \frac{\beta\rho_0\delta M_x}{1+\cosh\beta M_0}, \tag{4.47}$$

$$J_y(\mathbf{r},t) = \frac{\beta\rho_0\delta M_y}{1+\cosh\beta M_0}, \tag{4.48}$$

$$\rho_x(\mathbf{r},t) = \frac{(\rho_0+\delta\rho)\cosh\beta M_0}{1+\cosh\beta M_0} + \frac{\beta\rho_0\tanh\left(\frac{\beta M_0}{2}\right)\delta M_x}{1+\cosh\beta M_0}, \tag{4.49}$$

$$\rho_y(\mathbf{r},t) = \frac{\rho_0+\delta\rho}{1+\cosh\beta M_0} - \frac{\beta\rho_0\tanh\left(\frac{\beta M_0}{2}\right)\delta M_x}{1+\cosh\beta M_0}. \tag{4.50}$$

Unlike the LA, the EA model contains terms that are linear in δM_x and hence δR. While this does not suggest that a difference in behaviour between a metric and topological interaction *must* be observed in trajectories of the system, it highlights a discrepancy at linear order that could cause such a difference to appear. Given that the behaviour of the EA ABM differs under the above change while the LA ABM does not (Section 3.2), we propose that this change at linear order could be responsible for the macroscopic change observed.

4.3.3 Linearised equations and dispersion relations

Now that we have a form for our particle current and directional densities, we can examine the linearised field equations. We wish to show that, for a stable state where $\delta\rho$ and $|\delta\mathbf{m}|$ do not grow in time, $\delta\phi$ will be stable for the metric EA model and unstable for the other three model choices (topological EA, topological LA, metric LA). These findings would show that linear stability is sufficient to explain the different behaviours observed in the ABMs. We neglect the effects of the stochastic function $\boldsymbol{\xi}(\mathbf{r},t)$ here, as we wish to study the deterministic mean-field effects first.

Consider a function $f(\mathbf{r},t)$. We can express this function as a sum of its Fourier

components $\hat{f}_{\lambda,\mathbf{k}}$ as

$$f(\mathbf{r},t) = \sum_{\lambda,\mathbf{k}} \hat{f}_{\lambda,\mathbf{k}} e^{\lambda t} e^{i\mathbf{k}\cdot\mathbf{r}}. \tag{4.51}$$

If a mode $\hat{f}_{\lambda,\mathbf{k}} \neq 0$, the contribution of that mode to the function will grow or shrink in time depending on whether λ takes a positive or negative value respectively. We can plug Fourier expressions of $\delta\rho$, δm and $\delta\phi$ into (4.18, 4.24) and solve these equations to find values of λ in terms of $\mathbf{k}$ for which $\hat{f}_{\lambda,\mathbf{k}} \neq 0$. These values of λ are known as "dispersion relations", and they can tell us about the behaviour of the untransformed functions. If no value of $\mathbf{k}$ gives a value of λ with positive real part, the functions do not grow in time. Otherwise, there is at least one Fourier mode that grows exponentially in time and the function is not linearly stable.

Returning to the component form of the linearised neighbourhood magnetisation (4.43), we expand δR, δm and $\delta\phi$ in Fourier components. We then approximate the sum over all lattice sites $\mathbf{r}$ as an integral over space to obtain the Fourier components of the fluctuations of $\mathbf{M}$ as

$$\delta M(\mathbf{r},t) \approx 2\pi m_0 N R_0^2 \sum_{\lambda,\mathbf{k}} \left[\frac{\hat{\delta R}_{\lambda,\mathbf{k}}}{R_0} + \frac{J_1(kR_0)}{kR_0} \frac{\hat{\delta m}_{\lambda,\mathbf{k}}}{m_0} \right] e^{\lambda \mathbf{t}} e^{i\mathbf{k}\cdot\mathbf{r}}, \tag{4.52}$$

where $J_1(x)$ is the first Bessel function of the first kind, $k = |\mathbf{k}|$, and $\delta R_{\lambda,\mathbf{k}}$ is the Fourier transformation of $\delta R(\mathbf{r},t)$, which is zero for the metric interaction. Similarly,

$$\delta\Phi(\mathbf{r},t) \approx 2\pi N R_0^2 \sum_{\lambda,\mathbf{k}} \frac{J_1(kR_0)}{kR_0} \hat{\delta\phi}_{\lambda,\mathbf{k}}\, e^{\lambda t} e^{i\mathbf{k}\cdot\mathbf{r}}. \tag{4.53}$$

With these approximations, we can obtain dispersion relations for our PDEs. These will enable us to understand the linear stability of the equations.

LA model

To linear order, (4.18, 4.24) become

$$\partial_t \delta\rho = \left(-\partial_x + \frac{1}{2}\partial_{xx}\right)\delta\rho + \frac{\rho_0}{N\pi R_0^2}\left[-\partial_y\left(\delta\Phi + N\pi R_0^2\eta\right) + \frac{1}{2}\partial_{yy}|\delta\Phi + N\pi R_0^2\eta|\right], \tag{4.54}$$

$$\partial_t \delta m = \rho_0 - m_0 + \left(1 - \partial_x + \frac{1}{2}\partial_{xx}\right)\left(\delta\rho - \frac{\rho_0}{N\pi R_0^2}|\delta\Phi + N\pi R_0^2\eta|\right) - \delta m, \tag{4.55}$$

$$\partial_t \delta\phi = \frac{\rho_0}{N\pi m_0 R_0^2}\left[\left(1 + \frac{1}{2}\partial_{yy}\right)\left(\delta\Phi + N\pi R_0^2\eta\right) - \partial_y|\delta\Phi + N\pi R_0^2\eta|\right] - \delta\phi. \tag{4.56}$$

We first define $\alpha = 1 - \frac{m_0}{\rho_0}$. m_0 is bounded above by ρ_0 and below by 0, therefore $0 < \alpha < 1$. The first two terms of (4.55) suggest that, unless $\alpha \ll 1$, δm will grow in magnitude until the linear approximation no longer holds. If instead α is on the same order of magnitude as one or more of the other terms in the equation, δm can remain bounded.

In the absence of rotational diffusive noise ($\eta = 0$), the time evolution of $\delta\phi$ depends only on $\delta\Phi$ to a linear scale, so we can attempt to solve it directly through Fourier expansion. Using the linear approximations to J_y (4.45) and ρ_y (4.46), the Fourier transform of the fluctuations of the neighbourhood magnetisation (4.53) and the linearised PDE for the angular fluctuations to the magnetisation (4.56), and expanding the Bessel function $J_1(kR_0)$ in the angular fluctuations of $\mathbf{M}$ in powers of k, the Fourier modes of $\delta\phi$ for small k satisfy the equation

$$\lambda = \alpha \mp ik_y - \frac{k_x^2 + 5k_y^2}{8} + O\left(k^3, \alpha k_y, \alpha^2\right), \tag{4.57}$$

where the sign of k_y depends on whether $|\delta\phi| = \pm\delta\phi$. This shows that, unless $m_0 = \rho_0$ exactly (i.e. $\alpha = 0$), λ will be positive for sufficiently small k. If we still consider the underlying lattice, the magnitude of k is bounded below by $k_{\min} = \frac{2\pi}{L}$ where L is the length of one side of the lattice. Thus, there is a corresponding $\alpha_{\min}$ such that for $\alpha > \alpha_{\min}$, Equation (4.57) indicates that $\delta\phi$ will grow in time.

Let's now examine what happens to δm. If we consider fluctuations $\delta\rho$, δm that are constant in space (the $k = 0$ mode of the Fourier expansion) and substitute

in the $k = 0$ modes of the fluctuations in $\mathbf{M}$ (4.52, 4.53), (4.55) reduces to

$$\partial_t \delta m \approx \rho_0 \partial_t \delta p \approx \rho_0 \left(\alpha - \delta p - \delta\phi\right). \tag{4.58}$$

Thus, a fluctuation δm that is constant in space can grow in magnitude until $\delta p + \delta\phi \approx \alpha$. As such, linear fluctuations in the direction of motion are bounded and cannot grow uncontrollably.

Typical values from the ordered state in the agent-based models have $\alpha \sim 0.1 - 0.2 \gg \frac{k_{\min}^2}{8}$ (see Fig. 3.6), thus there exist small values of $\mathbf{k}$ corresponding to Fourier modes of $\delta\phi$ that will cause growth. Hence, there exists a long wavelength instability that causes the flock as a whole to turn while remaining in a highly ordered state, as seen in the ABMs. As this does not depend on the value of δR, this is independent of interaction neighbourhood choice, also as observed in the ABMs in Chapter 3. Thus, the linear stability analysis is sufficient to explain flock turning in the LA.

One final note before we turn our attention to the EA model. We have not included the rotational noise η in the dispersion relation, as it is not necessary for the fluctuations in $\delta\phi$ to grow. Rather, it is responsible for generating the fluctuations in the first place, ensuring that the $\alpha = 0$ state, for which turning is not expected to occur, is not an absorbing state. The other form of noise in this equation, $\boldsymbol{\xi}$, has a multiplicative prefactor proportional to $\sqrt{\alpha}$, thus it cannot play this role.

EA model

In the equations below, we define $\tau = \tanh\left(\frac{\beta M_0}{2}\right)$ for brevity. By the properties of hyperbolic functions, this gives the following relations

$$\cosh \beta M_0 = \frac{1+\tau^2}{1-\tau^2} \qquad \text{and} \qquad \sinh \beta M_0 = \frac{2\tau}{1-\tau^2}. \tag{4.59}$$

As the rotational noise is not required for turning to be observed in the topological EA model (see Fig. 3.3), we will set $\eta = 0$ here. Then, as above, we can write

the linearised evolution equations (4.18, 4.24) as

$$\partial_t \delta\rho = \left[-\tau\partial_x + \frac{1+\tau^2}{4}\partial_{xx} + \frac{1-\tau^2}{4}\partial_{yy}\right]\delta\rho - \frac{\beta m_0\rho_0(1-\tau^2)}{2}\partial_y\delta\Phi + \frac{\beta\rho_0(1-\tau^2)}{2}\left[-\partial_x + \frac{\tau}{2}\left(\partial_{xx} - \partial_{yy}\right)\right]\delta M, \tag{4.60}$$

$$\partial_t \delta m = \tau\rho_0 - m_0 + \tau\left(1 - \frac{1+\tau^2}{2\tau}\partial_x + \frac{1}{2}\partial_{xx}\right)\delta\rho - \delta m + \frac{\beta\rho_0(1-\tau^2)}{2}\left(1 - \tau\partial_x + \frac{1}{2}\partial_{xx}\right)\delta M, \tag{4.61}$$

$$\partial_t \delta\phi = \frac{\beta\rho_0(1-\tau^2)}{2}\left(1 + \frac{1}{2}\partial_{yy}\right)\delta\Phi - \delta\phi - \frac{(1-\tau^2)}{2m_0}\partial_y\left(\delta\rho - \beta\rho_0\tau\delta M\right). \tag{4.62}$$

Let's examine the second equation (4.61). To keep the linear assumption (4.37, 4.38) valid, we must have $\left|\frac{m_0}{\rho_0} - \tau\right| \ll 1$, as the $k = 0$ terms must be on the same scale as the next order terms to keep the system stable. We define a small constant quantity $\alpha' = \tau - \frac{m_0}{\rho_0}$ and drop terms of $O\left(\alpha'^2\right)$. Unlike α in the LA, α' can be negative. Again, we wish for α' to be small, otherwise the linear assumption will not hold true.

As the evolution of $\delta\rho$, δm and $\delta\phi$ do not depend on their own value only, we cannot solve a single equation individually to obtain a dispersion relation. Instead, we solve this by a Fourier transform and subsequent matrix inversion. Taking $\alpha' = 0$, this gives the following singular matrix equation

$$\begin{pmatrix} A_{\rho,\rho} - \lambda & A_{\rho,p} & A_{\rho,\phi} \\ A_{p,\rho} & A_{p,p} - \lambda & A_{p,\phi} \\ A_{\phi,\rho} & A_{\phi,p} & A_{\phi,\phi} - \lambda \end{pmatrix} \begin{pmatrix} \hat{\delta\rho}_{\lambda,\mathbf{k}} \\ \hat{\delta p}_{\lambda,\mathbf{k}} \\ \hat{\delta\phi}_{\lambda,\mathbf{k}} \end{pmatrix} = 0. \tag{4.63}$$

The definitions of $A_{i,j}$ and method of obtaining the solution of this equation can be found in Appendix D.

The matrix A has three distinct eigenvalues, each corresponding to a different dispersion relation. To determine the dynamics of the system and whether our small quantities grow or shrink in time, we examine the real part of these eigenvalues. While the eigenvalues take complicated forms, we can expand them for low values of $\mathbf{k}$ and $\epsilon = 1 - \tau^2 \ll 1$. We can assume that τ is very close to 1 in the ordered state as, for $\alpha' = 0$, τ is solved by the transcendental equation

$$\tau = \frac{m_0}{\rho_0} = \tanh\left(\frac{\beta N\pi R_0^2 m_0}{2}\right) = \tanh\left(\frac{\beta c\tau}{2}\right), \tag{4.64}$$

and $\beta c > 2$ for the ordered state (see Section 3.1.1). In the low $\mathbf{k}$ and low ϵ approximation, the eigenvalues λ_i are approximately given by

$$\Re[\lambda_1(\mathbf{k})] = -\frac{1}{2}k_x^2 - \frac{\epsilon}{4}\left(1 - \mathcal{M}\tilde{\beta}\right)k_y^2 - \frac{\tilde{\beta}\epsilon^2}{64}\left(\tilde{\beta}R_0^2 + 4\left(\mathcal{M}\tilde{\beta} - 1\right)\right)k_y^4, \quad (4.65)$$

$$\Re[\lambda_2(\mathbf{k})] = \frac{\tilde{\beta}\epsilon}{2} - 1 - \frac{\tilde{\beta}\epsilon}{4}\left[\left(\frac{R_0^2}{4} + \epsilon\right)k_x^2 + \left(\frac{R_0^2}{4} + 1 - \epsilon\right)k_y^2\right], \quad (4.66)$$

$$\Re[\lambda_3(\mathbf{k})] = \frac{\tilde{\beta}\epsilon}{2} - 1 - \frac{\tilde{\beta}\epsilon R_0^2}{16}k_x^2 - \frac{\tilde{\beta}\epsilon}{4}\left(1 + \frac{R_0^2}{4}\right)k_y^2, \quad (4.67)$$

where $\tilde{\beta} = \beta c = N\pi\rho_0\beta R_0^2$, the next highest order terms in k_x and k_y are strictly negative, $\mathcal{M} = 1$ for a metric interaction and $\mathcal{M} = 0$ for a topological interaction.

We note that the $\mathbf{k} = 0$ intercepts of $\Re[\lambda_2]$ and $\Re[\lambda_3]$ are negative when $\epsilon \ll 1$ and the second order terms in $\mathbf{k}$ are also negative, so these eigenvalues always have real part less than zero, and hence are stable modes of the Fourier expansion. The remaining eigenvalue gives $\lambda = 0$ when $\mathbf{k} = 0$, with the next highest order behaviour giving different results for the metric and topological models. We examine this eigenvalue in greater detail.

The first thing to notice is that for fluctuations along the axis of propagation ($|k_x| > 0, k_y = 0$), λ_1 has negative real part. This supports the assumption that fluctuations in the direction of propagation are short-lived, also found in other flocking systems [25]. We turn next to fluctuations perpendicular to the direction of motion ($|k_y| > 0, k_x = 0$). The behaviour of these fluctuations depends on the sign of $\mathcal{M}\tilde{\beta} - 1$, which changes between neighbourhood interaction types.

For a topological interaction, this term reduces to -1, which is negative. Thus, the k_y^2 term is negative and the fluctuations should die away. For a metric interaction, this varies with the system parameters. For a typical set that give an ordered state in the agent-based model (see Fig. 3.3), we have $\beta = 0.75$ and $c = 7$. This gives a prefactor $\mathcal{M}\tilde{\beta} - 1 \approx 4$. Thus, the prefactor of the k_y^2 term is positive, leading to exponentially growing fluctuations and an unstable Fourier mode. The k_y^4 term has a negative prefactor in the metric case, thus the fluctuations must be sufficiently long-range (small k) to cause growth.

4.3.4 Inconsistencies in the linear stability analysis

The behaviour of the LA ABM with either a topological or metric interaction both contain regions of parameter space where the system contains an ordered flock capable of undergoing stochastic turning. We demonstrated using linear stability analysis that a highly ordered and evenly-distributed flock is unstable to fluctuations causing it to change direction regardless of the interaction neighbourhood choice.

On the contrary, the EA ABM can exhibit both turning and non-turning ordered flocks for topological and metric interactions respectively. If the difference between the topological and metric models could be explained by linear stability analysis, we would expect to observe that the topological model is unstable to fluctuations causing the flock to turn, while the metric model is stable to such fluctuations. This is not what we observe from Section 4.3.3; rather the conclusion of the linear stability analysis for the EA model is that the opposite should be observed.

Before concluding that linear stability of the field equations is not sufficient to explain the behaviours of the EA ABM, we re-examine the assumptions that led to the dispersion relations that gave us (4.65). We identify ways the linear stability could break down as follows:

1. Truncating the equations of motion (4.18, 4.24) at third order in derivatives neglects terms that are sufficiently large to make a significant contribution to the linear dynamics.

2. The topological radius of interaction $R(\mathbf{r}, t)$ cannot be approximated to the form (4.6).

3. α' is not sufficiently small that we can solve for λ by treating $\alpha' = 0$.

Any assumptions made about the stochastic terms in (4.24) are not relevant here, such as the stochastic contribution to $\partial_t \rho$ being negligible compared to the deterministic term or polarisation on neighbouring sites being uncorrelated from one another, as stochastic contributions to a Langevin equation do not affect the linear stability of the dynamics. Note that the first two items in the list also apply to the LA model, where the linear stability predictions match the ABM observations.

Nevertheless, let's consider point 1. Returning to the position in the field equation derivation where the continuous space approximation was made, we instead keep the lattice terms in (4.12, 4.19, 4.20). Performing the linear stability analysis as in Section 4.3.3, the linearised equations of motion become

$$\begin{aligned}
\lambda\delta\rho_{\mathbf{k},\lambda} \approx & \left[\frac{1+\tau^2}{2}\left(\cos k_x - 1\right) - i\tau\sin k_x + \frac{1-\tau^2}{2}\left(\cos k_y - 1\right)\right]\delta\rho_{\mathbf{k},\lambda} \\
& + \beta\rho_0\frac{1-\tau^2}{2}\left[-i\sin k_x + \tau\left(\cos k_x - \cos k_y\right)\right]\delta M_{\mathbf{k},\lambda} \\
& - i\beta m_0\rho_0\frac{1-\tau^2}{2}\sin k_y\delta\Phi_{\mathbf{k},\lambda} \qquad (4.68) \\
\lambda\delta m_{\mathbf{k},\lambda} \approx & \ \tau\rho_0 - m_0 + \left[\tau\cos k_x - i\frac{1+\tau^2}{2}\sin k_x\right]\delta\rho_{\mathbf{k},\lambda} - \delta m_{\mathbf{k},\lambda} \\
& + \frac{\beta\rho_0(1-\tau^2)}{2}\left[\cos k_x - i\tau\sin k_x\right]\delta M_{\mathbf{k},\lambda} \qquad (4.69) \\
\lambda\delta\phi_{\mathbf{k},\lambda} \approx & \ \frac{\beta\rho_0(1-\tau^2)}{2}\cos k_y\delta\Phi_{\mathbf{k},\lambda} - \delta\phi_{\mathbf{k},\lambda} + i\frac{1-\tau^2}{2m_0}\sin k_y\left[\beta\tau\rho_0\delta M_{\mathbf{k},\lambda} - \delta\rho_{\mathbf{k},\lambda}\right]. \qquad (4.70)
\end{aligned}$$

For sufficiently small $\mathbf{k}$, these equations match the Fourier transformed versions of (4.60, 4.61, 4.62) (assuming $\tau\rho_0 = m_0$). Thus, we can rule truncation of equations of motion out as a cause of this discrepancy.

For a similar reason, we believe the approximation to the topological radius of interaction (point 2 above) to be adequate at the linear level. Therefore, point 3 (i.e. $\alpha' \neq 0$) is likely to be the cause of the discrepancy observed, due to it being a feature of the EA model only. In the case where $\alpha' \neq 0$, we discard Equation (4.63) and solve instead the equation

$$\begin{pmatrix} A_{\rho,\rho}-\lambda & A_{\rho,p} & A_{\rho,\phi} \\ A_{p,\rho} & A_{p,p}-\lambda & A_{p,\phi} \\ A_{\phi,\rho} & A_{\phi,p} & A_{\phi,\phi}-\lambda \end{pmatrix} \begin{pmatrix} \hat{\delta\rho}_{\lambda,\mathbf{k}} \\ \hat{\delta p}_{\lambda,\mathbf{k}} \\ \hat{\delta\phi}_{\lambda,\mathbf{k}} \end{pmatrix} = -\alpha' \begin{pmatrix} 0 \\ 1 \\ 0 \end{pmatrix} \delta_{\mathbf{k},0}\delta_{\lambda,0}, \qquad (4.71)$$

which adjusts the dispersion relation where $\lambda = 0$ and $\mathbf{k} = 0$ and should affect the eigenvalues for low $\mathbf{k}$. As the right hand side of Eq. (4.71) is no longer zero, it is not possible to solve the equation in the same way as before. As such, we leave the solution of this equation for $\alpha' \neq 0$ as an open problem.

While confirming the observations of the 2d ABMs with the linear stability analysis would be useful, our analysis thus far is sufficient to make a key observation. As none of the eigenvalues blow up as $\mathbf{k} \to \infty$, there exists a

numerical scheme that we can use to stably integrate the equations. In the next section, we will describe a numerical integration scheme along the lines of the 1d scheme from Section 2.3.

4.4 Numerical analysis

As we did for the 1d equations (2.22, 2.34), we can directly numerically analyse the equations and average over trajectories to obtain a quantifiable measure of the order in the system through the order parameter

$$\varphi = \frac{1}{L_x L_y} \left\langle \int |\mathbf{p}(\mathbf{r}, t)| \, d\mathbf{r} \right\rangle \tag{4.72}$$

where the average $\langle\rangle$ can be taken over t or realisations of the noise $\boldsymbol{\xi}(\mathbf{r}, t)$ due to ergodicity.

4.4.1 Numerical integration

We numerically integrate (4.18, 4.24) in much the same way as their 1d counterparts in Section 2.3. To reiterate that procedure, we use operator splitting to perform the stochastic update first, due to the presence of a complicated multiplicative prefactor, then perform the deterministic update by following the Euler-Maruyama approach that we introduced in Chapter 2 of replacing time and space derivatives with finite differences, using $\delta x = 1$ and $\delta t = 0.01$ (hence $N = 100$) again here.

Taking this step by step, we first split the vector equation for magnetisation evolution (4.24) into two scalar equations. To simplify dealing with the stochastic term, we choose to study the evolution of the magnitude m and angle ϕ of the magnetisation vector $\mathbf{m}$. The magnetisation vector component equations can be expressed as

$$\begin{aligned} \partial_t m(\mathbf{r}, t) &= \frac{1}{m}\left[m_x\left(J_x - \partial_x \rho_x + \frac{1}{2}\partial_{xx} J_x\right) + m_y\left(J_y - \partial_y \rho_y + \frac{1}{2}\partial_{yy} J_y\right)\right] \\ &\quad -m + \sqrt{\frac{2}{N\rho}(\rho^2 - m^2)}\xi_m(\mathbf{r}, t), \end{aligned} \tag{4.73}$$

$$\begin{aligned}\partial_t\phi(\mathbf{r},t) &= \frac{1}{m^2}\left[m_x\left(J_y-\partial_y\rho_y+\frac{1}{2}\partial_{yy}J_y\right)-m_y\left(J_x-\partial_x\rho_x+\frac{1}{2}\partial_{xx}J_x\right)\right]\\ &\quad+\sqrt{\frac{2}{m^2N\rho}(\rho^2-m^2)}\xi_\phi(\mathbf{r},t),\end{aligned}\tag{4.74}$$

where ξ_m and ξ_ϕ are Gaussian random variables with mean zero and variance 1 [63].

Next, we split the Hamiltonian into stochastic and deterministic parts [60], take the stochastic part of (4.73) and rewrite it in terms of a Fokker-Planck equation

$$\partial_t P(m,t)=\frac{1}{N\rho}\partial_{mm}\left[(\rho^2-m^2)P(m,t)\right].\tag{4.75}$$

We draw an intermediate value, m^{int}, from a beta distribution with parameters as in Chapter 2 and use that in the discretised deterministic equation. For the noise term in (4.74), we can take the Euler-Maruyama approach and add a Gaussian distributed random number with variance $\sigma^2=\frac{2\delta t(\rho^2-m^2)}{m^2N\rho}$, which is constant in ϕ.

Thus, the equations for numerically updating the particle density and magnetisation are

$$\begin{aligned}\rho_{i,j}(t+\delta t) &= \rho_{i,j}(t)(1-\delta t)+\delta t\left[\rho_{i-1,j}(t)P(\hat{\mathbf{x}}|\mathbf{M}^{\text{int}}_{i-1,j}(t))+\rho_{i+1,j}(t)P(-\hat{\mathbf{x}}|\mathbf{M}^{\text{int}}_{i+1,j}(t))\right.\\ &\quad\left.+\rho_{i,j-1}(t)P(\hat{\mathbf{y}}|\mathbf{M}^{\text{int}}_{i,j-1}(t))+\rho_{i,j+1}(t)P(-\hat{\mathbf{y}}|\mathbf{M}^{\text{int}}_{i,j+1}(t))\right],\end{aligned}\tag{4.76}$$

$$\begin{aligned}m_{i,j}(t+\delta t) &= \delta t\cos\phi_{i,j}(t)\left[\rho_{i-1,j}(t)P(\hat{\mathbf{x}}|\mathbf{M}^{\text{int}}_{i-1,j}(t))-\rho_{i+1,j}(t)P(-\hat{\mathbf{x}}|\mathbf{M}^{\text{int}}_{i+1,j}(t))\right]\\ &\quad+\delta t\sin\phi_{i,j}(t)\left[\rho_{i,j-1}(t)P(\hat{\mathbf{y}}|\mathbf{M}^{\text{int}}_{i,j-1}(t))-\rho_{i,j+1}(t)P(-\hat{\mathbf{y}}|\mathbf{M}^{\text{int}}_{i,j+1}(t))\right]\\ &\quad+m^{\text{int}}_{i,j}(t)(1-\delta t),\end{aligned}\tag{4.77}$$

$$\begin{aligned}\phi_{i,j}(t+\delta t) &= \delta t\frac{\cos\phi_{i,j}(t)}{m^{\text{int}}_{i,j}(t)}\left[\rho_{i,j-1}(t)P(\hat{\mathbf{y}}|\mathbf{M}^{\text{int}}_{i,j-1}(t))-\rho_{i,j+1}(t)P(-\hat{\mathbf{y}}|\mathbf{M}^{\text{int}}_{i,j+1}(t))\right]\\ &\quad-\delta t\frac{\sin\phi_{i,j}(t)}{m^{\text{int}}_{i,j}(t)}\left[\rho_{i-1,j}(t)P(\hat{\mathbf{x}}|\mathbf{M}^{\text{int}}_{i-1,j}(t))-\rho_{i+1,j}(t)P(-\hat{\mathbf{x}}|\mathbf{M}^{\text{int}}_{i+1,j}(t))\right]\\ &\quad+\phi_{i,j}(t)+\sqrt{\frac{2\rho_{i,j}(t)\delta t}{Nm^{\text{int}}_{i,j}(t)^2}\left(1-\frac{m^{\text{int}}_{i,j}(t)^2}{\rho_{i,j}(t)^2}\right)}\xi_{i,j}(t),\end{aligned}\tag{4.78}$$

with

$$m^{\text{int}}_{i,j}(t)=(2y^{\text{int}}_{i,j}-1)\rho_{i,j}(t),\tag{4.79}$$

where $y_{i,j}^{\text{int}}(t)$ are drawn from the distribution

$$y_{i,j}^{\text{int}}(t) \in Beta\left(\alpha = \frac{\frac{1}{2}\left(1+\frac{m_{i,j}(t)}{\rho_{i,j}(t)}\right)}{\exp\left[\frac{2\delta t}{N\rho_{i,j}(t)}\right]-1}, \beta = \frac{\frac{1}{2}\left(1-\frac{m_{i,j}(t)}{\rho_{i,j}(t)}\right)}{\exp\left[\frac{2\delta t}{N\rho_{i,j}(t)}\right]-1}\right). \tag{4.80}$$

and M_{int} is calculated from the intermediate magnetisation m_{int} and $\phi_{i,j}(t)$ as in (4.2).

4.4.2 Results of the numerical integration

The equations (4.76, 4.77, 4.78) are stable when directly numerically integrated, unlike in some other sets of field equations to describe flocking in 2d, e.g. [88]. They also remain physical, i.e. the density on any site never drops below 0 and is conserved globally, and the magnitude of the magnetisation on a site never exceeds that site's density. However, the trajectories generated by the field equations do not replicate some key behaviour observed in the ABMs. Crucially, the turning of an ordered flock observed in 3 of the 4 ABMs in Chapter 3 (see Fig. 3.2) is not seen under the same conditions in the trajectories of the field equations.

Fig. 4.3 highlights how, using the same parameters, the mean polarisation differs between the field equations and the ABMs. With the exception of the metric EA ABM, the magnitude of the polarisation in the ABMs decays with increasing density, while the magnitude of the polarisation for the field equations remains constant. This is likely due to the absence of any macroscopic turning for the field equations.

As the order parameter φ does not match between the field equations and the ABM, the quantitative agreement observed between the 1d field equations and ABM (Fig. 2.6) is not present in our 2d system.

To understand why the numerically integrated field equations generate trajectories displaying different behaviour than their corresponding ABM, we return to the linear stability analysis of the previous section. There, we demonstrated that the LA is linearly unstable to macroscopic turning in the absence of explicit noise ($\boldsymbol{\xi} = 0$), unlike in the numerically integrated results above. As we demonstrated that the behaviour in the 1d field equations was very sensitive to the form of the stochastic term (Section 2.2.4), and the linear stability was analysed for the deterministic term only, it is reasonable to assume that the stochastic term is

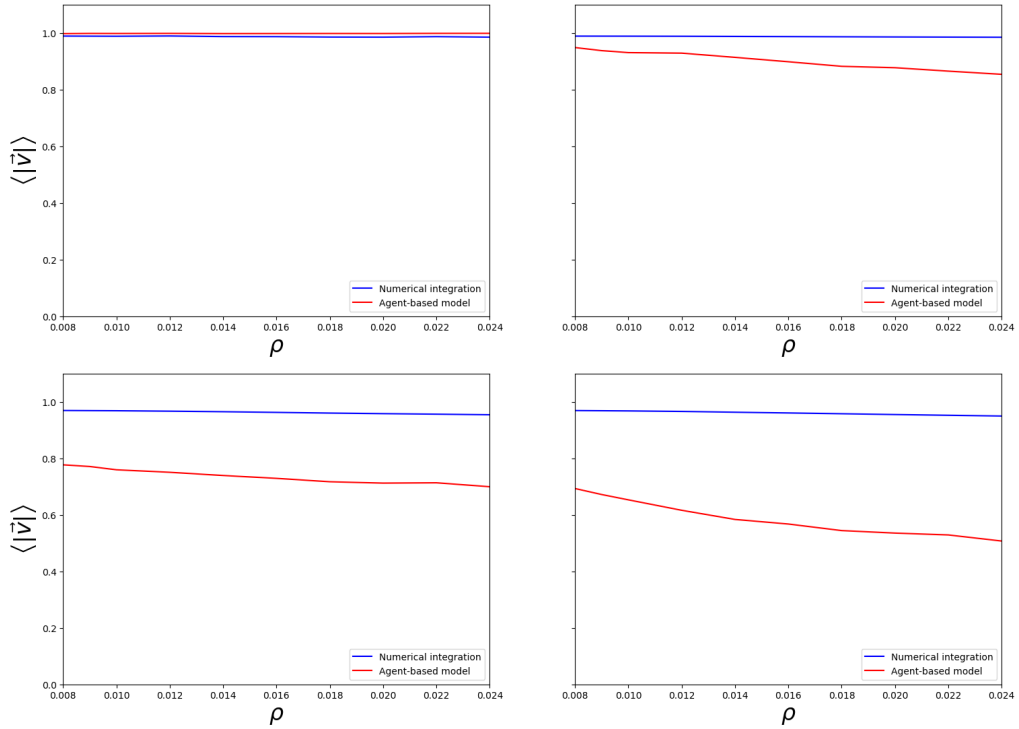

Figure 4.3 *Top: The order parameter in the ABM EA model vs the numerically integrated field equations as a function of system density with metric (left) or topological (right) interactions. Bottom: The order parameter in the ABM LA model vs the numerically integrated field equations as a function of system density with metric (left) or topological (right) interactions. For all four models, the order parameter for the numerically integrated SDE trajectories is close to 1 and does not change significantly as density increases. However, for trajectories of the ABMs that exhibit macroscopic turning in the ordered state (top right, bottom left and bottom right), the order parameter is lower than 1 and decreases further as density increases. This indicates that the macroscopic turning present in the topological EA and both LA ABMs is not observed in the trajectories of the numerically integrated field equations, as we see from Fig.s 3.2 and 3.3 that the order parameter drops as the flock changes direction. The ABM data was obtained using a stochastic update with scalar noise.* $L_x = L_y = 100$, $\beta = 0.75$, $\eta = 0.02$.

responsible for the unexpected behaviour in our numerical equations.

As we highlighted earlier in Section 4.1.4, we made the assumption in the derivation of our 2d Langevin equations that the autocorrelation of the polarisation $\mathbf{p}$ is negligible for $\mathbf{r} > 0$, enabling us to diagonalise the diffusion matrix in the Kramers-Moyal expansion. While we reasoned at the time that polarisation correlations in the ABMs suggested that the autocorrelation function dropped off rapidly, it is the only assumption made in our equation derivation that affects the stochastic term only, suggesting that the polarisation correlations do not drop off sufficiently fast that they are negligible. As such, more work is likely needed to obtain a more accurate stochastic term in the magnetisation Langevin equation (4.24).

While we have not confirmed through linear stability analysis that the deterministic terms of our Langevin equations (4.18, 4.24) act appropriately for our EA model, we assume that the same issue with the stochastic term arises in the numerical integration, resulting in the trajectories that do not conform to the trajectories in the ABM at the same point in parameter space.

4.5 Summary

We set out in this chapter to identify if we could derive field equations for density and magnetisation that generate trajectories matching those seen in related agent-based models, and to use those equations to explain why some flocks undergo macroscopic turning while others don't. Using linear stability analysis, we demonstrated that the form of the deterministic terms in our Langevin equations may be the determining factor in the presence or absence of turning, while the form of the stochastic term is likely responsible for obtaining the correct behaviour in numerical trajectories, as it was for the one-dimensional models in Chapter 2.

We used the Kramers-Moyal approximation [66, 78, 115] to derive a set of stochastic field equations describing the evolution of density and magnetisation in a family of related agent-based models on a square lattice. We re-used many key assumptions from Chapter 2 in this derivation, including an expansion from the lattice to continuous space, choosing the appropriate stochastic variables, and negligible correlations between neighbouring lattice sites. Some factors such as the radius of interaction and neighbourhood magnetisation required more careful

consideration due to the move to two spatial dimensions, the distinction between different interaction types, and increasing the range of interaction beyond a single site.

We turned next to linear stability analysis to explain the distinction between the macroscopically turning and non-turning models. For the LA, we demonstrated that the linearised evolution equations do not depend on the choice of metric or topological interaction. We subsequently derive the dispersion relation for the angle of the magnetisation and conclude that large wavelength fluctuations are capable of causing the flock to turn. This directly matches the behaviour of the agent-based simulations.

On the other hand, the linear stability analysis for the EA model is more complicated. The stability of the linearised equations of motion depend on whether a metric or topological interaction is used, as observed in the agent-based simulations. An approximate dispersion relation suggests that macroscopic turning should be observed for metric interactions only, not topological interactions as the agent-based simulations display.

While there are a number of reasons that linear stability analysis might have failed to duplicate the behaviour observed in agent-based systems, the most likely reason is the assumption that the linearised equations form a singular system of coupled equations. We expect that removing this assumption will be sufficient to demonstrate the expected behaviour, although more complicated techniques will be required to solve a nearly singular set of equations.

To illustrate that the field equations accurately represented behaviours observed in the ordered state of the agent-based models, we performed numerical integration of the field equations. The resulting simulations display some, but not all of the behaviour seen in the agent-based systems. Crucially, the macroscopic turning observed in the LA and the topological EA agent-based simulations is not exhibited at the same point in parameter space in the field equations. Rather, all models display an non-turning ordered state, as seen in the metric EA agent-based model. As the stochastic term was not present in the linear stability analysis that demonstrated the expected behaviour for the most part, the form of the diffusive stochasticity may be the cause of the incorrect behaviour observed.

Chapter 5

Discussion & conclusion

The work in this thesis shows the importance of the stochastic term in the dynamical (Langevin) equations describing a system of aligning self-propelled particles (SPPs) and introduces a method (the Kramers-Moyal approximation) of deriving these equations with an appropriate stochastic term. In the one-dimensional (1d) case, we demonstrated that deriving Langevin equations from the underlying microscopic dynamics can lead to a system of equations with trajectories matching those of the underlying agent-based models (ABMs). We further demonstrated how the Kramers-Moyal approximation could be used to identify the minimal requirements on the inter-particle interaction within a system of aligning SPPs in 1d to ensure an ordered coherent flock could form that was capable of turning. Turning to two dimensional (2d) models, we used the Kramers-Moyal approximation and linear stability analysis to explore how the ability of an ordered flock to spontaneously turn could be observed through the stochastic differential equations (SDEs) and ambitiously explored whether a simplified version of the Kramers-Moyal approximation could lead to SDEs with trajectories matching the behaviour of the underlying agent-based models. While there were some challenges with actually obtaining these equations for the 2d case, the work in this thesis demonstrates how a set of SDEs can be obtained from an agent-based system that match the dynamics of that system and outlines a practical way to obtain these equations in 1d.

We demonstrated in Chapter 2 that the form of the stochastic prefactor plays a large role in the dynamics of the SDEs. Using the wrong form of the stochastic prefactor could lead to behaviour that didn't match that of the agent-based model

(ABM) the SDEs were based on. In one of the systems of equations we studied, the stochastic term was so large that it overpowered the deterministic effects and an ordered flock was unable to form. We outlined a procedure to obtain a stochastic term that - when trajectories of the set of SDEs are obtained - matches the behaviour of the ABM without the need for arbitrary rescaling.

These results are significant in three primary ways. Firstly, we demonstrated that it is possible to obtain stochastic Langevin equations describing macroscopic properties directly from the microscopic interactions. Previous works [23, 112] have often made assumptions about the form of the stochastic term and added an arbitrary scaling factor to ensure behaviour matches. Secondly, we detailed the procedure to arrive at these equations, enabling the derivation of SDEs for a variety of other systems. Finally, we showcased that the SDEs generate trajectories that match the underlying mechanics of the ABM. We also highlighted how minor alterations to the stochastic prefactor can have outsized effects on the dynamics of the trajectories obtained, even removing the ability for an ordered state to exist.

With our ability to derive SDEs corresponding to agent-based systems, we explored the minimal requirements for a flock of aligning self-propelled particles (SPPs) in 1d to be able to alternate their direction stochastically. While there have been a number of works exploring 1d flocks as ABMs or differential equations [35, 46, 47, 82, 92], none had previously examined what factors were necessary for these flocks to change direction spontaneously in 1d. We demonstrated that a particle determining which direction to travel needed, at minimum, the ability to sample three particles chosen at random from its neighbourhood in order for a coherent flock to form capable of alternating direction. The "three particle minimum" that we demonstrated was needed for alternating flocks to exist *did* allow for a particle to select itself as one of those three. However, whether or not allowing that was necessary was also unclear from the literature.

We then outlined some preliminary findings from analysis into a few different variations of our base model, motivated by a desire to understand whether particles should include themselves in their neighbourhood, and by other 1d models that used larger neighbourhoods [46, 92] or directional neighbourhoods [47, 48]. By controlling whether or not a particle included itself in its own neighbourhood, we demonstrated that particles including themselves ("persistent" particles) allowed for a flock to exist for some non-zero noise strength, regardless of the neighbourhood chosen. Additionally, sampling from more sites tended to

result in higher order, and could even introduce order in systems of particles that did not include themselves in their own neighbourhood ("uncertain" particles). A potential avenue for further investigation in this area is to identify whether the ability of the system to form a coherent flock can be identified from the SDEs rather than by examining the ABMs. In this way, a better understanding of the interplay between microscopic interactions and macroscopic behaviour could be attained.

The results of Chapter 2 add to the work on self-propelled particle models in 1d [35, 46, 47, 82] by exploring how explicit stochastic terms can affect the trajectories of a system. They also explore the minimal interactions necessary for flocking to occur, adding to and reinforcing other works in the literature [32, 92] and contrasting with other agent-based systems such as run-and-tumble particles in which flocking is typically not present [109].

Examining the impact of different neighbourhoods on flocking dynamics in 1d was the inspiration for the latter half of this thesis; what if we could obtain SDEs for systems of aligning SPPs in 2d without arbitrarily scaling the noise term? If we could derive 2d SDEs in the same way as for 1d, might we be able to understand the factors that lead to stochastic turning in flocking models with a topological neighbourhood [4, 54] while leading to band formation in models with a metric neighbourhood [112, 116]?

In Chapter 3, we expanded our exploration of modifications to the 1d ABMs to consider the addition of another spatial dimension. We chose to examine lattice-based ABMs in 2d for two primary reasons. Firstly, while methods exist of deriving differential equations for off-lattice ABMs in 2d (see Section 1.3.2 for examples), none had previously been used to derive the stochastic term of those equations explicitly. For example, the phenomenological approach of Toner & Tu [112] typically includes an additive stochastic term in the velocity equation, while the Boltzmann equation approach [29] typically includes the stochastic nature of collisions and reorientation implicitly. Secondly, we had initially explored directly integrating the particle equations of motion to obtain SDEs for the evolution of density and velocity, in a similar manner to the approach of Chaté [29] and others. However, our approach ran into difficulties with the closure of the set of equations, as we were unable to neatly separate the deterministic and stochastic terms in the resulting SDEs.

We returned therefore to the Kramers-Moyal approximation that had served

us well for obtaining our 1d equations. The Kramers-Moyal approximation doesn't strictly require a finite number of states the particles can be in; however, dealing with infinite matrices is an additional complexity that is not needed to understand the factors necessary for turning, nor to demonstrate that the form of the stochastic term plays a large role in the dynamics of the system. As such, we constructed 2d agent-based systems based on a square lattice as a base from which we later derived SDEs. We introduced two different alignment interactions and two neighbourhood definitions, giving us four related lattice-based ABMs in 2d. We chose these alignment interactions such that, while similar in approach, spontaneous turning was not observed in one of the models but was observed for the remaining three. As these models were constructed for our purposes and had not been examined in previous works, we then demonstrated that the difference between these models was robust to changes in the mechanism of simulation. Additionally, we demonstrated that the lattice did not prevent the ability of a flock to turn, as one might have expected from introducing restrictions on the directions of motion of particles.

The phase-separated banding observed in 2d SPP ABMs with a metric neighbourhood and the macroscopic turning observed in 2d SPP ABMs with a topological neighbourhood are well-documented [4, 54], and was observed in our "exponentially-aligning" (EA) model. In contrast, the ability of an ordered flock to form and turn spontaneously in our "linearly-aligning" (LA) model has not been explored. Rather, the findings from simulations of the LA model contradict a belief that asymmetric interactions are necessary for an ordered flock to turn in 2d [27]. Exploring why simulations of the metric LA model do not result in band formation is challenging with the ABMs, but becomes more accessible if we can examine corresponding Langevin equations.

We begin Chapter 4 with a derivation of the stochastic Langevin equations for the ABMs introduced in the previous chapter, using the Kramers-Moyal approximation as in Chapter 2. As the later parts of Chapter 4 focus on comparisons between the SDEs for our four models, we derived a general equation for all interaction types covered in Chapter 3.

Based on the finding that the presence of an instability towards fluctuations perpendicular to the particle velocity can cause a flock to turn through propagation of that signal through the flock [3, 25], we conducted linear stability analysis on our SDEs to determine if stability arguments could explain the difference in behaviour between our systems. The neighbourhood definition had

no effect on the linear stability of the LA system, which is always unstable to perpendicular fluctuations and hence a flock can always turn spontaneously. This finding reinforces our result from Chapter 3 that non-reciprocal interactions are not strictly necessary for a flock to turn in a 2d system. Even when constrained to a lattice, the reciprocal interactions of the metric LA allowed the particles to form a flock capable of turning spontaneously.

Conducting linear stability analysis on the EA models was more challenging. Solving the equations required complicated matrix algebra that our analytical software was unable to perform. By making an additional assumption regarding the magnitude of the mean polarisation, we observed that the stability of an ordered flock under the EA model depended on the neighbourhood definition through fluctuations in the direction of motion. The addition of this simplification meant that we were unable to demonstrate the correct stability behaviour. To determine whether linear stability *is* sufficient to explain the behaviours observed in each of the topological and metric EA models, the small quantity approximated to be negligible (α') must be included and the equations solved more directly.

Linear stability analysis of differential equations has another benefit; if the small length-scale behaviour of differential equations is stable, there exists a numerical integration scheme that will generate trajectories of the differential equations that are also stable. We numerically integrated the SDEs obtained at the start of Chapter 4 to determine if the resulting trajectories matched the behaviour of the 2d ABMs, as they did for the 1d equations. Instead, we observed that all four models exhibited flocks that did not turn macroscopically and persisted travelling in the same direction. We determined that the likely cause of the observed mismatch was the assumption within the Kramers-Moyal approximation that correlations of density and polarisation were negligible beyond self-correlation. This assumption was necessary to ensure that the matrix of second order jump moments D was diagonal. However, if a suitable decomposition of the matrix of second order jump moments into the product of a matrix B and its transpose was found, the assumption of negligible correlations would no longer be necessary.

We close this work by discussing potential avenues of future research. The clearest direction of further study would be an exploration of the SDEs obtained through the Kramers-Moyal approximation with a non-diagonal D (and hence B). The elements of B are related to the stochastic prefactor g_i through the relation $g_i^2 = \sum_j b_{ij}^2$ for $i \in \{1, ..., 3L_xL_y\}$ [63]. For each variable $\psi \in \{\rho, p_x, p_y\}$, the stochastic prefactor $g_\psi(x)$ will depend only on $\rho(x)$, $\mathbf{p}(x)$ and their derivatives (i.e.

$g_\psi(x) = g_\psi[\rho, \mathbf{p}](x))$, although it would be preferable if higher order derivatives are negligible.

The ABMs in this work were toy models, not based directly on any physical system. Another avenue for future research would be to explore using the Kramers-Moyal approximation to obtain SDEs for ABMs that more closely resemble physical systems of birds, fish, insects, or other aligning self-propelled agents. Doing so may involve starting with off-lattice ABMs to more accurately represent the dynamics of agents, such as the constant-radius turning observed in flocks of birds [26]. Alternatively, one could examine the effect of further decoupling particle polarisation and particle velocity by introducing an internal "spin" (similar to the Inertial Spin Model [23]) with a continuous range of possible values.

We expect that in either an off-lattice system or one where a continuous spin variable was introduced, the field equations would look very similar to (4.18, 4.24). In moving to an off-lattice system, gradients, divergences and Laplacians would likely replace the directional derivatives in the deterministic terms, while an additional equation is needed in the case of the model adding a spin field. The details of J_x, J_y, ρ_x and ρ_y would depend on the exact interactions, though we expect that only the probability normalisation needs to be updated in a move to a continuous symmetry.

Additionally, as the results for 2d models in this work have considered a system in bulk, more interactions (e.g. a surface tension-like term [87]) may need to be added to ensure the flock does not diffuse and lose its cohesion. Agents in physical systems can often only interact with a subset of neighbours depending on which neighbours are within their field of view [44] or are within auditory range [48]. Obtaining accurate stochastic terms using the methods outlined in this work may prove useful in understanding the dynamics of these physical models.

Appendix A

The Kramers-Moyal approximation

The only possible transitions are those where the number of particles on a site i will decrease as a particle moves to a neighbouring site (or where a move from a neighbouring site will increase the density at i). The polarisation at both sites will also change in this move. I will denote $T^{\pm}_{r,l}(\rho_i, w_i)$ as the transition rate for a particle at site i facing right/left taking a step in the positive (right)/negative (left) direction. It will be a function of the density and momentum at that site only and has no explicit time dependence. Therefore, (1.50) can be expanded as

$$\begin{aligned}\frac{\partial P}{\partial t} &= \sum_{i=1}^{L} T_r^+\left(\rho_{i-1}+\frac{1}{N}, w_{i-1}+\frac{1}{N}\right) P\left(...\rho_{i-1}+\frac{1}{N}, \rho_i-\frac{1}{N}, ..., w_{i-1}+\frac{1}{N}, w_i-\frac{1}{N}, ..., t\right)\\ &\quad + T_l^+\left(\rho_{i-1}+\frac{1}{N}, w_{i-1}-\frac{1}{N}\right) P\left(...\rho_{i-1}+\frac{1}{N}, \rho_i-\frac{1}{N}, ..., w_{i-1}-\frac{1}{N}, w_i-\frac{1}{N}, ..., t\right)\\ &\quad + T_r^-\left(\rho_{i+1}+\frac{1}{N}, w_{i+1}+\frac{1}{N}\right) P\left(...\rho_i-\frac{1}{N}, \rho_{i+1}+\frac{1}{N}, ..., w_i+\frac{1}{N}, w_{i+1}+\frac{1}{N}, ..., t\right)\\ &\quad + T_l^-\left(\rho_{i+1}+\frac{1}{N}, w_{i+1}-\frac{1}{N}\right) P\left(...\rho_i-\frac{1}{N}, \rho_{i+1}+\frac{1}{N}, ..., w_i+\frac{1}{N}, w_{i+1}-\frac{1}{N}, ..., t\right)\\ &\quad - \left[T_r^+(\rho_i, w_i)+T_l^+(\rho_i, w_i)+T_r^-(\rho_i, w_i)+T_l^-(\rho_i, w_i)\right] P(\{\rho_i, w_i\}, t)\end{aligned} \tag{A.1}$$

To simplify this further, consider a set of operators $a_i^{\pm}$ and $b_i^{\pm}$ that act of a function $f(\{\rho_i, w_i\})$ such that

$$a_i^{\pm} f(\{\rho_i, w_i\}) = f\left(..., \rho_i \pm \frac{1}{N}, ...\right) \quad \text{and} \quad b_i^{\pm} f(\{\rho_i, w_i\}) = f\left(..., w_i \pm \frac{1}{N}, ...\right). \tag{A.2}$$

Using these operators and using the periodicity of the lattice, the master equation

can be expressed as

$$\begin{aligned}\frac{\partial P}{\partial t} &= \sum_{i=1}^{L}\left(a_i^+ b_i^+ a_{i+1}^- b_{i+1}^- - 1\right) T_r^+(\rho_i, w_i)P \\ &+ \left(a_i^+ b_i^- a_{i+1}^- b_{i+1}^- - 1\right) T_l^+(\rho_i, w_i)P \\ &+ \left(a_i^+ b_i^+ a_{i-1}^- b_{i-1}^+ - 1\right) T_r^-(\rho_i, w_i)P \\ &+ \left(a_i^+ b_i^- a_{i-1}^- b_{i-1}^+ - 1\right) T_l^-(\rho_i, w_i)P. \end{aligned} \tag{A.3}$$

Provided N is sufficiently large, ρ_i and w_i can be approximated as continuous variables. Under this assumption, the operators defined above can be approximated by the following Taylor expansion

$$a_i^{\pm} = 1 \pm \frac{1}{N}\frac{\partial}{\partial \rho_i} + \frac{1}{2N^2}\frac{\partial^2}{\partial \rho_i^2} + O\left(N^{-3}\right) \tag{A.4}$$

$$b_i^{\pm} = 1 \pm \frac{1}{N}\frac{\partial}{\partial w_i} + \frac{1}{2N^2}\frac{\partial^2}{\partial w_i^2} + O\left(N^{-3}\right) \tag{A.5}$$

The Kramers-Moyal approximation [52, 66, 78] involves truncating the above operators at the second order to obtain a Fokker-Planck equation. Under this approximation, and grouping terms under the same derivative, the Fokker-Planck equation for the above system becomes

$$\begin{aligned}\frac{\partial P}{\partial t} &= \frac{1}{N}\sum_{i=1}^{L}\partial_{\rho_i}\left(T_{r,i}^+ - T_{r,i-1}^+ + T_{l,i}^+ - T_{l,i-1}^+ + T_{r,i}^- - T_{r,i+1}^- + T_{l,i}^- - T_{l,i+1}^-\right)P \\ &+\partial_{w_i}\left(T_{r,i}^+ - T_{r,i-1}^+ - T_{l,i}^+ - T_{l,i-1}^+ + T_{r,i}^- + T_{r,i+1}^- - T_{l,i}^- + T_{l,i+1}^-\right)P \\ &+ \left(a_i^+ b_i^- a_{i+1}^- b_{i+1}^- - 1\right) T_l^+(\rho_i, w_i)P \\ &+ \left(a_i^+ b_i^+ a_{i-1}^- b_{i-1}^+ - 1\right) T_r^-(\rho_i, w_i)P \\ &+ \left(a_i^+ b_i^- a_{i-1}^- b_{i-1}^+ - 1\right) T_l^-(\rho_i, w_i)P. \end{aligned} \tag{A.6}$$

$$\frac{\partial P}{\partial t} = \sum_i \frac{\partial}{\partial \psi_i}\left(\frac{\langle \delta\psi_i \rangle}{\delta t}P\right) + \sum_{i,j}\frac{\partial^2}{\partial \psi_i \partial \psi_j}\left(\frac{\langle \delta\psi_i \delta\psi_j \rangle}{\delta t}P\right) \tag{A.7}$$

where $\delta\psi_i$ represents the possible changes in ψ_i in a single time-step δt.

Appendix B

Beta-type distribution

In Section 2.3, we describe separating a Langevin equation (2.33) into a deterministic and stochastic part to perform each step sequentially. We transform the variable p in the stochastic piece of our equation (2.38) to another variable $y = \frac{1}{2}(1+p)$, giving us

$$\partial_t P(y,t) = \frac{1}{N\rho}\partial_{yy}\left[y(1-y)P(y,t)\right]. \tag{B.1}$$

To more accurately simulate the above distribution with a beta distribution, we wish to calculate its mean $\bar{y}$ and variance σ^2. Given Equation (B.1), we can calculate the temporal evolution of $\bar{y}$ as

$$\begin{aligned}
\partial_t \bar{y} &= \frac{1}{N\rho}\int_0^1 dy\ y\partial_t P(y,t) \\
&= \frac{1}{N\rho}\int_0^1 dy\ y\partial_{yy}\left[y(1-y)P(y,t)\right] \\
&= \frac{1}{N\rho}\left[y\partial_y\left(y(1-y)P(y,t)\right)\right]_0^1 - \frac{1}{N\rho}\int_0^1 dy\ \partial_y\left[y(1-y)P(y,t)\right] \\
&= -\frac{1}{N\rho}\left[y(1-y)P(y,t)\right]_0^1 = 0,
\end{aligned} \tag{B.2}$$

where the probability distribution vanishes at $y \in \{0,1\}$. As the time derivative of the mean is 0, the mean is constant in time, i.e. $\bar{y} = y_0$.

We calculate the variance similarly by calculating the temporal evolution of

$\langle y(1-y)\rangle$

$$\begin{aligned}
\partial_t \langle y(1-y)\rangle &= \frac{1}{N\rho}\int_0^1 dy\ y(1-y)\partial_t P(y,t) \\
&= \frac{1}{N\rho}\int_0^1 dy\ y(1-y)\partial_{yy}\left[y(1-y)P(y,t)\right] \\
&= -\frac{1}{N\rho}\int_0^1 (1-2y)\partial_y\left[y(1-y)P(y,t)\right] dy \\
&= -\frac{2}{N\rho}\int_0^1 y(1-y)P(y,t)dy = -\frac{2}{N\rho}\langle y(1-y)\rangle\,. \qquad \text{(B.3)}
\end{aligned}$$

Thus, if we have $y(t) = y_0$ at time t_0, we have that at future times t,

$$\langle y(1-y)\rangle = y_0(1-y_0)e^{-2\frac{t-t_0}{N\rho}}\,, \qquad \text{(B.4)}$$

and hence the variance σ^2 is

$$\begin{aligned}
\sigma^2 &= \left\langle (y-y_0)^2\right\rangle = \left\langle y^2\right\rangle - y_0^2 \\
&= -\langle y(1-y)\rangle + \langle y\rangle - y_0^2 \\
&= -y_0(1-y_0)e^{-2\frac{t-t_0}{N\rho}} + y_0(1-y_0) \\
&= y_0(1-y_0)\left[1-e^{-2\frac{t-t_0}{N\rho}}\right]. \qquad \text{(B.5)}
\end{aligned}$$

Appendix C

Run-and-tumble velocity derivation

When the "run-and-tumble" interaction is added to the 1d model defined in Section 2.1, the update probabilities for a given site's density ρ_i and magnetisation m_i must be altered. In Section 2.5, we describe particles undergoing either an alignment step as in Section 2.1 with probability $1-r$ or a run-and-tumble step with probability r.

If a run-and-tumble step is chosen, the chosen particle will continue in the same direction (run) with probability $1-\eta$ and will change direction (tumble) and move in its new direction with probability η. Adding these new steps in, the change in density on a given site i over a single time-step is given by

$$\delta\rho_i(t) = \begin{cases} \frac{1}{N} & \text{with probability } \left(W^+_{i-1}\rho_{i-1} + W^-_{i+1}\rho_{i+1}\right)(1-r) \\ & \qquad\qquad +r(1-\eta)\left(\rho^+_{i-1} + \rho^-_{i+1}\right) \\ & \qquad\qquad +r\eta\left(\rho^-_{i-1} + \rho^+_{i+1}\right) \\ -\frac{1}{N} & \text{with probability } \rho_i \\ 0 & \text{otherwise} \end{cases}, \tag{C.1}$$

leading to jump moments for density of

$$\begin{aligned}\langle \delta\rho_i \rangle &= \frac{1-r}{2N}\left[\rho_{i+1}+\rho_{i-1}-v(p_{i+1})\rho_{i+1}+v(p_{i-1})\rho_{i-1}\right]-\frac{\rho_i}{N}\\ &+\frac{r}{2N}\left[\rho_{i-1}+\rho_{i+1}-(1-2\eta)\left(m_{i+1}-m_{i-1}\right)\right]\\ &=\frac{1}{2N}\left[\rho_{i+1}+\rho_{i-1}-2\rho_i-\left[v(p_{i+1})(1-r)+r(1-2\eta)p_{i+1}\right]\rho_{i+1}\right.\\ &\qquad\left.+\left[v(p_{i-1})(1-r)+r(1-2\eta)p_{i-1}\right]\rho_{i-1}\right],\\ &=\frac{1}{2N}\left[\rho_{i+1}+\rho_{i-1}-2\rho_i-\tilde{v}(p_{i+1})\rho_{i+1}+\tilde{v}(p_{i-1})\rho_{i-1}\right], \end{aligned} \tag{C.2}$$

where $\tilde{v}(p)$ is defined in (2.47), and

$$\begin{aligned}\left\langle \delta\rho_i^2 \right\rangle &= \frac{1-r}{2N^2}\left[\rho_{i+1}+\rho_{i-1}-v(p_{i+1})\rho_{i+1}+v(p_{i-1})\rho_{i-1}\right]+\frac{\rho_i}{N}\\ &+\frac{r}{2N}\left[\rho_{i-1}+\rho_{i+1}-(1-2\eta)\left(m_{i+1}-m_{i-1}\right)\right]\\ &=\frac{1}{2N^2}\left[\rho_{i-1}+\rho_{i+1}+2\rho_i-\left((1-r)v(p_{i+1})+r(1-2\eta)p_{i+1}\right)\rho_{i+1}\right.\\ &\qquad\left.+\left((1-r)v(p_{i-1})+r(1-2\eta)p_{i-1}\right)\rho_{i-1}\right]\\ &=\frac{1}{2N^2}\left[\rho_{i+1}+\rho_{i-1}+2\rho_i-\tilde{v}(p_{i+1})\rho_{i+1}+\tilde{v}(p_{i-1})\rho_{i-1}\right]. \end{aligned} \tag{C.3}$$

Note that (C.2) and (C.3) match (2.16) and (2.17) under the change $v(p) \to \tilde{v}(p)$ as claimed in Section 2.5.

The possible changes in magnetisation in a single time step are

$$\delta m_i(t) = \begin{cases} \frac{1}{N} & \text{with probability } (1-r)W_{i-1}^{+}\rho_{i-1}+\rho_i^{-} \\ & \qquad +r\left[(1-\eta)\rho_{i-1}^{+}+\eta\rho_{i-1}^{-}\right] \\ -\frac{1}{N} & \text{with probability } (1-r)W_{i+1}^{-}\rho_{i+1}+\rho_i^{+} \\ & \qquad +r\left[(1-\eta)\rho_{i+1}^{-}+\eta\rho_{i+1}^{+}\right] \\ 0 & \text{otherwise} \end{cases} \tag{C.4}$$

The jump moments for magnetisation now become

$$\begin{aligned}\langle \delta m_i \rangle &= \frac{1-r}{2N}\left[\rho_{i-1} - \rho_{i+1} + v(p_{i+1})\rho_{i+1} + v(p_{i-1})\rho_{i-1}\right] - \frac{m_i}{N} \\ &+ \frac{r}{2N}\left[\rho_{i-1} - \rho_{i+1} + (1-2\eta)\left(m_{i+1} + m_{i-1}\right)\right] \\ &= \frac{1}{2N}\left[\rho_{i-1} - \rho_{i+1} - 2m_i + \left((1-r)v(p_{i+1}) + r\left(1-2\eta\right)p_{i+1}\right)\rho_{i+1}\right] \\ &\qquad + \left((1-r)v(p_{i-1}) + r\left(1-2\eta\right)p_{i-1}\right)\rho_{i-1}\right] \\ &= \frac{1}{2N}\left[\rho_{i-1} - \rho_{i+1} - 2m_i + \tilde{v}(p_{i+1})\rho_{i+1} + \tilde{v}(p_{i-1})\rho_{i-1}\right], \end{aligned} \tag{C.5}$$

and

$$\begin{aligned}\left\langle \delta m_i^2 \right\rangle &= \frac{1-r}{2N^2}\left[\rho_{i-1} + \rho_{i+1} - v(p_{i+1})\rho_{i+1} + v(p_{i-1})\rho_{i-1}\right] + \frac{\rho_i}{N^2} \\ &+ \frac{r}{2N^2}\left[\rho_{i-1} + \rho_{i+1} - (1-2\eta)\left(m_{i+1} - m_{i-1}\right)\right] \\ &= \frac{1}{2N^2}\left[\rho_{i-1} + \rho_{i+1} + 2\rho_i - \left((1-r)v(p_{i+1}) + r(1-2\eta)p_{i+1}\right)\rho_{i+1}\right. \\ &\qquad \left. + \left((1-r)v(p_{i-1}) + r(1-2\eta)p_{i-1}\right)\rho_{i-1}\right] \\ &= \frac{1}{2N}\left[\rho_{i-1} + \rho_{i+1} + 2\rho_i - \tilde{v}(p_{i+1})\rho_{i+1} + \tilde{v}(p_{i-1})\rho_{i-1}\right], \end{aligned} \tag{C.6}$$

Similarly, (C.5) and (C.6) match (2.25) and (2.26) under the change $v(p) \to \tilde{v}(p)$ as claimed in Section 2.5.

Appendix D

Exponentially-aligning Fourier transform and matrix solution

In ordered state simulations of the exponentially-aligning (EA) agent-based models, we find that $\alpha' \ll 1$ and $\tau \approx \frac{m_0}{\rho_0} \approx 1$. In order to use a matrix solution, we must set $\alpha' = 0$ to obtain a set of linear equations for $\delta\rho$, δp and $\delta\phi$. We also introduce a small quantity $\epsilon = 1 - \tau^2$ for easy of labelling. We finally choose to define $\mathcal{T} = 1$ if we are considering a topological interaction and $\mathcal{T} = 0$ if a metric interaction is used.

In the equations below, we examine linear equations for δp rather than δm. The behaviour of the system will not change under this transformation, so we are free to choose the quantity that best suits our needs. We first must derive a linearised equation for the evolution of δp in time.

$$\begin{aligned}
\partial_t \delta p &\approx \partial_t \left[\frac{\delta m}{\rho_0} - \frac{p_0 \delta\rho}{\rho_0} \right] \\
&\approx \left[-\frac{\epsilon}{2}\partial_x + \frac{\tau\epsilon}{4}(\partial_{xx} - \partial_{yy}) \right] \frac{\delta\rho}{\rho_0} - \delta p \\
&+ \frac{\beta\epsilon}{2} \left[1 + \frac{\epsilon}{2}\partial_{xx} + \frac{\tau^2}{2}\partial_{yy} \right] \delta M + \frac{\beta m_0 \epsilon\tau}{2} \partial_y \delta\Phi
\end{aligned} \tag{D.1}$$

where δM and $\delta\Phi$ are the changes in the local magnetisation field (4.52, 4.53).

We can therefore write (4.60, D.1, 4.62) as

$$\partial_t \begin{pmatrix} \rho(\mathbf{r},t) \\ p(\mathbf{r},t) \\ \phi(\mathbf{r},t) \end{pmatrix} = \mathcal{A}_{\mathcal{T}}(\tilde{\beta},\epsilon,R_0) \begin{pmatrix} \rho(\mathbf{r},t) \\ p(\mathbf{r},t) \\ \phi(\mathbf{r},t) \end{pmatrix} \tag{D.2}$$

where $\mathcal{A}_{\mathcal{T}}$ is an operator acting on $\mathbf{r}$ with components given by (4.60, 4.61, 4.62), and $\tilde{\beta}$, η and R_0 are physical constants of the linearised system.

We next perform Fourier transformation on (D.2) by making the substitution

$$f(\mathbf{r},t) = \sum_{\mathbf{k},\lambda} e^{i\mathbf{k}\cdot\mathbf{r}+\lambda t} \hat{f}_{\mathbf{k},\lambda} \tag{D.3}$$

where $f \in \{\rho, p, \phi\}$. This leads to the following

$$\sum_{\mathbf{k},\lambda} [\lambda - A_{\mathbf{k}}] \begin{pmatrix} \rho_{\mathbf{k},\lambda} \\ p_{\mathbf{k},\lambda} \\ \phi_{\mathbf{k},\lambda} \end{pmatrix} e^{i\mathbf{k}\cdot\mathbf{r}+\lambda t} = 0 \tag{D.4}$$

where $A_{\mathbf{k}}$ is the operator $\mathcal{A}$ under the substitutions $\partial_x \to ik_x$ and $\partial_y \to ik_y$.

As (D.4) must hold for all values of $\mathbf{r}$ and t, we must have that λ are the eigenvalues of $A_{\mathbf{k}}$. To determine the leading behaviour of the eigenvalues, we look for the behaviour for low values of $\mathbf{k}$, keeping terms up to second order. Under the low $\mathbf{k}$ approximation, the matrix has components

$$A_{\rho,\rho} = -i\tau \left[1 - \frac{\tilde{\beta}\epsilon}{2}\mathcal{M}\right] k_x - \frac{k_x^2}{2} + \left[\frac{\epsilon}{4}\left(1 - \tilde{\beta}\tau^2\mathcal{M}\right)\right]\left(k_x^2 - k_y^2\right) \tag{D.5}$$

$$A_{\rho,p} = -\frac{\tilde{\beta}\epsilon\rho_0}{2}\left[ik_x + \frac{\tau}{2}(k_x^2 - k_y^2)\right] \tag{D.6}$$

$$A_{\rho,\phi} = -i\frac{\tilde{\beta}\epsilon\tau\rho_0}{2}k_y \tag{D.7}$$

$$A_{p,\rho} = \frac{\epsilon}{2\rho_0}\left[\tilde{\beta}\tau\mathcal{M} - ik_x - \frac{\tau}{2}\left(\frac{\tilde{\beta}R_0^2}{4} + 1 + \tilde{\beta}\epsilon\mathcal{M}\right)k_x^2 - \frac{\tau}{2}\left(\frac{\tilde{\beta}R_0^2}{4} - 1 + \tilde{\beta}\tau^2\mathcal{M}\right)k_y^2\right] \tag{D.8}$$

$$A_{p,p} = \frac{\tilde{\beta}\epsilon}{2} - 1 - \frac{\tilde{\beta}\epsilon}{4}\left[\left(\epsilon + \frac{R_0^2}{4}\right)k_x^2 + \left(1 - \epsilon + \frac{R_0^2}{4}\right)k_y^2\right] \tag{D.9}$$

$$A_{p,\phi} = i\frac{\tilde{\beta}\epsilon\tau^2}{2}k_y \tag{D.10}$$

$$A_{\phi,\rho} = -i\frac{\epsilon}{2m_0}\left[1 - \tilde{\beta}\tau^2\mathcal{M}\right]k_y \tag{D.11}$$

$$A_{\phi,p} = i\frac{\tilde{\beta}\epsilon}{2}k_y \tag{D.12}$$

$$A_{\phi,\phi} = \frac{\tilde{\beta}\epsilon}{2} - 1 - \frac{\tilde{\beta}\epsilon R_0^2}{16}k_x^2 - \frac{\tilde{\beta}\epsilon}{4}\left(1 + \frac{R_0^2}{4}\right)k_y^2 \tag{D.13}$$

where $\mathcal{M} = 1 - \mathcal{T}$. The eigenvalues are subsequently obtained by solving the equation $\det\left(A_{\mathbf{k}} - \lambda\mathcal{I}_3\right) = 0$, and the small $\mathbf{k}$ limits of these eigenvalues are given in equations (4.65, 4.66, 4.67).

Bibliography

[1] O. Al Hammal, H. Chaté, I. Dornic, and M. A. Muñoz. Langevin Description of Critical Phenomena with Two Symmetric Absorbing States. *Physical Review Letters*, 94(23):230601, 2005.

[2] C. Appert and S. Zaleski. Lattice gas with a liquid-gas transition. *Physical Review Letters*, 64(1):1–4, 1990.

[3] A. Attanasi, A. Cavagna, L. Del Castello, I. Giardina, T. S. Grigera, A. Jelic, S. Melillo, L. Parisi, O. Pohl, E. Shen, and M. Viale. Information transfer and behavioural inertia in starling flocks. *Nature Physics*, 10(9):691–696, 2014.

[4] M. Ballerini, N. Cabibbo, R. Candelier, A. Cavagna, E. Cisbani, I. Giardina, V. Lecomte, A. Orlandi, G. Parisi, A. Procaccini, M. Viale, and V. Zdravkovic. Interaction ruling animal collective behavior depends on topological rather than metric distance: Evidence from a field study. *Proceedings of the National Academy of Sciences*, 105(4):1232–1237, 2008.

[5] G. Baxter, R. A. Blythe, and A. J. McKane. Exact solution of the multi-allelic diffusion model. *Mathematical Biosciences*, 209(1):124–170, 2007.

[6] F. Benitez, C. Duclut, H. Chaté, B. Delamotte, I. Dornic, and M. A. Muñoz. Langevin Equations for Reaction-Diffusion Processes. *Physical Review Letters*, 117(10):100601, 2016.

[7] B. Benvegnen, H. Chaté, P. Krapivsky, J. Tailleur, and A. Solon. Flocking in One Dimension: Asters and Reversals. *Physical Review E*, 106(5):054608, 2022.

[8] E. Bertin. *Statistical Physics of Complex Systems*. Springer International Publishing, Cham, 2 edition, 2016.

[9] E. Bertin, M. Droz, and G. Gregoire. Boltzmann and hydrodynamic description for self-propelled particles. *Physical Review E - Statistical, Nonlinear, and Soft Matter Physics*, 74(2):022101, 2006.

[10] E. Bertin, M. Droz, and G. Grégoire. Hydrodynamic equations for self-propelled particles: microscopic derivation and stability analysis. *Journal of Physics A: Mathematical and Theoretical*, 42(44):445001, nov 2009.

[11] W. Bialek, A. Cavagna, I. Giardina, T. Mora, E. Silvestri, M. Viale, and A. M. Walczak. Statistical mechanics for natural flocks of birds. *Proceedings of the National Academy of Sciences*, 109(13):4786–4791, 2012.

[12] T. Biancalani, L. Dyson, and A. J. McKane. Noise-induced bistable states and their mean switching time in foraging colonies. *Physical Review Letters*, 112(3), 2014.

[13] G. Biroli and J. P. Garrahan. Perspective: The glass transition. *The Journal of Chemical Physics*, 138(12):12A301, 2013.

[14] R. A. Blythe. The Interplay of Replication, Variation and Selection in the Dynamics of Evolving Populations. In *Principles of Evolution: From the Planck Epoch to Complex Multicellular Life*, pages 81–118. Springer Berlin Heidelberg, 2011.

[15] J. Buhl, D. J. T. Sumpter, I. D. Couzin, J. J. Hale, E. Despland, E. R. Miller, and S. J. Simpson. From Disorder to Order in Marching Locusts. *Science*, 312(5778):1402–1406, 2006.

[16] M. Camperi, A. Cavagna, I. Giardina, G. Parisi, and E. Silvestri. Spatially balanced topological interaction grants optimal cohesion in flocking models. *Interface Focus*, 2(6):715–725, 2012.

[17] M. E. Cates. Active Field Theories. In *Active Matter and Non-equilibrium Statistical Physics*. Oxford University Press, 2022.

[18] M. E. Cates and J. Tailleur. Motility-Induced Phase Separation. *Annual Review of Condensed Matter Physics*, 6(1):219–244, 2015.

[19] J.-B. Caussin, A. Solon, A. Peshkov, H. Chaté, T. Dauxois, J. Tailleur, V. Vitelli, and D. Bartolo. Emergent Spatial Structures in Flocking Models: A Dynamical System Insight. *Physical Review Letters*, 112(14):148102, 2014.

[20] A. Cavagna, A. Cimarelli, I. Giardina, A. Orlandi, G. Parisi, A. Procaccini, R. Santagati, and F. Stefanini. New statistical tools for analyzing the structure of animal groups. *Mathematical Biosciences*, 214(1-2):32–37, 2008.

[21] A. Cavagna, A. Cimarelli, I. Giardina, G. Parisi, R. Santagati, F. Stefanini, and M. Viale. Scale-free correlations in starling flocks. *Proceedings of the National Academy of Sciences*, 107(26):11865–11870, 2010.

[22] A. Cavagna, L. Del Castello, S. Dey, I. Giardina, S. Melillo, L. Parisi, and M. Viale. Short-range interactions versus long-range correlations in bird flocks. *Physical Review E - Statistical, Nonlinear, and Soft Matter Physics*, 92(1):012705, 2015.

[23] A. Cavagna, L. Del Castello, I. Giardina, T. Grigera, A. Jelic, S. Melillo, T. Mora, L. Parisi, E. Silvestri, M. Viale, and A. M. Walczak. Flocking and Turning: a New Model for Self-organized Collective Motion. *Journal of Statistical Physics*, 158(3):601–627, 2015.

[24] A. Cavagna and I. Giardina. Bird Flocks as Condensed Matter. *Annual Review of Condensed Matter Physics*, 5(1):183–207, 2014.

[25] A. Cavagna, I. Giardina, and T. S. Grigera. The physics of flocking: Correlation as a compass from experiments to theory. *Physics Reports*, 728:1–62, jan 2018.

[26] A. Cavagna, I. Giardina, T. S. Grigera, A. Jelic, D. Levine, S. Ramaswamy, and M. Viale. Silent flocks: Constraints on signal propagation across biological groups. *Physical Review Letters*, 114(21):218101, 2015.

[27] A. Cavagna, I. Giardina, A. Jelic, S. Melillo, L. Parisi, E. Silvestri, and M. Viale. Nonsymmetric Interactions Trigger Collective Swings in Globally Ordered Systems. *Physical Review Letters*, 118(13):138003, 2017.

[28] C. Cercignani. The Boltzmann Equation. In *Slow Rarefied Flows*, volume 41, pages 1–28. Birkhäuser Basel, Basel, 2006.

[29] H. Chaté. Dry Aligning Dilute Active Matter. *Annual Review of Condensed Matter Physics*, 11(1):189–212, 2020.

[30] H. Chaté. Dry, aligning, dilute, active matter: A synthetic and self-contained overview. In *Active Matter and Nonequilibrium Statistical Physics*. Oxford University Press, 2022.

[31] H. Chaté, F. Ginelli, G. Grégoire, and F. Raynaud. Collective motion of self-propelled particles interacting without cohesion. *Physical Review E*, 77(4):046113, 2008.

[32] P. Chatterjee and N. Goldenfeld. Three-body interactions drive the transition to polar order in a simple flocking model. *Physical Review E*, 100(4):040602, 2019.

[33] D. Chen, Y. Sun, G. Shao, W. Yu, H. T. Zhang, and W. Lin. Coordinating directional switches in pigeon flocks: The role of nonlinear interactions. *Royal Society Open Science*, 8(9), 2021.

[34] J. F. Crow and M. Kimura. *An Introduction to Population Genetics Theory*. New York, Evanston and London: Harper & Row, Publishers, 1970.

[35] A. Czirók, A.-L. Barabási, and T. Vicsek. Collective Motion of Self-Propelled Particles: Kinetic Phase Transition in One Dimension. *Physical Review Letters*, 82(1):209–212, 1999.

[36] A. Czirók, M. Vicsek, and T. Vicsek. Collective motion of organisms in three dimensions. *Physica A: Statistical Mechanics and its Applications*, 264(1-2):299–304, 1999.

[37] L. P. Dadhichi, J. Kethapelli, R. Chajwa, S. Ramaswamy, and A. Maitra. Nonmutual torques and the unimportance of motility for long-range order in two-dimensional flocks. *Physical Review E*, 101(5):052601, 2020.

[38] D. S. Dean. Langevin equation for the density of a system of interacting Langevin processes. *Journal of Physics A: Mathematical and General*, 29(24):L613–L617, 1996.

[39] R. Dickman. Numerical study of a field theory for directed percolation. *Physical Review E*, 50(6):4404–4409, 1994.

[40] R. Dickman and A. Y. Tretyakov. Hyperscaling in the Domany-Kinzel cellular automaton. *Physical Review E*, 52(3):3218–3220, sep 1995.

[41] I. Dornic, H. Chaté, J. Chave, and H. Hinrichsen. Critical Coarsening without Surface Tension: The Universality Class of the Voter Model. *Physical Review Letters*, 87(4):045701, 2001.

[42] I. Dornic, H. Chaté, and M. A. Muñoz. Integration of Langevin Equations with Multiplicative Noise and the Viability of Field Theories for Absorbing Phase Transitions. *Physical Review Letters*, 94(10):100601, 2005.

[43] V. Dossetti. Cohesive motion in one-dimensional flocking. *Journal of Physics A: Mathematical and Theoretical*, 45(3):035003, 2012.

[44] M. Durve, A. Saha, and A. Sayeed. Active particle condensation by non-reciprocal and time-delayed interactions. *The European Physical Journal E*, 41(4):49, 2018.

[45] F. J. Dyson. Existence of a phase-transition in a one-dimensional Ising ferromagnet. *Communications in Mathematical Physics*, 12(2):91–107, 1969.

[46] L. Dyson, C. A. Yates, J. Buhl, and A. J. McKane. Onset of collective motion in locusts is captured by a minimal model. *Physical Review E*, 92(5):052708, 2015.

[47] R. Eftimie. Hyperbolic and kinetic models for self-organized biological aggregations and movement: a brief review. *Journal of Mathematical Biology*, 65(1):35–75, 2012.

[48] R. Eftimie. Simultaneous use of different communication mechanisms leads to spatial sorting and unexpected collective behaviours in animal groups. *Journal of Theoretical Biology*, 337:42–53, 2013.

[49] R. Eftimie. The Effect of Different Communication Mechanisms on the Movement and Structure of Self-Organised Aggregations. *Mathematical Modelling of Natural Phenomena*, 8(6):5–24, 2013.

[50] R. Eftimie, G. de Vries, and M. A. Lewis. Complex spatial group patterns result from different animal communication mechanisms. *Proceedings of the National Academy of Sciences*, 104(17):6974–6979, 2007.

[51] F. D. C. Farrell, M. C. Marchetti, D. Marenduzzo, and J. Tailleur. Pattern Formation in Self-Propelled Particles with Density-Dependent Motility. *Physical Review Letters*, 108(24):248101, jun 2012.

[52] C. W. Gardiner. *Stochastic methods: a handbook for the natural and social sciences*. Springer Berlin, 2009.

[53] F. Ginelli. The Physics of the Vicsek model. *European Physical Journal: Special Topics*, 225(11-12):2099–2117, 2016.

[54] F. Ginelli and H. Chaté. Relevance of metric-free interactions in flocking phenomena. *Physical Review Letters*, 105(16):168103, 2010.

[55] M. Goodrich, P. Sujit, S. Kerman, and B. Pendleton. *Enabling Human Interaction with Bio-Inspired Robot Teams: Topologies, Leaders, Predators, and Stakeholders*. Brigham Young University, 2011.

[56] R. Großmann, I. S. Aranson, and F. Peruani. A particle-field approach bridges phase separation and collective motion in active matter. *Nature Communications*, 11(1):5365, 2020.

[57] B. C. Hall. *Lie Groups, Lie Algebras, and Representations*, volume 222 of *Graduate Texts in Mathematics*. Springer International Publishing, Cham, 2015.

[58] H. Hatzikirou, L. Brusch, and A. Deutsch. From cellular automaton rules to a macroscopic mean-field description. In *Acta Physica Polonica B, Proceedings Supplement*, volume 3, pages 399–416, 2010.

[59] H. Hatzikirou and A. Deutsch. Cellular Automata as Microscopic Models of Cell Migration in Heterogeneous Environments. *Current Topics in Developmental Biology*, 81:401–434, 2008.

[60] H. Holden, K. H. Karlsen, and N. H. Risebro. Operator Splitting Methods for Generalized Korteweg–De Vries Equations. *Journal of Computational Physics*, 153(1):203–222, 1999.

[61] J. Jhawar and V. Guttal. Noise-induced effects in collective dynamics and inferring local interactions from data. *Philosophical Transactions of the Royal Society B: Biological Sciences*, 375(1807):20190381, 2020.

[62] J. Jhawar, R. G. Morris, U. R. Amith-Kumar, M. Danny Raj, T. Rogers, H. Rajendran, and V. Guttal. Noise-induced schooling of fish. *Nature Physics*, 16(4):488–493, 2020.

[63] J. Jhawar, R. G. Morris, and V. Guttal. Deriving Mesoscopic Models of Collective Behavior for Finite Populations. In *Handbook of Statistics*, volume 40, pages 551–594. Elsevier B.V., 2019.

[64] Y. Katz, K. Tunstrom, C. C. Ioannou, C. Huepe, and I. D. Couzin. Inferring the structure and dynamics of interactions in schooling fish. *Proceedings of the National Academy of Sciences*, 108(46):18720–18725, 2011.

[65] M. Kimura. Solution of a process of random generic drift with a continuous model. *Proceedings of the National Academy of Sciences*, 41(3):144–150, 1955.

[66] H. Kramers. Brownian motion in a field of force and the diffusion model of chemical reactions. *Physica*, 7(4):284–304, 1940.

[67] A. Krishnamoorthy and D. Menon. Matrix inversion using Cholesky decomposition. In *Signal Processing - Algorithms, Architectures, Arrangements, and Applications Conference Proceedings, SPA*, pages 70–72, 2013.

[68] J. M. Lewis and M. S. Turner. Density distributions and depth in flocks. *Journal of Physics D: Applied Physics*, 50(49):494003, 2017.

[69] H. Löwen and J. Dzubiella. Nonequilibrium pattern formation in strongly interacting driven colloids. *Faraday Discussions*, 123(1):99–105, 2003.

[70] K. Malakar, V. Jemseena, A. Kundu, K. Vijay Kumar, S. Sabhapandit, S. N. Majumdar, S. Redner, and A. Dhar. Steady state, relaxation and first-passage properties of a run-and-tumble particle in one-dimension. *Journal of Statistical Mechanics: Theory and Experiment*, 2018(4):043215, 2018.

[71] M. C. Marchetti, J. F. Joanny, S. Ramaswamy, T. B. Liverpool, J. Prost, M. Rao, and R. A. Simha. Hydrodynamics of soft active matter. *Reviews of Modern Physics*, 85(3):1143–1189, 2013.

[72] D. Martin, H. Chaté, C. Nardini, A. Solon, J. Tailleur, and F. van Wijland. Fluctuation-induced phase separation in metric and topological models of collective motion. *Physical Review Letters*, 126(14):148001, aug 2020.

[73] N. D. Mermin and H. Wagner. Absence of ferromagnetism or antiferromagnetism in one- or two-dimensional isotropic Heisenberg models. *Physical Review Letters*, 17(22):1133–1136, 1966.

[74] J. Michaud. Continuous time limits of the utterance selection model. *Physical Review E*, 95(2):022308, 2017.

[75] S. Mishra, A. Baskaran, and M. C. Marchetti. Fluctuations and pattern formation in self-propelled particles. *Physical Review E*, 81(6):061916, 2010.

[76] E. Moro and H. Schurz. Boundary Preserving Semianalytic Numerical Algorithms for Stochastic Differential Equations. *SIAM Journal on Scientific Computing*, 29(4):1525–1549, 2007.

[77] M. Moussaïd, D. Helbing, and G. Theraulaz. How simple rules determine pedestrian behavior and crowd disasters. *Proceedings of the National Academy of Sciences of the United States of America*, 108(17):6884–6888, 2011.

[78] J. Moyal. Stochastic processes and statistical physics. *Journal of the Royal Statistical Society. Series B*, 11(2):150–210, 1949.

[79] J. M. Nava-Sedeño, H. Hatzikirou, R. Klages, and A. Deutsch. Cellular automaton models for time-correlated random walks: Derivation and analysis. *Scientific Reports*, 7(1):16952, 2017.

[80] J. M. Nava-Sedeño, A. Voß-Böhme, H. Hatzikirou, A. Deutsch, and F. Peruani. Modelling collective cell motion: are on- and off-lattice models equivalent? *Philosophical Transactions of the Royal Society B: Biological Sciences*, 375(1807):20190378, 2020.

[81] E. Ó Laighléis, M. R. Evans, and R. A. Blythe. Minimal stochastic field equations for one-dimensional flocking. *Physical Review E*, 98(6):062127, 2018.

[82] O. J. O'Loan and M. R. Evans. Alternating steady state in one-dimensional flocking. *Journal of Physics A: Mathematical and General*, 32(8):L99–L105, feb 1999.

[83] N. T. Ouellette. A physics perspective on collective animal behavior. *Physical Biology*, 19(2):021004, 2022.

[84] R. Pawula. Generalizations and extensions of the Fokker- Planck-Kolmogorov equations. *IEEE Transactions on Information Theory*, 13(1):33–41, 1967.

[85] R. D. Peacock, E. D. Kuligowski, and J. D. Averill, editors. *Pedestrian and Evacuation Dynamics*. Springer US, Boston, MA, 2011.

[86] D. J. G. Pearce, A. M. Miller, G. Rowlands, and M. S. Turner. Role of projection in the control of bird flocks. *Proceedings of the National Academy of Sciences*, 111(29):10422–10426, 2014.

[87] D. J. G. Pearce and M. S. Turner. Density regulation in strictly metric-free swarms. *New Journal of Physics*, 16(8):082002, 2014.

[88] A. Peshkov, S. Ngo, E. Bertin, H. Chaté, and F. Ginelli. Continuous Theory of Active Matter Systems with Metric-Free Interactions. *Physical Review Letters*, 109(9):098101, 2012.

[89] P. Protter. *Stochastic Integration and Differential Equations*, volume 21 of *Stochastic Modelling and Applied Probability*. Springer Berlin Heidelberg, Berlin, Heidelberg, 1990.

[90] S. Ramaswamy. The Mechanics and Statistics of Active Matter. *Annual Review of Condensed Matter Physics*, 1(1):323–345, 2010.

[91] S. Ramaswamy. Active matter. *Journal of Statistical Mechanics: Theory and Experiment*, 2017(5):054002, 2017.

[92] J. R. Raymond and M. R. Evans. Flocking regimes in a simple lattice model. *Physical Review E*, 73(3):036112, 2006.

[93] C. W. Reynolds. Flocks, herds and schools: A distributed behavioral model. *ACM SIGGRAPH Computer Graphics*, 21(4):25–34, 1987.

[94] H. Risken. *The Fokker-Planck Equation*. Springer Series in Synergetics. Springer Berlin Heidelberg, Berlin, Heidelberg, 1984.

[95] P. Romanczuk, M. Bär, W. Ebeling, B. Lindner, and L. Schimansky-Geier. Active Brownian particles. *The European Physical Journal Special Topics*, 202(1):1–162, 2012.

[96] M. Romensky, V. Lobaskin, and T. Ihle. Tricritical points in a Vicsek model of self-propelled particles with bounded confidence. *Physical Review E*, 90(6):063315, 2014.

[97] M. Romensky, D. Scholz, and V. Lobaskin. Hysteretic dynamics of active particles in a periodic orienting field. *Journal of The Royal Society Interface*, 12(108):20150015, 2015.

[98] D. I. Russell and R. A. Blythe. Noise-Induced Dynamical Transition in Systems with Symmetric Absorbing States. *Physical Review Letters*, 106(16):165702, 2011.

[99] M. J. Schnitzer. Theory of continuum random walks and application to chemotaxis. *Physical Review E*, 48(4):2553–2568, 1993.

[100] M. R. Shaebani, A. Wysocki, R. G. Winkler, G. Gompper, and H. Rieger. Computational models for active matter. *Nature Reviews Physics*, 2(4):181–199, 2020.

[101] X.-q. Shi and H. Chaté. Self-Propelled Rods: Linking Alignment-Dominated and Repulsion-Dominated Active Matter. *arXiv: 1807.00294*, 2018.

[102] A. B. Slowman, M. R. Evans, and R. A. Blythe. Jamming and Attraction of Interacting Run-and-Tumble Random Walkers. *Physical review letters*, 116(21):218101, 2016.

[103] P. Sollich, F. Lequeux, P. Hébraud, and M. E. Cates. Rheology of Soft Glassy Materials. *Physical Review Letters*, 78(10):2020–2023, 1997.

[104] A. P. Solon, J.-B. Caussin, D. Bartolo, H. Chaté, and J. Tailleur. Pattern formation in flocking models: A hydrodynamic description. *Physical Review E*, 92(6):062111, dec 2015.

[105] A. P. Solon, H. Chaté, and J. Tailleur. From Phase to Microphase Separation in Flocking Models: The Essential Role of Nonequilibrium Fluctuations. *Physical Review Letters*, 114(6):068101, feb 2015.

[106] A. P. Solon and J. Tailleur. Revisiting the Flocking Transition Using Active Spins. *Physical Review Letters*, 111(7):078101, 2013.

[107] J. Tailleur, G. Gompper, M. C. Marchetti, J. M. Yeomans, and C. C. Salomon. *Active matter and nonequilibrium statistical physics : lecture notes of the Les Houches Summer School*. Oxford University Press, 1 edition, 2023.

[108] R. Temam. *Navier-Stokes equations: theory and numerical analysis.* North-Holland Publishing Company, 2016.

[109] A. G. Thompson, J. Tailleur, M. E. Cates, and R. A. Blythe. Lattice Models of Nonequilibrium Bacterial Dynamics. *Journal of Statistical Mechanics: Theory and Experiment*, 2011(02):P02029, 2010.

[110] J. Toner. Why walking is easier than pointing: Hydrodynamics of dry active matter. *arXiv*, 2018.

[111] J. Toner and Y. Tu. Long-Range Order in a Two-Dimensional Dynamical XY Model: How Birds Fly Together. *Physical Review Letters*, 75(23):4326–4329, 1995.

[112] J. Toner and Y. Tu. Flocks, herds, and schools: A quantitative theory of flocking. *Physical Review E*, 58(4):4828–4858, 1998.

[113] J. Toner, Y. Tu, and S. Ramaswamy. Hydrodynamics and phases of flocks. *Annals of Physics*, 318(1 SPEC. ISS.):170–244, 2005.

[114] N. G. van Kampen. A power series expansion of the master equation. *Canadian Journal of Physics*, 39(4):551–567, 1961.

[115] N. G. van Kampen. *Stochastic Processes in Physics and Chemistry.* Elsevier, 2007.

[116] T. Vicsek, A. Czirók, E. Ben-Jacob, I. Cohen, and O. Shochet. Novel type of phase transition in a system of self-driven particles. *Physical Review Letters*, 75(6):1226–1229, 1995.

[117] T. Vicsek and A. Zafeiris. Collective motion. *Physics Reports*, 517(3-4):71–140, 2012.

[118] X. Yang and M. C. Marchetti. Hydrodynamics of Turning Flocks. *Physical Review Letters*, 115(25):258101, 2015.

[119] C. A. Yates, R. Erban, C. Escudero, I. D. Couzin, J. Buhl, I. G. Kevrekidis, P. K. Maini, and D. J. T. Sumpter. Inherent noise can facilitate coherence in collective swarm motion. *Proceedings of the National Academy of Sciences*, 106(14):5464–5469, 2009.